Biophysical characterisation of PEGylated proteins and highly concentrated protein solutions

Plesner, Bitten

Publication date:
2011

Document Version
Peer reviewed version

Citation for published version (APA):
Plesner, B. (2011). *Biophysical characterisation of PEGylated proteins and highly concentrated protein solutions.* Roskilde Universitet.

Biophysical characterisation of PEGylated proteins and highly concentrated protein solutions

Bitten Plesner

PhD Thesis
Department of Science
Roskilde University, Denmark
October 2010

Abstract

During the past decade the field of developing highly concentrated protein solutions, especially antibodies, have grown significantly within the pharmaceutical industry. In spite of the growing interest, the distinctive properties of concentrated solutions remains only sporadically explored experimentally. In fact, most biophysical work has strived to investigate solutions, which are as dilute as the experimental method permits, so that forces between protein molecules and restricted volume effects are practically absent, and the intrinsic stability of the protein can be unravelled. Therefore, a major obstacle for a deeper understanding of concentrated protein solutions currently appears to be a shortage of experimental data. Thus, we have investigated the thermodynamic stability of chicken egg lysozyme by Differential Scanning Calorimetry (DSC) with respect to protein concentration, pH and added salt. Despite excluded volume effects the data indicate that lysozyme is destabilised at high protein concentration. It is suggested that the lowered thermodynamic stability at high protein concentration reflects electrostatic repulsion between the native protein molecules or electrostatic attraction between the unfolded protein molecules. This unfavourable effect is speculated to be less severe in the more flexible denatured state and hence to displace the thermal equilibrium towards unfolding.

Besides the commercial approach to develop highly concentrated protein solutions, proteins do in fact often exist in solutions far from ideal and at high concentrations or in crowded environments and protein-protein interactions will in these cases contribute to the stability of the protein. There are several challenges involved in working with highly concentrated protein formulations, most of these regarding the decreased stability of the protein such as the concentration dependent degradation route of aggregation. In order to prevent e.g. aggregation there are several ways of improving the stability of the protein. Excipients as sugars, salts or amino acids can be added the formulation to increase the stability of the protein formulation. Another way of improving the stability, decreasing the risk of aggregation and increasing the solubility is covalently to attach a polymer e.g. a poly-ethylene-glycol (PEG) group to the protein. There are a range of advantages in using PEGylation in therapeutic application in the pharmaceutical industry. It has been shown that PEGylating a protein prolongs its half-life in the circulatory system, increase the drug efficiency dramatically, mask and reduce immune-recognition and clearance from the body, protect from enzymatic or chemical degradation, enhance hydrodynamic size and reduce glomerular filtration.

We have investigated the effects of PEGylation and GlycoPEGylation on Bovine Serum Albumin (BSA) and recombinant human Factor VIIa (rFVIIa), respectively using classical biophysical characterisation tools. Biophysical characterisation of pharmaceutical proteins is widely used throughout the whole drug development process as an invaluable tool to determine possible changes in the structural, thermal and kinetic stability of the protein in question. The effects of PEGylation on the structural, thermal and functional stability of BSA were investigated using BSA and six linear, monoPEGylated BSA compounds, and the effects of GlycoPEGylation on the structural, kinetic and thermal stability of rFVIIa were investigated using rFVIIa and linear 10 kDa and branched 40 kDa GlycoPEGylated recombinant human FVIIa derivatives. In addition the effects of GlycoPEGylation on the molar hydrodynamic volume of recombinant human FVIIa were investigated. In general the secondary and tertiary structure of BSA and rFVIIa measured by Circular Dichroism (CD) was maintained upon PEGylation and GlycoPEGylation, respectively. In contrast, the thermal stability of both model proteins was affected by the covalently attached PEG polymer. For BSA the apparent unfolding temperature, T_m, measured by DSC decreased with PEGylation, whereas T_m for rFVIIa increased with GlycoPEGylation. The temperature of aggregation, T_{agg}, measured by Dynamic Light Scattering (DLS) increased with PEGylation or GlycoPEGylation for both proteins in questions. Possible functional changes of BSA after PEGylation were estimated

by Isothermal Titration Calorimetry (ITC), where the binding of Sodium Dodecyl Sulphate (SDS) to BSA and PEGylated BSA was analysed. At 25 °C two distinct classes of binding sites (high affinity and low affinity) for BSA and one class of binding site (low affinity) for PEGylated BSA were identified. The binding isotherm was modelled assuming independence and thermodynamic equivalence of the sites within each class. Thus BSA appears to have an altered functionality (binding profile) upon PEGylation. This observation is supported by Surface Plasmon Resonance (SPR) measurements, which indicate changes in the binding between BSA and anti-BSA compared to PEGylated BSA and anti-BSA. These biophysical characteristics are all independent of the molecular weight of the attached polymer chain.

From a pharmaceutical formulation point of view altering the salt concentration in the protein buffer is of interest in relation to its effect on the protein stability, and thus we have investigated the effect of calcium chloride on the structural, kinetic and thermal stability of rFVIIa and its two GlycoPEGylated compounds using three different $CaCl_2$ concentrations and the same biophysical characterisation tools as mentioned above. From the obtained results it is concluded that Glyco-PEGylation postpones the calcium induced thermal destabilisation of rFVIIa, and a much higher calcium concentration also postpones the thermally induced aggregation of rFVIIa. The thermally induced aggregation of the GlycoPEGylated rFVIIa compounds is unaffected by an increasing calcium chloride concentration.

In addition, the effects of GlycoPEGylation on the molar hydrodynamic volume of rFVIIa were investigated using capillary viscometry and mass spectrometry to measure the intrinsic viscosity and the molecular mass. The results show that the molar hydrodynamic volume of the conjugated protein is not just an addition of the molar hydrodynamic volume of the PEG and the protein. The molar hydrodynamic volume of the GlycoPEGylated protein is larger than the volume of its composites. These results suggest that both the linear and the branched PEG are not wrapped around the surface of rFVIIa but chains are significantly stretched out when attached to the protein.

Resumé

Udviklingen af højkoncentrerede protein formuleringer, især antistoffer, i den farmaceutiske industri har været støt stigende i løbet af det sidste årti. Men på trods af den stigende interesse er der kun få eksperimentelle studier til karakterisering af disse opløsningers egenskaber. Dette skyldes primært, at de fleste eksperimentelle teknikker er designet til at undersøge fortyndede opløsninger, hvor påvirkningerne mellem proteinmolekylerne og påvirkningerne fra 'resticted volume' nærmest er forsvundet, og stabiliteten af det enkelte proteinmolekyle kan belyses. Den største forhindring i en dybere forståelse af koncentrerede proteinopløsninger synes derfor at være manglen på eksperimentelle data. Derfor har vi undersøgt den termodynamiske stabilitet af lysozym med differentiel skanningskalorimetri i forhold til ændringer i proteinkoncentrationen, pH og tilsat salt. De opnåede resultater indikerer at lysozym destabiliseres ved høj proteinkoncentration på trods af påvirkningerne fra 'excluded volume'. En forklaring herpå kunne være, at den lavere termodynamiske stabilitet ved høj proteinkoncentration skyldes elektrostatisk frastødning mellem de native proteinmolekyler eller elektrostatisk tiltrækning mellem de udfoldede proteinmolekyler. Denne ufordelagtige effekt tænkes at være mindre kraftig i det mere fleksible, udfoldede stadie, og derfor forskydes den termodynamiske ligevægt hen mod udfoldning.

Udover den kommercielle tilgangsvinkel til udviklingen af højkoncentrerede proteinopløsninger, så findes proteiner ofte naturligt i langt fra ideelle opløsninger, i høj koncentration eller i trængte omgivelser, og i disse tilfælde vil protein-protein interaktionerne bidrage væsentligt til proteinets stabilitet. I arbejdet med højkoncentrerede proteinopløsninger er der involveret adskillige udfordringer, primært relateret til den reducerede stabilitet som for eksempel den koncentrationsafhængige aggregering. Proteiner kan dog behandles kemisk og derved kan blandt andet aggregering forbygges. For eksempel kan tilsætningsstoffer som sukkere, salte eller aminosyrer tilsættes for at øge stabiliteten af proteinformuleringen. En anden mulig måde at øge stabiliteten, nedsætte aggregeringsrisikoen og forbedre opløseligheden er ved kovalent at binde en bio-polymer som f.eks. poly-etylen-glykol (PEG) gruppe til proteinet. Der er en lang række fordele ved at benytte PEGylering som terapeutisk applikation i den farmaceutiske industri. Det er påvist at protein PEGylering forlænger proteinets halveringstid i kredsløbet, øger lægemidlets effekt, reducerer immungenkendelse og udskillelsen fra kroppen, beskytter mod enzymatisk eller kemisk nedbrydning, forøger den hydrodynamiske størrelse og reducerer filtreringen gennem nyren.

Vi har undersøgt PEGylerings- og GlycoPEGyleringseffekten på både Bovin Serum Albumin (BSA) og rekombinant human Faktor VIIa (rFVIIa) ved bruge af klassiske biofysiske karakteriseringsværktøjer. Biofysisk karakterisering af farmaceutiske proteiner er udbredt i hele forsknings- og udviklingsfasen som et uvurderligt værktøj til at undersøge mulige ændringer i den strukturelle, termiske og kinetiske stabilitet af det pågældende protein. Effekten af PEGylering på BSA og 6 mono-PEGylerede BSA species blev undersøgt med henblik på ændringer i den strukturelle, termiske og funktionelle stabilitet, og effekten af GlycoPEGylering på rFVIIa, 10 kDa lineær og 40 kDa forgrenet glycoPEGyleret rFVIIa blev undersøgt med henblik på ændringer i den strukturelle, kinetiske og termiske stabilitet. Derudover blev ændringer i det hydrodynamiske volumen af rFVIIa som følge af GlycoPEGylering undersøgt. Den sekundære og tertiære struktur af BSA og rFVIIa blev undersøgt med Cirkulær Dichroism (CD), og begge proteiner havde bevaret deres struktur efter hhv. PEGylering og GlycoPEGylering. Den termiske stabilitet, derimod, var påvirket af PEGylering. Udfoldningstemperaturen, T_m, for BSA faldt med PEGylering, hvorimod T_m for rFVIIa steg med GlycoPEGylering. Aggregeringstemperaturen, T_{agg}, blev målt med Dynamisk Lysspredning (DLS), og denne steg med PEGylering eller GlycoPEGylering for begge undersøgte proteiner. Mulige funktionelle ændringer af BSA pga. PEGylering blev undersøgt med Isotermisk Titreringskalorimetri (ITC), hvor bindingen mellem Natrium Dodecyl-Sulfat

(SDS) og BSA/PEGyleret BSA blev målt. Ved 25 ℃ blev to forskellige slags bindingssteder (høj og lavaffinitet) identificeret på BSA, hvorimod en slags bindingssted (lavaffinitet) blev fundet for PEGyleret BSA. Bindingsisotermen blev modelleret under forudsætning af at bindingsstederne, både høj- og lavaffinitet, var uafhængige og termodynamisk set ens. BSA synes derfor at have en ændret funktionalitet (bindingsprofil) som følge af PEGylering. Denne observation understøttes af Surface Plasmon Resonance (SPR) bindingsstudier, der indikerer ændringer i bindingen mellem BSA og anti-BSA sammenlignet med bindingen mellem PEGyleret BSA og anti-BSA. Samtlige biofysiske karakteristika er uafhængige af molekylvægten af den bundne PEG polymer.

Ændringer af saltkoncentrationen i en proteinbuffer er ud fra et farmaceutisk formuleringssynspunkt ofte interessant eftersom det påvirker proteinets stabilitet, og vi har derfor undersøgt effekten af at ændre kalciumkloridindholdet i bufferen på den strukturelle, kinetiske og termiske stabilitet af rFVIIa og to GlycoPEGylerede varianter heraf. Vi benyttede tre forskellige $CaCl_2$ koncentration og de samme karakteriseringsværktøjer, som blev nævnt ovenfor. På baggrund af de opnåede resultater vi konkluderede, at GlycoPEGylering udskyder den calcium inducerede termiske destabilisering af rFVIIa, og at en tilpas høj kalciumkloridkoncentration også udsatte den termisk inducerede aggregering af rFVIIa. Den termisk inducerede aggregering af de GlycoPEGylerede rFVIIa varianter var upåvirket af ændringen i kalciumkloridkoncentrationen.

Kapillærviskometri og massespektrometri blev benyttet til at måle hhv. grænseviskositet og molekylmasse af rFVIIa og to GlycoPEGylerede rFVIIa varianter for dermed at kunne estimere eventuelle ændringer i det hydrodynamiske volumen af rFVIIa som følge af GlycoPEGylering. Resultaterne viste at det molære volumen af det konjugerede protein ikke blot er en addition af det molære hydrodynamiske volumen af PEG og protein. Det hydrodynamiske volumen af GlycoPEGyleret rFVIIa er større end den samlede volumen af komplekssets komponenter sammenlagt. Resultaterne tyder på, at både den lineære og den forgrenede PEG polymer ikke omslutter overfladen på det konjugerede protein, men derimod tyder resultaterne på at PEG kæderne strækker sig ud og væk fra proteinet.

Overordnet set afspejler de opnåede resultater med PEGylerede og GlycoPEGylerede proteiner i dette studie resultaterne publiceret i litteraturen. Gennem PEGylering eller GlycoPEGylering af en protein opnår man en reduceret termisk induceret aggregeringstendens, bevarer den sekundære og tertiære struktur, påvirker bindingsegenskaberne og et større hydrodynamisk volumen.

Acknowledgements

Preface

This dissertation entitled "**Biophysical characterisation of PEGylated proteins and highly concentrated protein solutions**" is submitted to meet the requirements for obtaining the PhD degree at the Department of Science, Roskilde University, Denmark. The PhD project was carried out under the guidelines of the Industrial PhD Programme and funded by The Danish Council for Technology and Innovation and Novo Nordisk A/S. The work was carried out under the supervision of Professor, PhD Peter Westh and Associate Professor, PhD Søren Hvidt, both at Roskilde University and Research Scientist, PhD Anders Dybdal Nielsen at Novo Nordisk A/S.

The experimental work was performed in the Research Unit for Functional Biomaterials, Department of Science, Roskilde University, Denmark and Department of CMC Analytical Support, CMC, Novo Nordisk A/S, Denmark and at the Department of Chemical and Process Engineering at the University of Canterbury, New Zealand. The PhD project was carried out from August 2007 to October 2010 in collaboration between Roskilde University and Novo Nordisk A/S.

Aim of the thesis

The aim of the thesis is bipartite, and the thesis treats both highly concentrated protein solutions and PEGylated proteins in solution.

Highly concentrated protein solutions

While most of the studies on highly concentrated protein solutions have aimed to shed light on antibody solutions due to the immediate interest from the pharmaceutical industry, we have investigated a well-known and well characterised protein at high concentrations in aqueous solutions. This study primarily contributes to the discussion on which of these two opposite forces dominate at high protein concentration; the effect of excluded volume phenomena or electrostatic interactions. Lysozyme is a highly soluble, globular protein with an isoelectric point of 10.5-11. The latter dictates a high positive charge at low and intermediate pH values and we found that this was sufficient to essentially prevent aggregation, which is otherwise dominating thermal denaturation at high protein concentration. As a result we were able to study reversible unfolding and hence single out the thermodynamic functions at various salt concentrations even at very high protein load.

PEGylated proteins

PEGylating proteins affect a number of the biophysical properties of the bioconjugated protein. We focus on the changes in the binding properties, the thermal, kinetic and struc-

tural stability as well as hydrodynamic volume upon PEGylation. Two different model systems were chosen; Bovine Serum Albumin and recombinant human Factor VIIa which were PEGylated and GlycoPEGylated respectively. The possible altered binding properties of a PEGylated protein as compared to the unmodified protein are investigated by Surface Plasmon Resonance and ITC, two complementary techniques for measuring binding properties of proteins. These measurements contribute specifically to further elucidate the changes in the pharmacokinetic profile of PEGylated proteins as described in section 1.2.1. The thermal stability is investigated by Differential Scanning Calorimetry (DSC), which is mainly used to describe possible changes in the apparent unfolding temperature. The thermogram is also used for predicting whether the protein aggregates upon unfolding or stays in solution. Dynamic Light Scattering (DLS) has been used to describe the aggregation behaviour of PEGylated proteins and their unmodified counterparts, as the postponed aggregation is one of the most characteristic features of a PEGylated protein compared to the unmodified protein. Another key feature obtained by PEGylation is the increased hydrodynamic volume, which is estimated by measuring the intrinsic viscosity and the molecular mass. The change in the intrinsic viscosity is measured by an Ubbelohde viscometer. Finally the secondary and tertiary structure of BSA and rFVIIa as well as their PEGylated or GlycoPEGylated counterparts have been measured by Circular Dichroism (CD) in order to investigate possible changes in the protein structure upon PEGylation. These techniques represent a wide range of classical biophysical characterisation tools, and the obtained results all reflect pharmaceutically relevant properties of the potential protein drug.

Outline of the thesis

The thesis consists of 8 chapters and is divided into three parts. Part I consists of chapter 1 and this chapter is intended as an introduction to the fundamental subjects covered in the thesis and includes a short description of the scientific results obtained and reported in part II and part III. The chapters in part II and part II are either constructed as research papers or as short introductions to the less common biophysical techniques used, followed by experimental results of that technique. Due to this composition of the thesis, there are some overlapping introduction and materials and methods sections on BSA in chapters 3 and 4 and on rFVIIa in chapters 5, 6 and 7.

Part II, Highly Concentrated Protein Solution, consists of one chapter.

Chapter 2 describes the effect of surface charge on the thermal stability of highly concentrated lysozyme solutions.

Part III, PEGylated proteins, consists of five chapters.

Chapter 3 treats the effects of PEG size on the structure, function and stability of PEGylated BSA. This manuscript entitled **Effects of PEG size on the structure, function and stability of PEGylated BSA** was submitted to European Journal of Pharmaceutics and Biopharmaceutics in December 2010.

Chapter 4 gives a short introduction to Surface Plasmon Resonance, SPR, followed by experimental results on PEGylated BSA.

Chapter 5 describes the biophysical characterisation of GlycoPEGylated recombinant human Factor VIIa. This manuscript entitled **Biophysical Characterisation of GlycoPEGylated recombinant human Factor VIIa**, was submitted to International Journal of Pharmaceutics in September 2010 and accepted for publication in December 2010.

Chapter 6 also describes the biophysical characterisation of GlycoPEGylated recombinant human Factor VIIa but focuses on the effect of $CaCl_2$ on the stability of GlycoPEGylated rFVIIa. This manuscript entitled **The effect of GlycoPEGylation on the physical stability of human rFVIIa with increasing calcium chloride concentration** was submitted to European Journal of Pharmaceutics and Biopharmaceutics in September 2010 and accepted for publication in December 2010.

Chapter 7, which treats the hydrodynamic volume changes of rFVIIa due to GlycoPEGylation. This manuscript entitled **The hydrodynamic volume changes of Factor VIIa due to GlycoPEGylation** was submitted to Journal of Pharmaceutical and Biomedical Analysis in October 2010.

Chapter 8, the concluding remarks.

Three appendices are included in the thesis. Appendix A contain additional data on Highly Concentrated Lysozyme Solutions measured by High Resolution Ultrasonic Spectroscopy (HRUS). The content of appendices B and C refers to work in relation to Surface Plasmon Resonance and has been placed as appendices as the work is not fully developed but serves as a basis for further exploration and development in the future. The content of appendix B has been presented as a poster on the 2009 Colorado Protein Stability Conference.

Throughout the report several abbreviations and symbols are used.

AUC Analytical Ultracentrifugation

BSA Bovine Serum Albumin

C_p Heat capacity

CD Circular Dichroism

CV Column Volume

ΔH Enthalpy change

DLS Dynamic Light Scattering

DSC Differential Scanning Calorimetry

ELISA Enzyme-Linked ImmunoSorbent Assay

EMA European Medicines Agency

FDA Federal Drug Agency

FTIR Fourier Transform Infra Red Spectroscopy

η Viscosity

HSA Human Serum Albumin

IEC Ionic Exchange Chromatography

IFN Interferon

IM Intramuscular

IP Intraperitoneal

ITC Isothermal Titration Calorimetry

IV Intravenous

K Binding constant

k_a Association rate constant

k_d Dissociation rate constant

K_D Equilibrium constant

MALDI-TOF Matrix Assisted Laser Desorption Ionisation - Time of Flight

mAb Monoclonal Antibody

MW Molecular Weight

n Refractive index

N Number of binding sites

NMR Nuclear Magnetic Resonance

PBS Phosphate Buffered Saline

PEG Poly(ethylene) glycol

rFVIIa Recombinant Human Factor VIIa

R_g Radius of gyration

R_H Viscosity radius

R_{max} Maximum SPR response

RU Response Units from SPR measurements

S Entropy

SC Subcutaneous

SDS Sodium Dodecyl Sulfate

SDS-PAGE Sodium Dodecyl Sulfate Poly-Acrylamide Gel Electrophoresis

SEC Size Exclusion Chromatography

SPR Surface Plasmon Resonance

SANS Small Angle Neutron Scattering

SAXS Small Angle X-ray Scattering

T_{agg} Temperature of aggregation

T_m Temperature of unfolding

T_{onset} Onset temperature

TF Tissue Factor

V_H Hydrodynamic Volume

Two fundamental terms are recurring throughout the thesis: PEGylation and GlycoPEG-ylation. PEGylation refers to the covalent attachment of poly-ethylene-glycol (PEG) to a protein and does not take the PEGylation method into account. GlycoPEGylation refers to a specific PEGylation method, where glycosyltransferases is used to attach PEG to glycan residues, the enzyme based GlycoPEGylation technology. All the investigated proteins, which have been PEGylated by the GlycoPEGylation technology, have been denoted GlycoPEGylated. However both the PEGylated and GlycoPEGylated proteins are proteins whereto a PEG polymer has been attached.

Contents

Part I

Introduction

1 Introduction

Since the late 1980s the number of protein pharmaceuticals has increased dramatically due to recombinant DNA technology. By then only three recombinant protein products were on the US market, while twenty antibody products and almost 150 protein-based products are now available [1]. Proteins provide a number of unique possibilities with regard to treatment for human diseases and conditions including diabetes, cancer and haemophilia. But even though the development of more pharmaceutical proteins appear to help in curing many diseases, the benefits of the protein drug will not be fully utilised unless the protein is stable throughout the whole process. As the number of therapeutic protein products in the pharmaceutical industry continues to increase, protein stability, chemically as well as physically, will continue to be a relevant issue [1, 2].

1.1 Highly concentrated proteins solutions

Proteins often exist in concentrated solutions or in crowded environments, where the biophysical properties of aqueous protein solutions are characterised by a pronounced non-ideality. During the past decades there has been a growing interest within both the pharmaceutical industry and the scientific society in general to explore the origin of this non-ideality. The focus on highly concentrated protein solutions has increased dramatically during the last decades as the use of antibodies as pharmaceutical drug has gained ground [3, 4]. This growing interest is primarily due to the fact that high protein concentration liquid formulation typically is required to better address the therapeutical goal and patient convenience of subcutaneous (SC), self-administration of the biopharmaceuticals. The SC route of delivery is appealing for protein based pharmaceutical products that require frequent and chronic administration. SC administration is easier compared to the intravenous route (IV) of delivery, which often requires administration in a hospital or similar facility. In combination with a relevant device, SC administration allows home administration for the patient. SC administration often requires high protein concentration due to volume limitations (<1.5 mL) and high dose requirements (50 mg/mL or even higher) [5] and the development of a dosage form in the concentration range 50-200 mg/mL with adequate stability and deliverability presents a technical challenge [6]. As seen in table 1.1 most of the marketed monoclonal antibodies are administered by intravenous injection due to the high doses.

The development of highly concentrated protein products includes several potential challenges with respect to manufacturing, formulation, analysis and delivery. Relevant issues in relation to pharmaceutical formulations are macromolecular crowding, the concentration-

Brand Name	Antibody Type	Dose Route of Administration	Indication
Orthoclone-OKT3	IgG_2, Murine	1 mg/mL (liquid, IV)	Transplant rejection
Remicade	IgG_1, Chimeric	3-10 mg/kg (lyophilizate, IV)	Crohn's disease, rheumatoid arthritis
Herceptin	IgG_1, humanized, CDR-grafted	160 mg (lyophilizate, IV)	Breast cancer
Mylotarg	IgG_4, humanized, CDR-grafted	9 mg/m^2 (lyophilizate, IV)	Myeloid leukemia
Humira	IgG_1, Human	50 mg/mL (Liquid, SC)	Rheumatoid arthritis
Simulect	IgG_1, Murine	450 mg (lyophilizate, IV)	Transplant rejection
Synagis	IgG_1, humanized, CDR-grafted	15 mg/kg (lyophilizate, IM)	Respiratory syncytial virus

Table 1.1: A short list of some of the approved and marketed Antibody (mAb) drugs [3, 4].

dependent aggregation and tendency to form viscous solutions due to the high potential of intermolecular interactions. It is crucial to obtain further knowledge about the various factors influencing the stability of highly concentrated protein formulations for the further development of these pharmaceutical products.

In spite of this growing interest in the special properties of concentrated protein solutions remains only sparsely explored [7]. A lot of the obtained biophysical information is based on dilute solutions resulting in the absence of forces between protein molecules as well as restricted volume effects [7]. Most of the classic biophysical characterisation methods are simply not designed to measure highly concentrated protein solutions. Sensitive instruments requiring very small quantities have been dominating the market of biophysical characterisation instruments. Especially instruments requiring small quantities have been of great importance due to the shortage of sample material which in the early discovery phases often is only available in very few milligrams. However, due to the growing interest especially from the pharmaceutical industry in investigating highly concentrated protein solutions more and more experimental techniques are now available for these purposes. Currently the major limitation for further understanding of concentrated protein solutions appears to be a shortage of experimental data.

In relation to biophysical characterisation of highly concentrated protein solutions a few papers are worth mentioning. One of the most comprehensive studies on the biophysical

stability of proteins at high concentration has been done by Guo et al. [8]. Guo et al. studied the colloidal and conformational stability of proteins in highly concentrated solutions by Fourier Transform Infra Red Spectroscopy (FTIR), Dynamic Light Scattering (DLS) and Circular Dichroism (CD). Based on the results obtained Guo et al. conclude that the conformational and colloidal stability of a protein is determined by a variety of factors. Guo et al. also state that while the prediction of excluded volume theory should conformationally stabilise proteins at high concentrations, other factors such as pH, kinetics, protein dynamics, and intermolecular charge-charge effects may affect the overall stability of proteins at high concentrations under certain conditions. Harn et al. [9] have investigated highly concentrated monoclonal antibody formulations by various biophysical methods including UV spectroscopy, fluorescence spectroscopy, FTIR, CD and DSC. Harn et al. concludes that UV spectroscopy and fluorescence spectroscopy demonstrate a decrease in the apparent thermal melting temperature of $\sim$ 5-20 °C of the proteins with increasing protein concentration. In contrast, DSC thermograms and CD thermal experiments suggest a minor degree of stabilization ($\sim$ 2 °C) of the antibodies although protein association could be responsible for these observations. Matheus et al. [10] have studied highly concentrated protein formulations using FTIR and nano-DSC. Matheus et al. conclude that FTIR is preferred over nano-DSC for analysis of high-concentration protein formulations because the protein can be measured without prior dilution, that is at real solution conditions without the fear of artificial changes in the protein's physical state. In another study by Matheus et al. from the same year [11], they report the use of Fourier-transform infrared (FTIR) spectroscopy in determining the protein melting temperature of highly concentrated liquid IgG$_1$ antibody in various formulations. Matheus et al. conclude, that T_m(FTIR) values did not necessarily correspond to the storage stability at 40 °C analyzed by means of SEC-HPLC and SDS-PAGE. Therefore T_m(FTIR) should only be employed as supportive information to the results from both real-time and accelerated stability studies. Liu et al. [12] have studied the effect of reversible protein self-association on the viscosity of concentrated monoclonal antibody solutions using capillary viscometer or cone-plate rheometer. Liu et al. concludes that the reversible multivalent self-association of this protein appears to be mediated mainly by electrostatic interactions of charged residues and results in unusually high viscosity of this monoclonal antibody in solution at low ionic strength conditions. Patel et al. [13] have investigated an analytical method to calculate the complex modulus and viscosity of high concentration protein solutions from measurements using quartz crystal microbalance with dissipation monitoring (QCM-D). Patel et al. concluded that the characterisation of the rheological properties of high concentration antibody solutions provided insight into protein-protein interactions, and the presented methodology demonstrates a straightforward way to determine the viscoelastic properties using ultrasonic rheology without the drawbacks of numerical fitting.

1.1.1   Crowding theory and excluded volume phenomena

Studies on the structure and function of proteins have traditionally been performed on solutions which are dilute. However, many physiological media do have considerable macromolecular content, and all together the macromolecular species occupy a substan-

tial fraction (10% or larger) of the fluid volume [14]. In general at low concentration, the stability of a protein is mostly dependent on intramolecular interactions and hydration effects, whereas at high concentration, protein-protein interactions are more dominant [8]. At high concentration intramolecular interactions as apolar and electrostatic effects, hydrogen bonds and van der Waals forces might also be altered. Furthermore covalent alternations such as deamidation, oxidation, rupture of peptide bonds and broken disulfide bridges are also very concentration dependent [8].

More than 35 years ago Laurent showed that adding a water-soluble polymer to a protein solution resulted in a significant reduction of the solubility of the protein, suggesting that the thermodynamic activity of the protein was changed due to the exclusion of protein from that fraction of solution volume occupied by polymer [15]. During the 1980s it became the general conception that

> ...in solutions containing a total protein concentration comparable to that found in physiological media, the exclusion of a given protein molecule from the combined volume occupied by other protein molecules can have energetic consequences which are comparable in magnitude to those of commonly invoked inter- and intramolecular electrostatic and hydrophobic interactions [14].

The theoretical fundament of this conception was provided by Minton and coworkers in a number of papers throughout the past three decades [14, 16–23]. The heart of this statistical mechanical approach is to describe the effect of concentration on the Gibbs free energy of the protein molecule. Differentiation of the free energy function with respect to temperature, pressure and composition subsequently enables a comprehensive thermodynamic description of the system. In its simplest form, this theory only accounts for the steric accessibility (i.e. volume exclusion) but more sophisticated versions of the theory also provide some descriptions of electrostatic interactions. While crowding theory has been successful in accounting for some experimental data such as osmotic pressure and diffusion rates [18, 24] it is far from sufficient to rationalize - let alone predict - the physical properties of concentrated protein solutions in general. For example, little information can be derived on hydrodynamic properties such as viscosity, which are of obvious importance. Also, conjugates such as glycosylated or PEGylated proteins, which are not readily described as a hard-sphere, are not easily applicable to the theory. When applying excluded volume theory or crowding theory to a model system, it is important to distinguish between media, which are termed *crowded* and media which are termed *concentrated*, because *in vitro* no single macromolecular species will occur at high concentration but, taken together, the macromolecules occupy a significant fraction (typically 20-30 %) of the total volume [22]. In other words a crowded media is one, where no single macromolecular species is present at high concentration, but all species taken together occupies a significant fraction of the volume of the medium, and a concentrated medium is one where one specific macromolecule occupy a significant fraction of the medium [23].

In the simple version of the excluded volume theory, it predicts that at high concentration of inert macromolecules, e.g. a protein, should be stabilised in the native state relative

to any less compact unfolded or partially folded state of the protein, and in these cases the inert macromolecules are referred to as background molecules or crowding agents. The assumption here being that the background molecules interact with the reactants exclusively through steric exclusion, which is arising from the impenetrable nature of each macromolecule [22]. Steric repulsion models have successfully predicted and accounted for changes in a variety of reactions and processes where addition of inert volume-excluding macromolecules have been added. These reactions include protein folding and the formation of protein-protein complexes [25]. However steric exclusion is not entirely non-specific and it is evident that crowding will have an influence on protein aggregation within more complex heterogeneous media too. This is not depending on but in addition to the influence of other interactions and for this reason these must also be taken into account when seeking to understand reaction rates and equilibria in such media [22, 25].

The excluded volume theory predicts that crowded fluids will promote self-association and hetero-association of proteins [19]. Hence, the conformational stability of the protein is thought to increase while the colloidal stability is thought to decrease. The theory, however, is not directly applicable to proteins without alternations and reservations as proteins are not inert macromolecules. The well-defined secondary and tertiary structure of a protein may change upon stress, and the protein may be more prone to interact more with other proteins. The degree of interaction depends on concentration, temperature and buffer composition.

The continuous progress within the pharmaceutical industry for the development of highly concentrated antibody solutions call for further experimental investigations of the non-ideal properties of concentrated proteins solutions as described earlier in this section. One of these experimental investigations could be to study the effect of concentration, pH and salt on the thermal stability of highly concentrated protein solution mimicking an antibody. In this context we investigated the thermodynamic stability of chicken egg lysozyme by Differential Scanning Calorimetry (DSC) with respect to protein concentration, pH and added salt (see Chapter 2). Lysozyme is chosen due to its high solubility and unusually high isoelectric point. The latter ensures a high positive surface charge at low pH, and it turned out that this surface charge was high enough to prevent aggregation, which is otherwise dominating thermal denaturation at high protein concentration. This experimental setup enabled us to study reversible unfolding and hence single out the thermodynamic functions even at very high protein load, an aspect we believe, based on the current literature, needs to be studied in further detail. Due to the extensive amount of literature on various subjects in relation to dilute lysozyme solutions [8, 10, 26–46] new results obtained by studying lysozyme at high concentration can be correlated to those at low concentration, and differences relating to concentration issues will appear more clearly.

As seen in figure 1.1 at all the investigated pH values the apparent unfolding temperature, T_m, decreases with increasing protein concentration at low salt concentration. Thus despite excluded volume effects the data indicate that lysozyme is thermally destabilised at high protein concentration. At high salt concentration the picture is different, as T_m

decreases with increasing protein concentration at low pH, whereas T_m increases with increasing protein concentration at high pH.
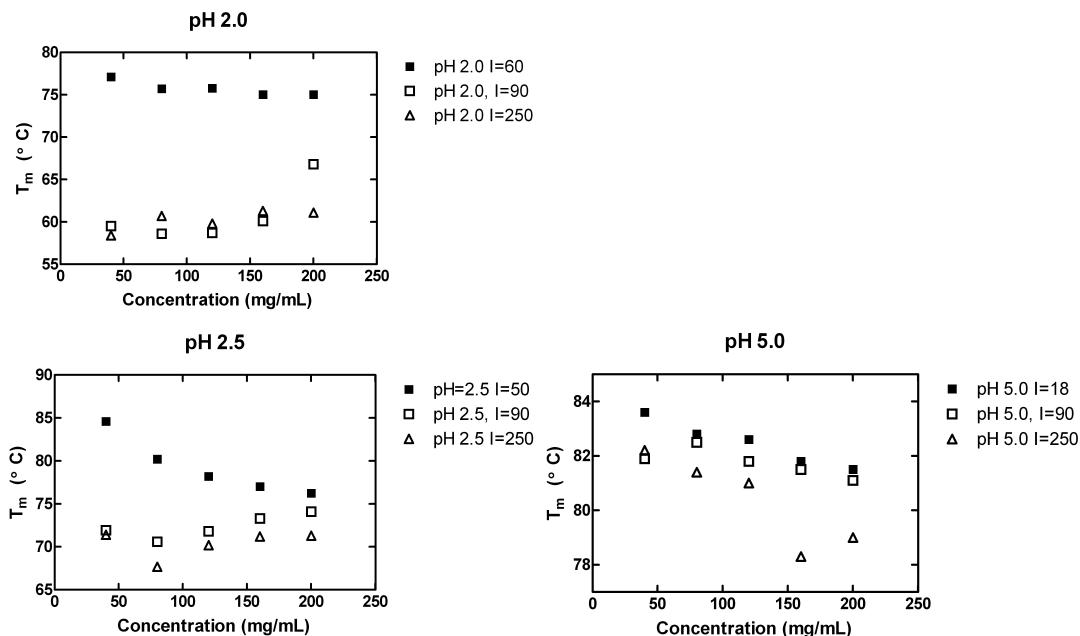
Figure 1.1: The apparent unfolding temperature is plotted as a function of lysozyme concentration. The three figures show the pH depending differences in T_m at different salt concentration. I is the salt concentration in mM. To illustrate the variations in T_m further, the ranges on the y-axis are different in each figure.

The results of this study can generally be categorised in one of two ways either (i) the apparent unfolding temperature decreases with increasing protein concentration or (ii) the apparent unfolding temperature increases with increasing protein concentration, both of which depends on pH and salt concentration. It is suggested that the lowered thermodynamic stability at high protein concentration reflects either electrostatic repulsion between the native protein molecules or electrostatic attraction between the unfolded protein molecules. This unfavourable effect is speculated to be less severe in the more flexible denatured state and hence to displace the thermal equilibrium towards unfolding.

There are several challenges involved in working with highly concentrated protein formulations, most of these regarding the decreased stability of the protein such as the concentration dependent degradation and aggregation. In order to prevent e.g. aggregation there are several ways of stabilising the protein. Excipients as sugars, salts, surfactants or amino acids can be added the formulation to increase the stability. A another way of improving the stability, decreasing the risk of aggregation and increasing the solubility is

to covalently attach a polymer e.g. a poly-ethylene-glycol (PEG) to the protein, a method of modification which has been used in the pharmaceutical industry for the past decades.

1.2 PEGylated proteins in solution

The process of covalently attaching a PEG polymer to a protein, called PEGylation, was first described in the 1970s by Davis and Albuchowsky and subsequently reported in two key papers, one on catalase modification [47] and one on albumin modification [48]. Frank Davis and his colleagues generated the findings regarding the effect of PEGylation. They showed that besides protecting the protein from degrading during drug delivery, PEGylation improves the pharmacokinetic and pharmacodynamic properties of the protein drug by increasing water solubility, reducing renal clearance and limiting toxicity [49]. Modification of pharmaceutical proteins with hydrophilic polymers such as poly-ethylene-glycol (PEGylation) is an established method for prolonging the circulatory half-life of proteins, reducing self-aggregation, increasing water solubility and decreasing antibody recognition, and it has been used successfully in several marketed proteins [50, 51]. In table 1.2 a few of the PEGylated drugs on the current marked are listed.

Brand Name	Product	PEG size (kDa)	Indication	Year (approved)
PEGasys®	PEG-IFN-α-2a (interferon)	40	Hepatitis	2001
PEG-Intron®	PEG-IFN-α-2b (interferon)	12	Hepatitis	2000
Neulastra®	PEG-filgrastim (granulocyte colony-) (stimulating factor)	20	Neutropenia	2002
Oncaspar®	PEG-aspargase (asparaginase)	5	Cancer	1994
Somavert®	PEG-visomant (growth hormone)	4-5 $\times$ 5	Acromegaly	2003

Table 1.2: A short list of some of the PEGylated protein drugs on the current marked [52–54].

PEG, -$(CH_2$-CH_2-$O)_n$-, is a highly soluble, amphiphilic polyether diol. PEG is not charged in solution. X-ray structural analysis shows that PEG chains can adopt two very different structural conformations: a zigzag, random coil structure for shorter chains, or a winding, helical structure for longer chains [55]. These two extreme conformations are reversible in water and dependent on solution conditions [56]. The oxygen atoms allow for hydration of the highly mobile polymer chains resulting in the formation of three water bridges per monomer unit [52, 57, 58]. For this reason the PEG chains are heavily hydrated and consequently they have a large excluded volume which among other things inhibits the

approach of another molecule. The hydration of the PEG chain determines the overall hydrodynamic properties of PEG bioconjugates [59].

Most of the benefits of PEGylated proteins reflect the properties of the PEG polymer itself [60]. Generally the polymer is prepared by anionic polymerisation, which provides a number of molecular sizes. PEG contains two OH end groups, both of which can be activated for chemical PEGylation purposes [61]. The polymerisation process can be controlled such that the molecular weight distribution is narrow, so the PEGs on the market today are much less polydisperse than those employed initially [59, 62]. Still, the polydispersitivity should be taken into account when PEGylating peptides or other low molecular weight drugs as the molecular weight of the PEG can be a significant part of the molecular weight of the whole complex.

PEG is EMA[1]- and FDA-approved for use as a vehicle or base in foods, cosmetics and pharmaceuticals including in injectable, topical, rectal and nasal formulations [49]. PEG shows little toxicity and is cleared from the body, intact, through the kidneys (PEGs <30 kDa) or through the liver or faeces (PEGs >30 kDa) [52, 59]. In general PEGylation reduces kidney clearance simply because PEGylation makes the hydrodynamic volume of a pharmaceutical molecule larger, and the kidney filters molecules according to size, the larger the molecule the slower the clearance. As mentioned earlier, the binding of water makes the PEGylated compounds function as though they are much larger than a corresponding soluble protein of the same mass [49]. This is confirmed by e.g. gel electrophoresis.

1.2.1 Pharmacokinetics

There are many benefits from PEGylating a pharmaceutical drug. One is the altered pharmacokinetics, which already was observed by Abuchowski et al. [47] in 1977. When PEGylating a protein the new molecule will exhibit different pharmacokinetic and pharmacodynamic properties from the parent drug, although it acts on the same target. A reduced binding affinity is often the result of the steric hindrance by the large conjugated PEG polymer. This reduction is often compensated by a prolonged circulation time which together with the reduced immunogenicity creates an overall improved pharmacokinetic profile, which often result in not only an improved efficacy, but also a reduced dosing frequency and an increased patience compliance [52]. The efficacy of a PEGylated protein drug is illustrated in figure 1.2, and discussed in a thorough review by Fishburn [52], where comparative pharmacokinetic and pharmacodynamic parameters from PEGylated proteins and their parent unmodified protein drugs in several *in vivo* animal models are represented. In the review by Fishburn 15 PEGylated enzymes, cytokines, hormones and antibodies have been tested in mice, rats and monkeys. These data show an 100 fold increase in the half-life and a 60 % retained activity on average [52]. Harris et al. [63] have reported similar data in a 2001 review.

---

[1] Abbreviation for European Medicines Agency, which had the acronym EMEA until December 2009.
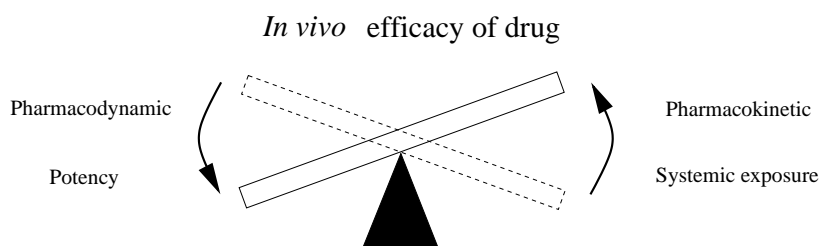
Figure 1.2: PEGylation alters the *in vivo* efficacy of drugs by altering the balance between their pharmacodynamic (PD) and pharmacokinetic (PK) properties. The decrease in potency can be due to a reduced binding affinity which can be compensated for by the increase in the overall exposure caused by a prolonged circulation time. The resulting change in the PK-PD profile provides an overall improved therapeutic efficacy, adapted from [52].

The prolonged circulation time which is one of the main characteristics of a PEGylated protein is primarily a result of two effects; the low clearance through the kidney and the protection from proteolytic degradation, the latter being one of the largest challenges in manufacturing viable protein drugs. The low clearance is a result of the heavily hydrated PEG polymer which increases the effective molecular size of the PEG conjugate. The protection from proteolytic degradation is a result of the constantly mobile PEG moiety which impairs access for proteolytic enzymes. It is the perception that this mechanism also underlies the reduced immunogenicity of PEG-proteins, as the PEG polymer minimises the exposure of antigens and thus reduces or even prevents the formation of neutralising antibodies [52]. Some examples of different classes of PEGylated protein drugs are found in table 1.3, and in the literature. Bailon et al. [51] report that PEGylated α-interferon, Pegasys®, retains only 7% of the antiviral activity of the native protein. It still shows a greatly improved performance *in vivo* compared with the unmodified enzyme because of the improved pharmacokinetics. Stennicke et al. [64] have shown that GlycoPEGylated recombinant Factor VIIa (rFVIIa) has a significantly lower clearance and an increased half-life compared to a variety of rFVIIa from animal species . Hinds and Kim [65] investigated the effect of chemically coupling a single low molecular weight PEG on the physical and pharmacological properties of insulin, and reported that PEGylation of insulin almost completely eliminated the immunogenicity, allergenicity and antigenicity of the conjugated protein. In addition, Yang et al. [66] have studied the effect of PEGylation on the pharmacokinetic profile of anti-TNF-alpha scFv. The studies showed that PEGylated scFv has a 100-fold prolonged circulation life in mice compared to comparable clinical antibodies. Clark et al. [67] have studied the effect of PEGylation on derivatives of human growth hormone (hGH), and their studies showed, that the clearance of hGH in rats was inversely proportional to effective molecular weight (which changed with the number of PEGs attached), and that the potency (*in vivo* and *in vitro*) was increased by about 10-fold compared with unmodified hGH. They concluded that PEGylation improved the hormone's clearance properties, which even at the expense of reducing receptor

binding affinity, would lead to dramatic increases in hormone efficacy.

Class	Molecule	PEG size (kDa)	PEGs per Molecule	Mechanism of Action
Enzymes	Adenosine deaminase	5	Multiple	Proteolytic protection reduced immugenicity
	Asparaginase	5	Multiple	Reduced immugenicity
Cytokines	Interferon - α2a	40	1	Increase size to slow renal clearance
	Interferon - α2b	12	1	Increase size to slow renal clearance
Hormones	GH antagonist	5	4-5	Protection from protease
	Growth hormone	20	1	Protection from protease
Antibodies	Fab' fragments	5, 25, 40	Multiple	Increase size to slow renal clearance
	Anti-TNFα Fab'	nd [a]	1	Increase size to slow renal clearance
Nucleic acids	Anti VEGF[b] aptamer	40	1	Slow diffusion away from site of action of in vitreous tumor
	Anti PDGF[c] aptamer	40	1	Increase size to slow renal clearance

[a] nd, not disclosed
[b] VEGF, vascular-endothelial growth factor
[c] PDGF, platelet-derived growth factor

Table 1.3: Different classes of drugs benefit from different altered properties of the PEG-ylated protein, adapted from [52].

1.2.2   PEG polymer size and shape

The PEG polymer size does also play a role in the immunological properties of the PEG-ylated protein. First and foremost several studies have shown that by increasing the number of conjugated polymers or the PEG polymer size the immunogenicity and anti-genicity decrease [58], and it was found that branched were more effective than the linear ones in improving the immunological properties of proteins. Veronese et al. [68] found that the binding of branched 10 kDa PEG to asparaginase reduced the antigenic character of the protein about 10-fold as compared to the counterpart obtained by modification with 5 kDa PEG, and Caliceti et al. [69] found that branched 10 kDa PEG reduced the uricase immunogenicity and antigenicity more efficiently than the linear 5 kDa polymer, see figure 1.3. Harris et al. [63] argue that attachment at multiple sites will increase the likelihood of steric interference at the active site of the native protein, which will result in a possible

inhibition or reduction of the activity. Monfardini et al. [70] have shown that branched PEG polymers have increased the pH and thermal stability as well as increased the resistance to proteolytic digestion compared with linear PEG conjugates. These results suggest that high molecular weight and branched structures are more efficient in preventing the approach of anti-protein antibodies and do improve the immunogenicity more efficiently.
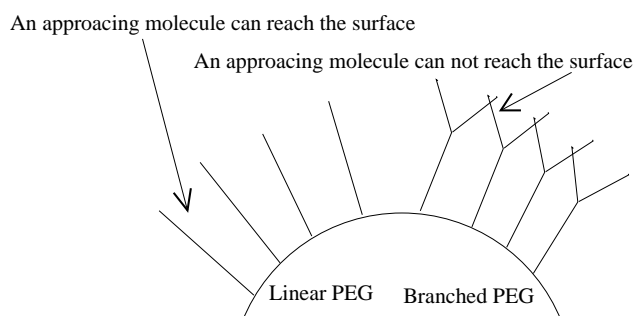

Figure 1.3: The branched PEG decreases the probability of an approaching molecule reaching the surface of the protein compared to the linear PEG. Adapted from [63] and [71].

A side effect of having an efficient prevention of an approaching molecule is also expressed in the lower biological activity. Veronese et al. [72] showed that when PEGylating the enzyme uricase, the residual PEGylated enzyme activity was 32 % of the starting one using a branched PEG, whereas it was only 2.5 % if a linear PEG of the same mass was used.

1.2.3   PEG-protein linkage

It is crucial to ensure that the linkage between the PEG moiety and the protein drug is stable in order to ensure that the pharmaceutical advantages are maintained. Normally PEGylation of a protein is achieved either chemically or enzymatically.

Chemical PEGylation

The chemical PEGylation process is attained by the formation of linkages between a surface available amino acid and an active carbonate, active ester, aldehyde or tresylate derivative of PEG [73]. The modification of the terminal hydroxyl group of PEG is synthesised chemically, and the PEG is activated through the substitution of the hydroxyl group by an electrophilic functional group [74]. Subsequently, the activated PEG can be covalently bound to a specific amino acid, most often lysine or the N-terminus of the protein. The PEG derivatives which are used for amine coupling include N-hydroxysuccinimidyl-activated esters (producing an amide linkage), PEG-epoxide (amine linkage), PEG-carbonyl imidazole (urethane linkage), PEG-tresylate (amine linkage) and PEG-aldehyde (amine linkage). The thiol groups in cysteine can also be used for PEGylation, in this case a PEG-maleimide is among the most utilised [63], see figure 1.4 for the reaction mechanism. In a typical PEGylation reaction process where the lysines or

N-terminal amines are PEGylated, the PEG will be attached to one or several potential sites on the protein. Each of these PEGylated compounds represents one isoform, and the compounds will differ in either degree of PEGylation (mono-, di- or triPEGylated) or site of PEGylation. Most studies on chemical PEGylation refer to liquid phase conjugation, but Suo et al. [75] has developed a method for solid phase chemical conjugation, and with haemoglobin as a model protein Suo et al. obtained a yield of 75%, in comparison to the yield of 30 % obtained in the liquid phase.
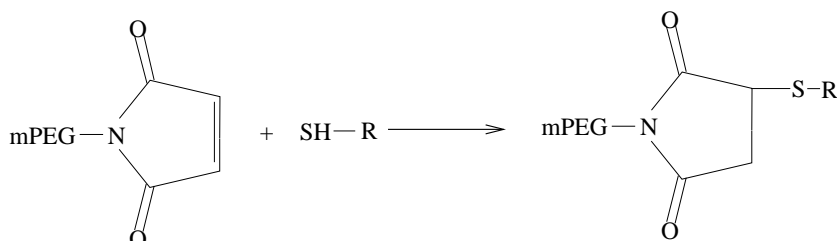

Figure 1.4: The Michael reaction. The PEG-maleimide is reactive under acidic conditions, and is often used when PEGylating thiol groups [76].

We have used chemical PEGylated with PEG-maleimide to PEGylate BSA, see section 3.2 and section 4.2.

Enzymatic PEGylation

Enzymatic PEGylation take advantage of the fact that enzymes can recognise and specifically modify a single or a few amino acid residues in the native protein [77]. As an example of site specific enzymatic PEGylation Sato [78] have used transglutaminase (TGase). Here alkylamine derivatives of PEG could be site-specifically incorporated into intact or modified proteins without decreasing the bioactivities. However the incorporation site of the TGase-catalyzed modification is limited to the substrate Gln residues for TGases. Additionally DeFrees et al. [79] have designed a strategy for site-directed enzymatic PEGylation using glycosyltransferases to attach PEG to O-glycans. Here the enzymatic N-Acetylgalactosamine (GalNAc), an amino sugar derivative of galactose) glycosylation at specific serine and threonine residues in proteins expressed without glycosylation in *Escherichia coli*, followed by enzymatic transfer of sialic acid conjugated with PEG to the introduced GalNAc residues. DeFrees et al. have demonstrated this method of site directed enzymatic attachment of large PEG moieties to three recombinant therapeutic proteins including interferon-αb2, and they suggest that this method enables the manufacture of long-acting protein drugs with greater structural homogeneity compared with chemically PEGylated proteins [80].

The enzyme based GlycoPEGylation technology, which uses glycosyltransferases to attach PEG to N-glycans has been used to produce the GlycoPEGylated recombinant human Factor VIIa, which has been characterised in chapters 5, 6 and 7.

1.2.4   Location of the conjugation site

The location of the conjugation site is another important parameter which can influence the immunogenic and antigenic properties of a PEGylated protein.

Vanwetswinkel et al. [81] have investigated recombinant staphylokinase (Sak-STAR), where variants were obtained by substituting lysines and serines with cysteines, which were subsequently modified with one or two 5, 10 or 20 kDa PEG polymers. Vanwetswinkel et al. found that there were significant differences in the pharmacokinetic parameters among the 5 kDa PEGylated compounds, depending on the site of conjugation. They found pronounced differences between PEGylated compounds having two 5 kDa PEG polymers or one 10 kDa PEG polymers at different conjugation sites. The authors suggest that these observations are a result of the PEG polymer being attached to amino acids which may be exposed to antibody binding or proteolytic enzymes. In addition, Francis et al. [80] have reported that conjugation chemistry can have a dramatic influence on the immunogenicity of the conjugated protein. Thus, in order to obtain the best immunological properties of the PEGylated compound it is important to choose the polymer conjugation site carefully.

Caliceti and Veronese [58] report that in relation to cost effectiveness, therapeutic efficacy and regulatory acceptability the mono- or diPEGylated proteins using high molecular weight PEGs are preferred compared to mixtures of multi-PEGylated protein compounds using low molecular weight PEGs. This is primarily due to the fact that mono- or diPEGylated proteins with high PEG molecular weight in themselves demonstrate enhanced bio-pharmaceutical properties as well as high biomolecular activity compared to the multi-PEGylated proteins with low molecular weight PEGs.

Route of administration

There are several parameters to consider when choosing the proper route of administration. These parameters include among others the molecular weight of the PEG polymer and the degree of PEGylation as this will be reflected in the volume of distribution and the half-life of the PEGylated protein drug [82]. Both intramuscular (I.M.) and subcutaneous (S.C.) adminstration could slow down both adsorption and diffusion and thus the PEGylated drug from reaching the bloodstream for further circulation. In such cases the PEGylated protein might act as a depot, however the degradation may also be increased. Thus the intravenous (I.V.) route of administration might be preferred.

Veronese et al. [83] have studied the pharmacokinetic effect of administering PEG-superoxide dismutase (PEG-SOD) by intravenous, intraperitoneal, subcutaneous and intramuscular injection, see figure 1.5. This study showed that compared to the intravenous route (100 %) the bioavailability of SOD was 71, 54 and 29 % after intraperitoneal, intramuscular and subcutaneous adminstration, respectively. Compared to the native SOD, the bioavailability were in general 100 fold higher, regardless of which route of administration was used. As as seen on figure 1.5, the time for maximal concentration peak is higher when using I.M. and S.C. injection compared to the two other adminstration routes [58].
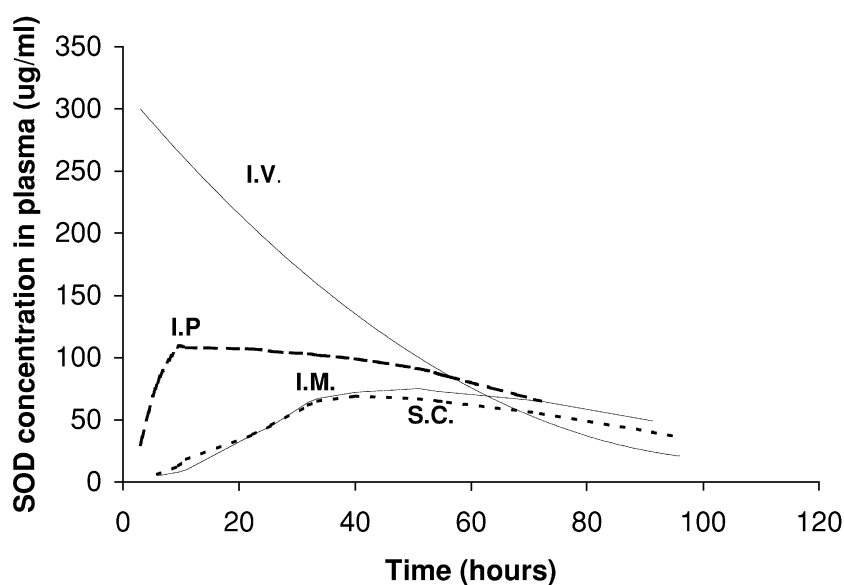
Figure 1.5: Pharmacokinetic profiles of PEG-superoxide dismutase (SOD) in rats after intravenous, intraperitoneal, intramuscular and subcutaneous administration, adapted from [58].

1.2.5   Purification of PEGylated proteins

Chromatographic methods are used to both purify and characterise PEGylated proteins as these methods have both preparative and analytical purposes. Besides from purifying the PEGylated protein by removing PEGylation byproducts and unconverted reactant, information regarding the characteristics of the molecule is also obtained.

Ionic Exchange Chromatography (IEC)

The most common chromatographic method for purifying PEGylated proteins is IEC, and this method has been successfully used to separate several different monoPEGylated proteins from their native counterparts including interleukin 2, papain, caricain, glycyl endopeptidase and human granulocyte colony-stimulating factor, [84, 85]. Fee [85] states three ways in which PEG can affect the charge properties of the protein. First of all, the PEG polymer may weaken the electrostatic interactions by shielding the surface charges. Second of all, the conjugation of PEG to charged residues can affect the isoelectric point (pI) of the protein conjugate. Finally, the PEG polymer bind by hydrogen bonding to some of the surface available amino acids and thus raise or reduce their pKa and in this way affect the charge versus pH behaviour. An observation reported by both Fee [85] and Pabst et al. [86] regarding IEC is that the heavily PEGylated proteins (longer chain length or di-, tri-PEGylated species) elute at a lower ionic strength than their less heavily PEGylated counterparts. Pabst et al. [86] also report a very large decrease in the dynamic binding capacity of PEGylated BSA species compared to the native BSA. These observations are

explained by modulation of the electrostatic interactions associated with the binding of the neutral PEG chain to the charged surface amino acids and an increased mass transfer resistance due to the large size of the PEGylated molecule [85, 86].

Size Exclusion Chromatography (SEC)

SEC can be used to purify a PEGylated sample as well as determine the PEGylation extent, keeping in mind that the elution volumes for SEC relates to the protein size not the molecular weight [85]. The PEGylation extent of a PEGylated protein can be determined qualitatively [87]. SEC is useful as a desalting method, and due to the large hydrodynamic radius of PEGylated proteins small by-product molecules will also be removed during the SEC experiment, and can also be used to separate the native protein from its PEGylated compounds. Generally, the best peak separation is obtained if the proteins differ in molecular weight by no less than two times [85].

Both chromatographic methods have been used to purify PEGylated BSA, see section 3.2 and section 4.2.

1.2.6 Biophysical properties

Thorough characterisation and knowledge about the distribution of the PEGylated compounds are important throughout the whole development process of a PEGylated pharmaceutical drug, which includes formulation changes, process changes and up-scaling [63]. Biophysical characterisation can provide crucial and essential information about the structural, thermal, kinetic and functional stability, all of which can be used in the further development steps.

Structural and thermal stability

Despite the reported altered properties of the PEGylated protein compared to the unmodified protein in relation to prolonged circulation time and reduced activity, most studies report an unchanged secondary and tertiary structure of the protein upon PEGylation. Hinds and Kim [65] have studied PEGylation of insulin by Circular Dichroism (CD), and conclude that PEGylation did not substantially alter insulin's secondary/ tertiary structure. Meng et al. [88] have also used CD to investigate the effect of PEGylation using human serum albumin (HSA) as the model protein. Meng et al. report, that the CD spectra of the conjugates showed that PEGylation of HSA has only little influence on the secondary structure of HSA, whereas Freitas and brahao Neto [89] have studied 5 kDa mono-PEGylated lysozyme with CD and FTIR, and concluded, that the protein structure of lysozyme did not change with PEGylation. Digilio et al. [90] have conducted Nuclear Magnetic Resonance (NMR) spectroscopy on monoPEGylated derivatives of human growth hormone-releasing factor, fragment 1-29. Digilio et al. report that lysine PEGylation does not alter the tendency of the peptide to adopt a stable R-helix conformation, nor does it induce appreciable conformational mobility in the proximity of the PEGylation sites. Dhalluin et al. [91] have studied the thermal and kinetic stability of monoPEGylated human recombinant Interferon-α_{2a}, and they report an unchanged secondary and tertiary

structure upon PEGylation too. Furthermore Dhalluin et al. conclude, that PEGylated interferon-α_{2a} compound has a significantly decreased tendency for heat induced irreversible aggregation, coupled with a slightly elevated denaturation melting temperature. In addition, Ramon et al. [92] studied the conjugation of interferon-α2b (IFN-α2b) to a branched 40 kDa polyethylene glycol with several methods including ELISA and thermal stability (storage at 60 ℃). Ramon et al. concluded, that the immunorecognition against IFN was reduced by the attached PEG moiety, and that PEGylation markedly enhanced the thermal stability of IFN-α2b. Stigsnaes et al. [93] investigated the effect of 5 kDa mono-PEGylation on the conformation and physical stability of glucagon during purification and freeze-drying using FTIR, CD and Thioflavin T asays. Stigsnaes et al. report that the formation of intermolecular β-sheet was less apparent for 5 kDa PEG-glucagon, and that no fibrillation was detected. Stigsnaes et al. conclude, that 5 kDa PEG-glucagon showed a significantly improved physical stability during purification and freeze-drying compared to glucagon. In addition, Hinds and Kim [65] studied the fibril formation of insulin and PEGylated insulin compounds by accelerated shake tests, and conclude that PEGylation significantly increase the fibrillation-resistance, mainly due to steric blocking and increased physical stability.

Even though there appears to be a number of biophysical characterisation studies done on the effect of protein PEGylation, no fundamental study exists which encompasses the effect of PEGylation and different PEG chain lengths on the thermal and kinetic as well as the structural stability. Measuring the thermally induced unfolding and subsequent aggregation by DSC and DLS, and combining this with the thermally induced changes in tertiary structure of an unmodified protein and its PEGylated counterpart has yet to be done. A combination of these methods will enable us to relate changes in the tertiary structure with the formation of aggregates while the overall heat uptake or release is monitored. This would give us a good platform for interpreting the behaviour of PEGylated proteins upon heating.

We have used three complementary classical biophysical characterisation methods which all illustrate each different aspects of the protein unfolding or aggregation processes. The biophysical characterisation has been done on two different protein model systems; Bovine Serum Albumin (BSA) and the more pharmaceutically relevant recombinant human Factor VIIa (rFVIIa). BSA was monoPEGylated with 6 linear PEG ranging from 5 to 60 kDa (chapter 3), and rFVIIa was GlycoPEGylated with a 10 kDa linear PEG or a 40 kDa branched PEG (chapters 5 and 6).

Structural Characterisation

The secondary structure and tertiary structure of both BSA and rFVIIa and their PEGylated and GlycoPEGylated compounds have been measured by Circular Dichroism (CD). The structural information obtained with far-UV-CD and near UV-CD scans shows that both the secondary structure and the tertiary structure of rFVIIa are maintained upon GlycoPEGylation and the structures do not change with PEG chain length nor with the PEG conformation (linear or branched), see figure 1.6.
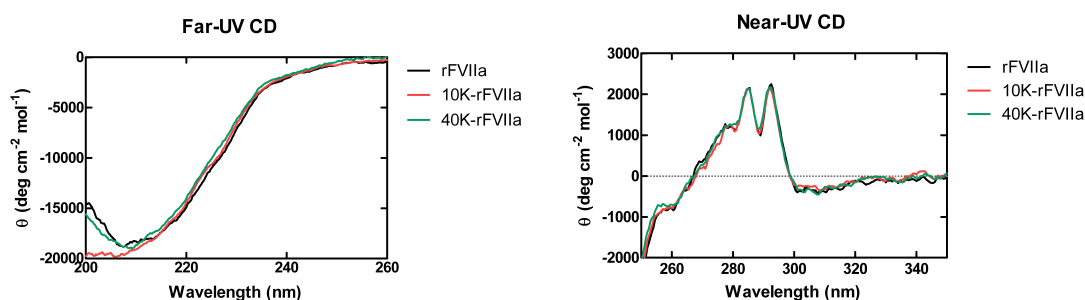
Figure 1.6: Far-UV CD scan and near-UV CD scan of rFVIIa, 10 kDa PEG-rFVIIa and 40 kDa PEG-rFVIIa. The far-UV CD scans show only little variation between the spectrum of 10 kDa PEG-rFVIIa and the two spectrums of rFVIIa and 40 kDa PEG-rFVIIa, and the near-UV CD scans show that GlycoPEGylation has no notable effect on the tertiary structure (near-UV CD) of rFVIIa.

The secondary structure and tertiary structure of BSA is also maintained upon PEGylation (fig. 3.2 and fig. 3.3).

Thermal stability

While the secondary and tertiary structure appear to be maintained upon PEGylation and GlycoPEGylation, the thermal stability of both model proteins was affected by the covalently attached PEG polymer. For BSA the apparent unfolding temperature, T_m, measured by DSC decreased with PEGylation (fig. 1.7), whereas T_m for rFVIIa increased with GlycoPEGylation (fig. 1.8). The temperature of aggregation, T_{agg} (see fig. 1.8 for definition), measured by Dynamic Light Scattering (DLS) increased with PEGylation or GlycoPEGylation for both proteins in questions (fig. 1.7 and fig. 1.8).

The apparent unfolding temperature, T_m decreases for BSA and increases for rFVIIa upon PEGylation and GlycoPEGylation, a result which indicates that the alterations in the thermal stability upon covalently attaching a PEG moiety is very protein specific. All the PEGylated BSA compounds seems to be unfolding at a lower temperature than unmodified BSA, whereas unmodified rFVIIa unfolds at a lower temperature than its GlycoPEGylated compounds. For both model proteins it is evident that a longer PEG chain length does not contribute more to the stability of the protein than a short PEG chain. Rather, it appears that the thermal stability is independent of the molecular weight of the attached PEG polymer. For both model proteins the temperature of aggregation, T_{agg}, increased markedly with PEGylation and GlycoPEGylation, and the unfolded state of the proteins appear to be stabilised.
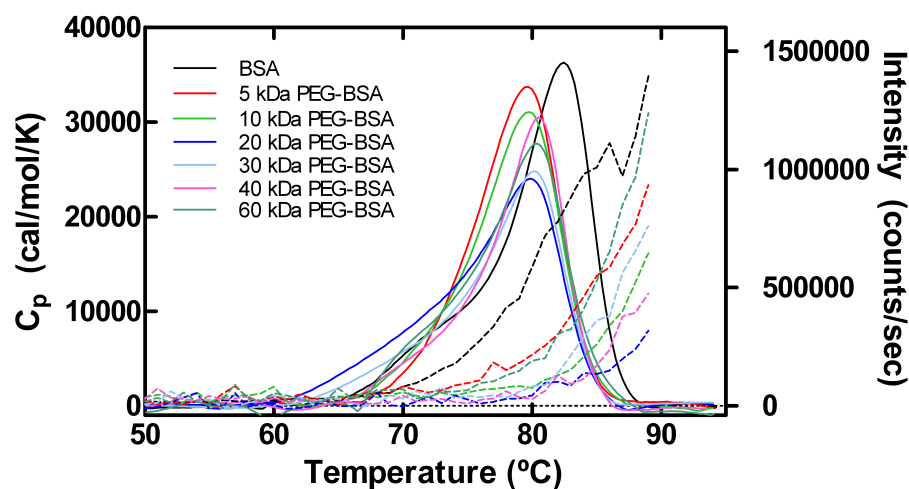
Figure 1.7: DSC scan and DLS measurements of BSA and the 6 PEGylated BSA species with various covalently attached linear PEGs. The DSC scans reveal that PEGylation slightly decreases the apparent unfolding temperature, T_m. The DLS measurements are plotted with the DSC scans, and as expected, the aggregation temperature, T_{agg}, increases with PEGylation.

Formulation

The effect of altering the salt concentration in the buffer was also investigated in the case with GlycoPEGylated rFVIIa (chapter 6). As with lysozyme (chapter 2) the thermal stability of rFVIIa and its GlycoPEGylated compounds also depend on the concentration of $CaCl_2$ in the buffer (fig. 1.8 and table 1.4). Three different $CaCl_2$ concentrations were used: 10 mM, 35 mM and 100 mM.

From the thermograms in fig 1.8 it is evident, that the thermal stability of rFVIIa depends on both $CaCl_2$ content and GlycoPEGylation. The apparent unfolding temperature of rFVIIa decreases at 35 mM and 100 mM $CaCl_2$ compared to 10 mM $CaCl_2$, whereas 10 kDa PEG-rFVIIa and 40 kDa PEG-rFVIIa are not thermally destabilised until the $CaCl_2$ concentration reaches 100 mM. There is a significant difference between the appearances of the thermograms after T_m has been reached. From the DSC thermograms and the LS intensities for the GlycoPEGylated rFVIIa compounds, it appears that GlycoPEGylation delay the thermally induced aggregation of rFVIIa at 10 mM $CaCl_2$ and 35 mM $CaCl_2$. At 100 mM $CaCl_2$ the unmodified rFVIIa and the GlycoPEGylated rFVIIa compounds display similar aggregation behaviour.

In relation to the biophysical characterisation of rFVIIa and GlycoPEGylated rFVIIa, it is noticeable how all three compounds display different aggregation behaviours at 100 mM
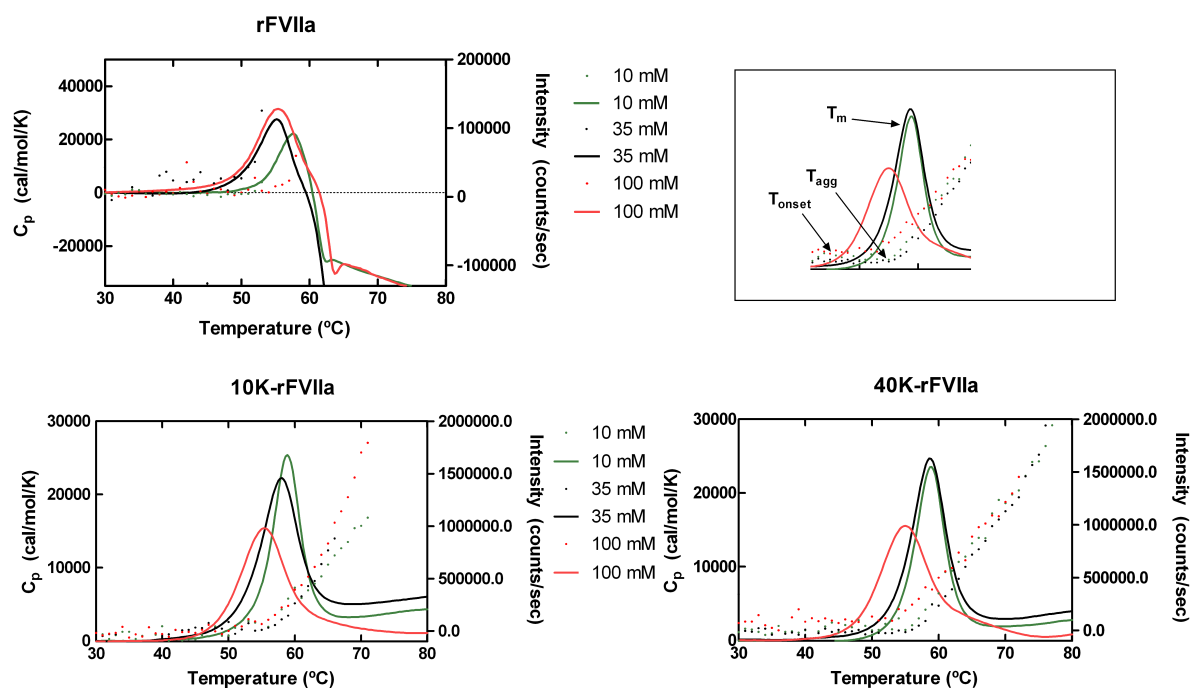
Figure 1.8: DSC thermograms and LS intensity measurements of rFVIIa, 10 kDa PEG-rFVIIa and 40 kDa PEG-rFVIIa are plotted as a function of temperature in buffers with 3 different $CaCl_2$ concentrations. The dotted line correspond to the LS intensity, the solid line correspond to the DSC thermogram. The insert illustrate where the onset temperature, T_{onset}, the temperature of aggregation, T_{agg}, and the apparent unfolding temperature, T_m, are found. The rFVIIa aggregates formed close to T_{agg} were too large for the LS detector to measure, and continuous intensity measurements as a function of temperature were impossible after 53 ℃ for rFVIIa.

$CaCl_2$ as compared to the lower calcium concentrations. At 100 mM $CaCl_2$ the aggregation is not only postponed for all the investigate proteins, native and GlycoPEGylated, the difference between T_{onset} and T_{agg} is 10-11 degrees as opposed to 1-5 degrees at lower $CaCl_2$ concentrations. The main conclusion form these results is that GlycoPEGylation postpones the calcium induced thermal destabilisation of rFVIIa, and a much higher calcium concentration also postpones the thermally induced aggregation of rFVIIa. The thermally induced aggregation of the GlycoPEGylated rFVIIa compounds is unaffected by an increasing calcium chloride concentration.

Lumry-Eyring model

For all the investigated PEG-protein systems the unfolding and aggregation pathway can be described by a model put forward by Lumry and Eyring in 1954 [94]. According to the Lumry Eyring model, irreversible protein denaturation involves at least two steps. The

	T_{onset} (℃) (DSC)	T_m (℃) (DSC)	ΔH (kJ/mol) (DSC)	T_{agg} (℃) (LS)	(T_{onset}-T_{agg})
10 mM CaCl$_2$					
rFVIIa	50.9±0.2	57.7±0.2	NA	50.8±0.4	0.1
10 kDa PEG-rFVIIa	53.3±0.1	59.0±0.2	140	57.1±0.2	-3.8
40 kDa PEG-rFVIIa	52.9±0.1	59.0±0.2	134	57.9±0.9	-5
35 mM CaCl$_2$					
rFVIIa	49.0±0.1	55.2 ±0.2	NA	49.8±0.7	-0.8
10 kDa PEG-rFVIIa	51.0± 0.1	58.0 ±0.2	140	56.8±0.3	-5.8
40 kDa PEG-rFVIIa	52.3±0.1	58.6±0.2	153	57.7±0.2	-5.4
100 mM CaCl$_2$					
rFVIIa	48.3±0.1	55.1±0.2	NA	59.3±0.4	-11
10 kDa PEG-rFVIIa	47.6±0.2	55.3±0.2	147	59.2±0.4	-11.6
40 kDa PEG-rFVIIa	47.1±0.1	55.0±0.2	156	56.7±0.2	-9.6

Table 1.4: The onset temperature T_{onset}, the T_m and corresponding enthalpy measured by DSC, the aggregation temperature, T_{agg}, measured by LS and the difference between T_{onset} and T_{agg}. The extraction of the enthalpy of unfolding of rFVIIa is not possible due to the irreversibility of the denaturation process.

first step is the reversible unfolding of the native protein (N), characterised by the rate constants, k_1 and k_2. This step is followed by an irreversible change of the unfolded protein (D), into an inactivated, irreversible aggregate (A), characterised by the rate constant k_3. The unfolded state, D, is characterised by having some tertiary structure.

$$N \underset{k_2}{\overset{k_1}{\rightleftharpoons}} D \overset{k_3}{\rightarrow} A \qquad K = \frac{k_1}{k_2}$$
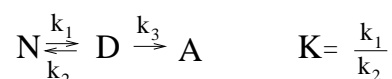
Figure 1.9: The Lumry Eyring model, N is the native protein, D is the unfolded protein and A is the aggregated protein.

Thus we suggest that the covalent attachment of a PEG polymer to a protein (BSA or rFVIIa) slightly increases the equilibrium constant K (lowers T_m) but has a stronger, reducing effect on k_3, so that the aggregation of the denatured (D) is slowed down. The general suppression of protein aggregation by PEG observed here is in accord with earlier reports [65, 95] and the suggestion that this is mainly due to changes in k_3 (and not K) has also been put forward before [65]. Steric hindrance of favourable peptide-peptide contacts appears to be a likely course for the effect of PEG on k_3, but the lack of a correlation of PEG size and T_{agg} suggests that other as of yet unidentified factors may be involved in

the PEG induced increase of the colloidal stability. In particular in relation to the study on the effect of calcium, it is suggested that rFVIIa (unmodified and GlycoPEGylated) in general is stabilised by electrostatic interactions which are weakened by the addition of $CaCl_2$, and that $CaCl_2$ might interact preferentially with the protein in the unfolded state, 'D'. Both effects stabilise the aqueous 'D' state, as the equilibrium constant K increases and the rate constant k_3 decreases with increasing calcium concentration, leading to a lower apparent T_m and a higher T_{agg}.

Binding properties

Even though the structure of the PEGylated proteins appears to be maintained upon PEGylation, the binding properties of the protein can be altered. Kubetzko et al. [96] have constructed a site-specifically PEGylated variants of anti-p185(HER-2) antibody fragments in the format of a monovalent single-chain variable fragment and a divalent mini-antibody and characterized the antigen binding properties using Surface Plasmon Resonance (SPR). Kubetzko et al. found that the attachment of a 20-kDa PEG moiety led to a reduction in apparent affinity of approximately 5-fold, despite a maintained immunoreactivity of the antibody fragments upon PEGylation. In relation to the obtained results, Kubetzko et al. suggest that PEGylation can alter the binding-competent fraction of both ligands and receptors significantly and that this may help to explain some of the beneficial effects of PEGylation *in vivo*. Larson et al. [97] investigated 5 kDa or 20 kDa multi-PEGylated monoclonal anti-GAD antibodies with CD, ^{1}H-NMR and ELISA. The ^{1}H NMR analysis of the modified antibody showed reasonably similar results from 5 to 60 PEG per antibody, and the CD spectra of the polyclonal rabbit IgG showed only small differences at variously modified antibody. The ELISA method revealed that the binding affinity of anti-GAD was lower for all PEG modifications with respect to unmodified anti-GAD, and binding to GAD or anti-mouse-IgG decreased as the degree of modification increased. Wang et al. [98] have investigated the effect of PEGylation on human galectin-2 and report that PEGylation enhanced the protein's stability towards aggregation but did not alter the binding properties.

There are several ways of investigating possible changes in the binding properties of proteins and how these properties can be altered upon PEGylation. One way is to study ligand binding; another is to study the binding between a protein and it's antibody. These two methods elucidate different aspects of the binding process and can be used complementary. To illustrate possible alterations in the ligand binding properties of proteins due to PEGylation, we have investigated the ligand binding properties of BSA and 6 linear, monoPEGylated BSA compounds with Isothermal Titration Calorimetry (ITC) (chapter 3). We chose BSA as a model protein because previous studies of the binding of serum albumins have examined the thermodynamics and stoichiometry of fatty acids or mimics of these (like SDS) to BSA with ITC [99–101]. As the experimental foundation on the unmodified protein already was present, the effects of PEGylation were elucidated by comparing the experimental results obtained with the various PEGylated BSA molecules with the literature values.

At 25 ℃ two distinct classes of binding sites (high affinity and low affinity) for BSA and one class of binding site (low affinity) for PEGylated BSA were identified (fig. 1.10). The binding isotherm was modelled assuming independence and thermodynamic equivalence of the sites within each class. Thus BSA appears to have an altered functionality (binding profile) upon PEGylation. These biophysical characteristics are all independent of the molecular weight of the attached polymer chain.
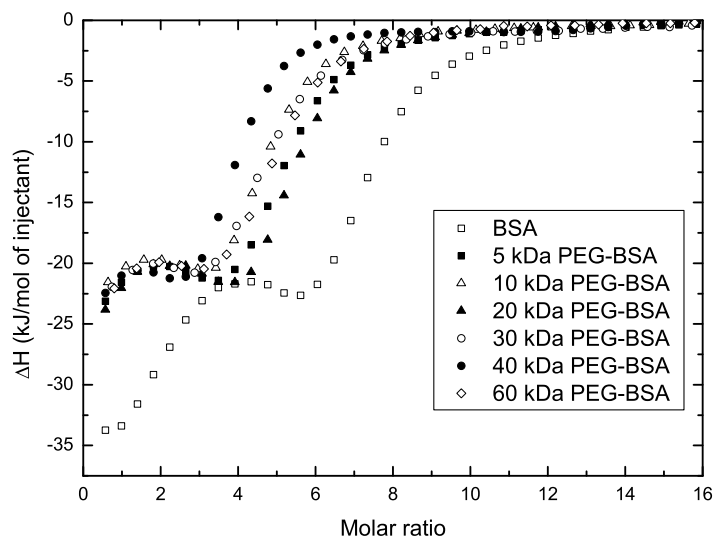

Figure 1.10: Enthalpograms showing the binding of SDS to native BSA and the 6 PEGylated BSA compounds. The ordinate shows the observed enthalpy change ΔH_{obs} in kJ per mole SDS injected, and the abscissa is the concentration of SDS expressed by the surfactant: protein molar ratio. Visually and thermodynamically, there is a significant difference between the binding profiles of the native BSA compared to the PEGylated BSA species. The enthalpogram for native BSA show two inflection points and three plateaus are found, whereas the PEGylated BSA species all have only one inflection point and two plateaus. This indicates that SDS binds differently to native BSA compared to PEGylated BSA.

It is noticeable how little variation there is within the parameters characterising the low affinity sites of the 6 PEGylated BSA compounds. The function of PEGylated BSA seems to be the same whether a small PEG polymer chain or a long PEG polymer chain is attached. Crystallographic and thermodynamic investigations of the these sites on structurally similar serum albumin have revealed that the binding sites for negatively charged ligands with large acyl chains can be roughly divided into two classes: high affinity and low affinity, and that within each class the binding parameters are similar

[99, 102, 103]. It has been suggested that the hydrophobic regions of PEG would interact with the hydrophobic clusters on the protein surface, resulting in a structure of the PEG-protein complex, where PEG is coiled on the protein surface [104]. This may explain the change in the binding properties of BSA upon PEGylation. The PEG polymer may compete with SDS for interaction sites on the protein surface and thus weaken SDS-BSA affinities; although control ITC experiments in which an 8 kDa PEG polymer was titrated to unmodified BSA failed to show direct binding.

Besides investigating the effect of PEGylation on the binding properties of BSA with ITC, we have also investigated these properties with Surface Plasmon Resonance (SPR) (Chapter 4). The binding kinetics of BSA and PEGylated BSA to anti-BSA is investigated with two identical but reversed assay orientations. The SPR response to the binding of BSA or PEGylated BSA to anti-BSA is depending significantly on PEGylation, and it applies to both assay orientations that the binding between anti-BSA and unmodified BSA results in the largest SPR response compared to the binding between anti-BSA and the PEGylated BSA compounds. The SPR response due to complex formation between anti-BSA and PEGylated BSA seems to be independent of the molecular weight of the grafted PEG moiety, which is in accordance with the binding results we obtained with ITC. In addition, we observed that the rate of association was unaffected of PEGylation, molecular weight of the attached PEG polymer as well as assay orientation, and overall K_D appeared to be slightly depending on PEGylation, but independent of the molecular weight of the attached PEG polymer and of the orientation of the assay.

Hydrodynamic volume

When developing a pharmaceutical protein solution intended for injection, the viscosity of the solution plays a key role. In the end it is the viscosity which determines how easy it will be and how long time it will take to press the solution through the syringe. The final viscosity of an aqueous protein solution can be estimated from knowledge of the intrinsic viscosity or the molar hydrodynamic volume of the protein in question together with the concentration of protein in solution. Investigations regarding possible changes in the molar hydrodynamic volume of a pharmaceutical protein upon PEGylation are of high relevance in the drug development process, and we have examined the change in molar hydrodynamic volume of recombinant human Factor VIIa (rFVIIa) upon GlycoPEGylation by measuring the intrinsic viscosity and the molar mass of rFVIIa, PEG and two different GlycoPEGylated rFVIIa compounds, a 10 kDa linear GlycoPEGylated rFVIIa and a 40 kDa branched GlycoPEGylated rFVIIa (see Chapter 7). The results show that the molar hydrodynamic volume of the conjugated protein is not just an addition of the molar hydrodynamic volume of the PEG and the protein. The molar hydrodynamic volume of the GlycoPEGylated protein is larger than the volume of its composites. These results suggest that both the linear and the branched PEG are not wrapped around the surface of rFVIIa but chains are significantly stretched out when attached to the protein, see figure 1.11.
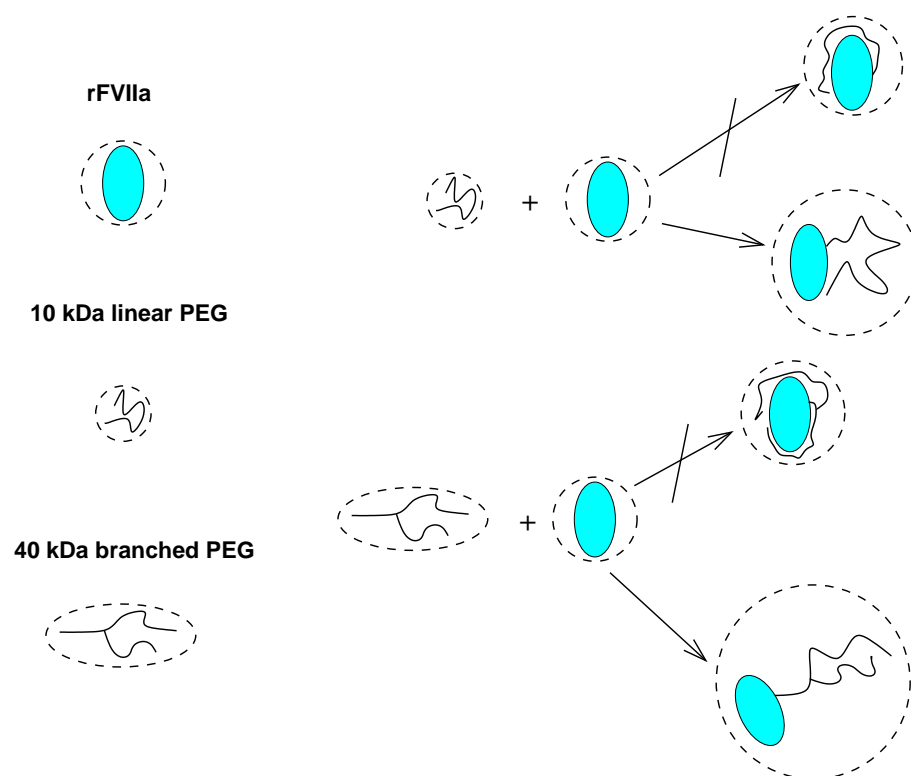
Figure 1.11: The molar hydrodynamic volume of rFVIIa, pure PEG and GlycoPEGylated rFVIIa. The molar hydrodynamic volumes of the conjugated protein indicate that the PEG polymer is not wrapped around the protein; on the contrary it appears to be stretched out from the protein surface.

Further reading

The intentions of this part of the thesis was to give the reader an introduction to and background knowledge on and a short description of the data obtained on the two subjects treated in part II and III. Part II and III are a more detailed description of experiments, result and discussions of the two subjects and the chapters are all constructed as research papers, four of them have been submitted, two have been accepted for publication (chapter 5 and 6) and two are currently under peer review (chapter 3 and 7).

Part II

Highly Concentrated Protein Solutions

2 Thermal stability of Lysozyme at high concentrations: Effect of surface charge

Abstract

The non-ideal properties of concentrated proteins solutions are attracting increasing interest. However the experimental analysis of the relatively strong intermolecular interactions and the excluded volume effects which may modulate the stability of the protein remain sparse. Here the thermodynamic stability of chicken egg lysozyme was investigated by DSC with respect to protein concentration, pH and added salt. Despite excluded volume effects the data indicate that lysozyme is destabilised at high protein concentration and low salt concentration. This indicates that electrostatic interactions favour protein unfolding in the investigated systems. The results generally emphasized the role of intermolecular electrostatic interactions for the stability of lysozyme at high concentration. Thus, in de-salted solutions the unfolding temperature, T_m, decreased at all investigated pH values as the protein concentration was raised from 40 to 200 mg/ml. At pH 2.0 and 2.5, where lysozyme is highly charged, this tendency seems to be reverted so that T_m increased with protein concentration by the addition of 250 mM NaCl. At pH 5.0, on the other hand, where the estimated net charge was lower than at pH 2.0 and 2.5, T_m decreased slightly at all investigated salt concentrations. It is suggested that the lowered thermodynamic stability at high protein concentration reflects electrostatic repulsion between the native protein molecules or electrostatic attraction between the unfolded protein molecules. This unfavourable effect is speculated to be less severe in the more flexible denatured state and hence to displace the thermal equilibrium towards unfolding.

Keywords: highly concentrated protein solutions, protein stability, surface charge, electrostatic interactions, DSC.

2.1 Introduction

Concentrated protein solutions are characterised by a pronounced non-ideality, which becomes particularly strong above 10-20 % by weight [105]. This is of interest e.g. for the understanding of enzyme catalysis in vivo, where very high protein concentrations (10-35 %) may significantly modify kinetic parameters measured in dilute systems [106].

Theoretical aspects of the work on highly concentrated protein solutions include the macromolecular crowding theory or excluded volume theory developed by Minton and co-workers

[20, 21]. In the simple case of inert molecules, this theory predicts that the equilibrium of a highly concentrated protein solution will shift towards the native state of the protein; away from the less compact, unfolded state and thus that the thermal stability of the native conformation will increase at high concentration. These excluded volume effects are related to the mutual impenetrability of inert macromolecules and hence mutual steric repulsion, yielding an increased conformational stabilisation at higher protein concentration [8]. However, contributions to the chemical potential from the intramolecular electrostatic effects as well as a number of intermolecular interactions including van der Waals forces and hydrogen bonding may change considerably with increasing protein concentration. This, in turn, may affect the chemical potential of the native and denatured states of the protein differently and hence shift the thermodynamic stability in a more complex fashion.

Within the pharmaceutical industry there is a growing interest in investigating proteins in highly concentrated solutions primarily due to the increasing interest in highly concentrated antibody solutions. The administration of highly concentrated protein drugs, especially antibodies [3, 4, 9, 107], is often associated with the subcutaneous route of delivery. This route of administration most often requires a higher concentration of the protein drug due to the limited volume given. In spite of the growing interest, the distinctive properties of concentrated solutions remains only sporadically explored experimentally [9, 22]. In fact, most biophysical work has strived to investigate solutions, which are as dilute as the experimental method permits, so that forces between protein molecules and restricted volume effects are practically absent, and the intrinsic stability of the protein can be unravelled. Therefore, a major obstacle for a deeper understanding of concentrated protein solutions currently appears to be a shortage of experimental data. There are a number of works concerning the conformation, interactions and colloidal stability of proteins in crowded systems [105, 108–111], but data on thermodynamic, hydrodynamic and catalytic properties are sparse. In some cases, the concentrated solutions need to be diluted prior to analysis due to experimental limitations [112], but this strategy clearly holds a risk of making mistakes in relation to evaluation of the protein stability. Dilution can significantly change for example the kinetics of irreversible processes as protein aggregation and storage stability.

We have used chicken egg lysozyme as a model protein to investigate the influence of pH, and added salt on the thermal stability of lysozyme at high concentration. Lysozyme is an adequate model protein for this work as it is a highly soluble, globular protein with an isoelectric point of 10.5-11. The latter dictates a high positive net charge at low and intermediate pH values and it turned out that this was sufficient to essentially prevent aggregation, which is otherwise dominating thermal denaturation at high protein concentration. As a result we were able to study reversible unfolding and hence single out the thermodynamic functions even at very high protein load. The structure, folding mechanisms and stability of dilute lysozyme solutions have been studied intensively over the past decades [8, 10, 26–44]. This includes thermal stability and unfolding pathways as a function of pH [8, 30–32], buffer concentration [8, 45], and denaturants such as guanidinium chloride and urea [8, 31, 40, 42, 46]. This wealth of information provides

a unique opportunity of interpreting high concentration lysozyme data, a subject which still remain to be investigated.

2.2   Materials and Methods

Materials

Chicken Egg Lysozyme (L7651) was purchased from Sigma-Aldrich (St. Louis, MO, USA). Lysozyme stock was prepared by dissolving the protein in MilliQ water (Millipore 0.22 μm). The solution was subsequently filtered (0.45 μm). The solution was diluted with Milli Q water and then concentrated through an Amicon tube (Millipore, Carrigtwohill, Ireland), repeating the procedure 6 times to remove excess ions. At high protein concentration lysozyme has a significant buffering capacity, and the current preparations consistently had a pH of 4.1 at 200 mg/mL. The pH was subsequently adjusted with 1 M NaOH or 1 M HCl (VWR, Briare, France). The salt concentration of the solution was determined by the amount of NaOH or HCl added to the most concentrated sample i.e. the sample requiring most acid/base to achieve the desired pH. After adjustment of pH, the concentrated samples were diluted with a NaCl-buffer with the same salt concentration as the concentrated protein solution and pH was adjusted again. In this way, series of the low-salt samples, with identical concentration of salt and protein concentrations from 40-200 mg/ml could be prepared at three different pH values. The concentration of added NaCl was 60 mM for pH 2.0, 50 mM for pH 2.5 and 18 mM for pH 5.0. In addition to this "low-salt" series, we prepared analogous solutions by adding either 90 mM NaCl ("medium-salt") or 250 mM NaCl ("high-salt") to the solvents. Again, these medium and high salt solutions were prepared at pH 2.0, 2.5 and 5.0 and with a lysozyme concentration ranging from 40-200 mg/mL., The concentration of lysozyme was determined using diluted solutions, the published extinction coefficient 37.860, [113] and A280 measurements. The solutions were kept at -20 ℃ until used. All experiments are made in duplicates.

Differential Scanning Calorimetry (DSC)

DSC experiments were performed with a Perkin Elmer Pyris 1 DSC with auto sampler (Waltham, MA). An empty steel sample pan with lid was used as reference and the scans were preformed with a scan rate of 10 ℃/min. All samples were heated from 5 ℃ to 110 ℃, cooled from 110 ℃ to 5 ℃ and re-heated from 5 ℃ to 110 ℃. DSC data was analysed using Origin software from MicroCal Inc. (Northampton, MA). A baseline was subtracted prior to analysis. The apparent denaturation temperatures (T_m) values were determined as the temperature corresponding to the maximum heat capacity (C_p). The enthalpy is calculated from the area under the peak bound by the baseline. The difference in heat capacity is found as described in [30], and the uncertainties are determined based on 3 different tangents on each side of the peak.

Protein pKa (PROPKA)

The online programme PROPKA [114, 115] was used to estimate the value of the surface charge of the lysozyme molecule as a function of pH. PDB file number *2vb1* was used [116]. PROPKA uses all the available amino acids of the native and unfolded protein, respectively, in calculating the total surface charge of the given conformational state. The amino acids individual contributions to the total surface charge depend on their individual location within the protein. In the native state the amino acids are categorised as buried, at the surface or bonded, the latter only apply to cysteine. In the unfolded state pKa values are similar to the actual pKa values for the given amino acids (personal communication; Associate Professor Jan H. Jensen).

2.3 Results and Discussion

DSC thermograms

The DSC scans were conducted so that all the samples were heated, cooled and re-heated. We found that although the samples had been heated 20-40 ℃ above T_m in the first heating scan, the enthalpy change was only reduced by 5-10% in the subsequent heating scan. Thus, it seems reasonable to assume, that the denaturation process around T_m occurs close to equilibrium with a small contribution from coupled, kinetically controlled processes such as aggregation, see figure 2.1.

Figure 2.2 shows two families of raw DSC data for low-salt/pH 2.5 (fig. 2.2a) and high-salt/pH 5.0 (fig. 2.2b), respectively. In both of these examples the apparent unfolding temperature of lysozyme decreases with increasing concentration of the protein. The tendency is particularly pronounced at low pH and low salt concentration (fig. 2.2a).

To further illustrate the observed decrease in the apparent unfolding temperature with increasing lysozyme concentration, T_m is plotted as a function of the protein concentration for all the investigated systems (fig. 2.3). It appears that for the low-salt samples (fig. 2.3, low salt) T_m consistently decreases with protein concentration. However, this trend is changed by the addition of salt (fig. 2.3, medium salt and high salt).

The observed variations in T_m due to changes in pH are also found in a very comprehensive work by Pfeil and Privalov [30–32]. They found T_m values of 48 ℃ at pH 1.5 and 78 ℃ at pH 4.5 by using a 1 mg/mL lysozyme, 100 mM NaCl buffer [30]. Both values are comparable to the values obtained in this work.

Enthalpy

The unfolding enthalpy is calculated for all the DSC thermograms by integrating the area under the peak. The enthalpy at infinite dilution is found by plotting the unfolding enthalpy as a function of concentration at different pH values. Using linear regression and subsequently extrapolating to zero result in values in the range of 240-750 kJ/mol, see figure 2.4. The enthalpies at low lysozyme concentration (40 mg/mL) are outliers, but repeated experiments have given the same result. The values of the enthalpies are
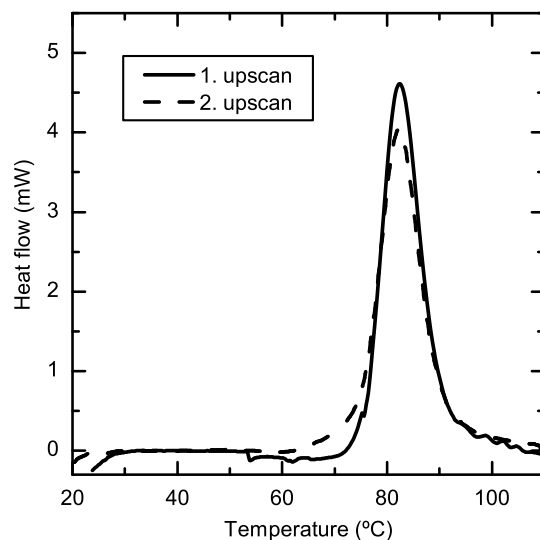
Figure 2.1: Thermograms of the first and second up scans of a 120 mg/mL lysozyme sample, pH 5.0, 18 mM NaCl. The small difference in peak size ($\sim 6\%$) corroborates the view that the denaturation may be described as a simple unfolding equilibrium.
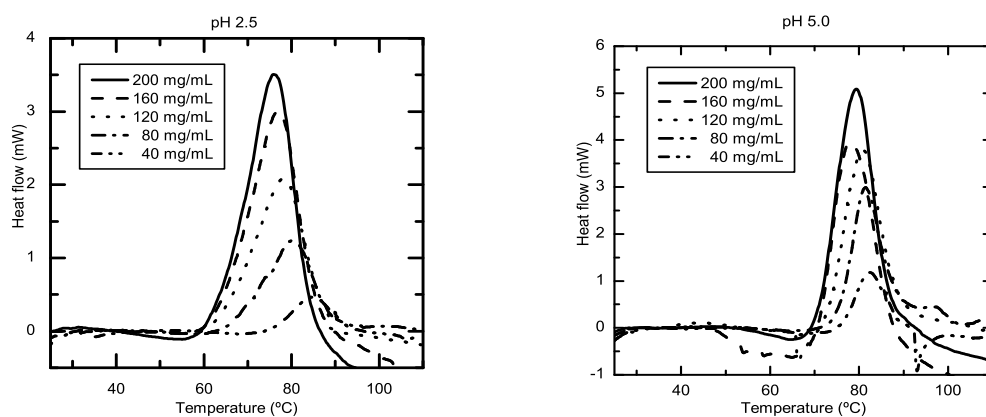
(a) DSC thermograms obtained at pH 2.5 and low salt concentration.

(b) DSC thermograms obtained at pH 5.0 and high salt concentration.

Figure 2.2: DSC thermograms of various concentrations of lysozyme at pH 2.5/low salt and 5.0/high salt.
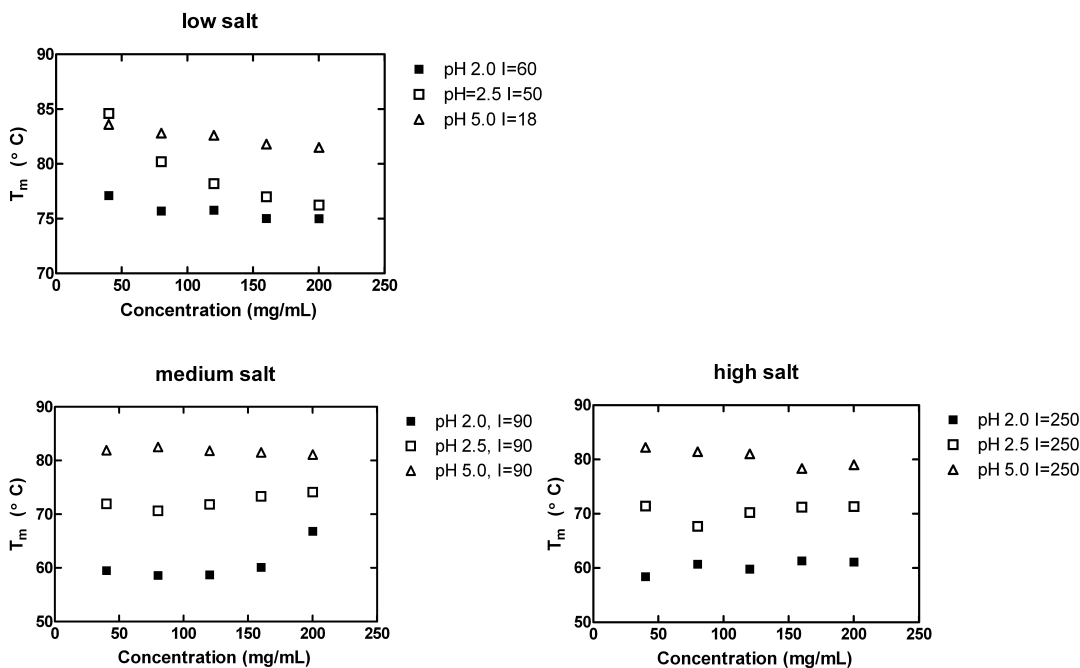
Figure 2.3: The unfolding temperature, T_m, of lysozyme at different salt concentrations. The legend, I, represent the salt concentration in the solution.

comparable to values obtained by Pfeil and Privalov [30–32].

Heat capacity

The heat capacity change associated with the unfolding of the protein is found as described in section 2.2. The values for the heat capacity are positive and independent of pH and attain values of 8 ± 2 kJ mol^{-1}K^{-1}, when disregarding the enthalpies obtained at 40 mg/mL. This value is in the range of the values found in the literature [30–32].

The interactions in the pH range from 2.0 to 5.0 are particularly interesting, as the protein is far from its pI and consequently highly charged. The results obtained in this work illustrate the interrelationships of protein concentration and the well known pH [30–32] and salt effects on the thermodynamic stability.

At low salt concentration T_m decreases with increasing protein concentration at all pH values, (fig. 2.6) and it seem reasonable to assume, that at low salt concentration the contributions to the overall protein stability is dominated by other effects than the excluded volume effect. The excluded volume theory stipulates that the increase in volume associated with increasing concentration of macromolecules will increase the chemical potential of the unfolded species relative to the native state. This in turn will shift the equilibrium towards the native state and hence result in an increase in T_m with increasing

Figure 2.4: The plot shows corresponding values of ΔH as a function of concentration. The filled squares correspond to measurements at pH 2.0, the open squares correspond to measurements at pH 2.5 and the filled triangles correspond to measurements at pH 5.0, all at different salt concentrations. The enthalpies at low lysozyme concentration are outliers, but repeated experiments have given the same result.
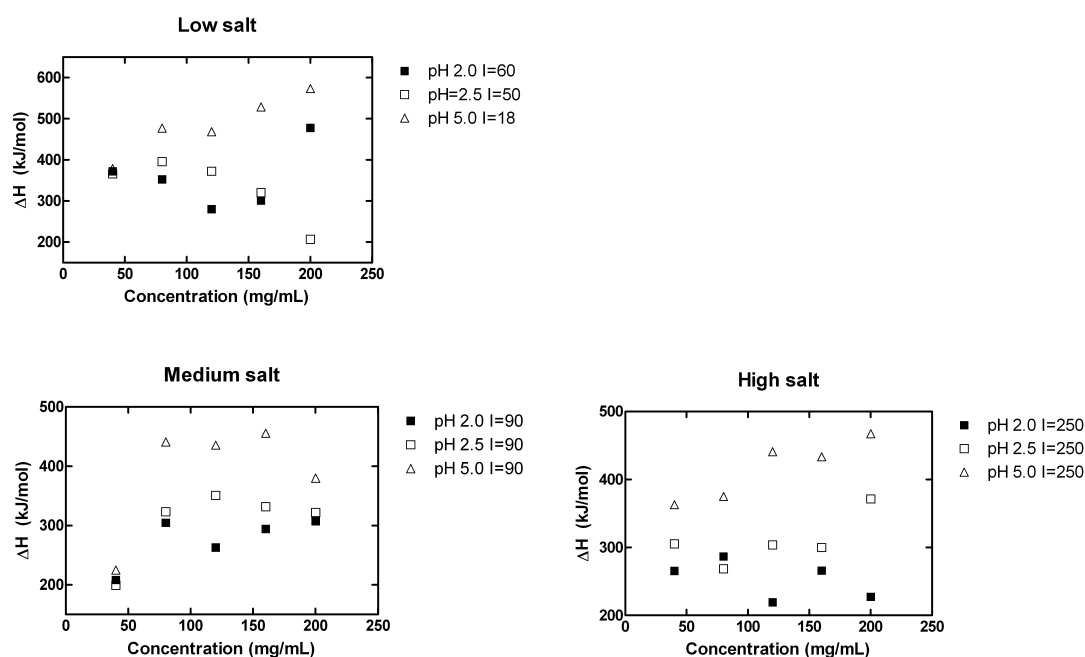
protein concentration. However from the unfolding temperatures obtained at low salt concentration, it is observed that the native state of lysozyme is destabilised with increasing concentration. At both medium and high salt concentration T_m decreases with increasing concentration at high pH, whereas T_m increases with increasing concentration at low pH (fig. 2.3).

These results indicate that the thermal stability of lysozyme in a highly concentrated environment is particularly influenced by electrostatic interactions, as the changes in T_m with concentration are highly influenced by the salt concentration in the solution. These electrostatic interactions can to a certain extent be quantified by values of the pH-depending surface charge. The surface charge of lysozyme has been calculated using PROPKA. The native lysozyme molecule has a surface charge of ~18 at pH 2, see figure 2.5. This value has been experimentally validated [30–32].

The pH-dependent surface charge values are obtained on the basis of calculation of difference in pKas of all the proteins amino acids, including the N and C terminals, as a function of pH. From the theoretical calculations illustrated in figure 2.5 it is clear, that at
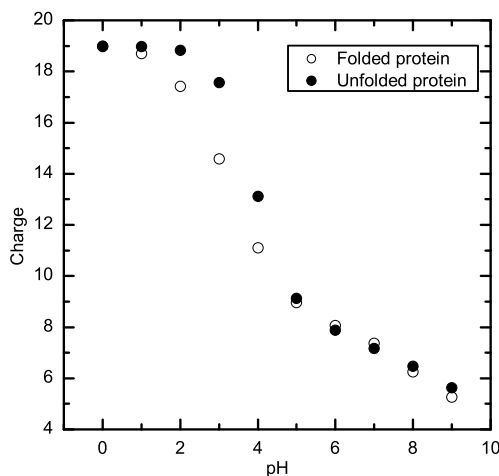
Figure 2.5: The surface charge of lysozyme as a function of pH, calculated by PROPKA [114, 115] using the lysozyme pdb-file: 2vb1 [116]. The filled circles correspond to the unfolded protein; the open circles correspond to the folded protein.

low pH the unfolded state of lysozyme has a higher surface charge than the native state. This difference in surface charge can be explained by the fact that more amino acids are exposed, and then able to contribute to the overall charge, when the protein is unfolded as compared to the native, folded protein.

In figure 2.6 it is seen how the apparent unfolding temperature, T_m, changes as the salt concentration increases within each pH series. From this figure it is clear that the thermal stability of lysozyme at pH 2.0 and pH 2.5 are influenced the most by the increase in salt concentration. For these low pH measurements T_m decreases significantly as the salt concentration increases, the effect being most pronounced at low protein concentration. This may indicate that the electrostatic interactions are strongest at low protein concentration and at low pH. The change in salt concentration from medium to high salt does not seem to affect the unfolding temperature much.

For the thermal stability measurements of lysozyme at pH 5.0, the effect of increasing the salt concentration is not as marked as it was the case with the low pH measurements. There are only small variations in T_m with increasing salt concentration, and not until the salt concentration is increased to 250 mM an effect is found, and then only at the 160 mg/mL and 200 mg/mL.

Overall the thermal stability results indicate that the intermolecular interactions of lysozyme are dominated by electrostatic interactions. This effect is pronounced at low pH and at
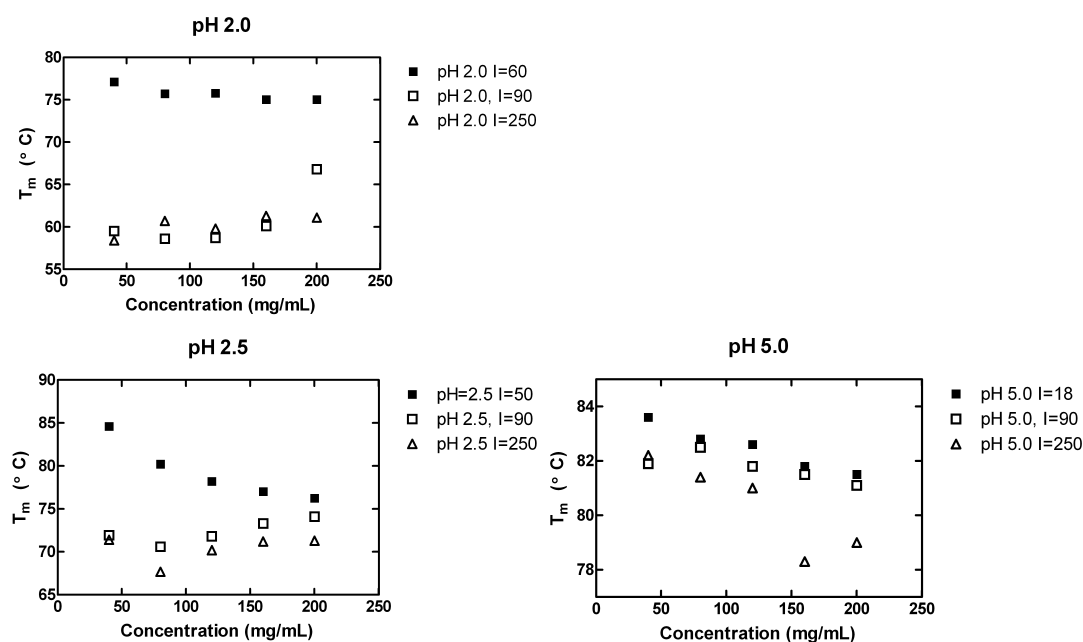
Figure 2.6: The apparent unfolding temperature is plotted as a function of protein concentration. The three figures show the pH depending differences in T_m at different salt concentration. To illustrate the variations in T_m further, the ranges on the y-axis are different in each figure.

low salt concentrations, indicating that the interactions between the unfolded species of lysozyme are more favourable than interactions between the native protein molecules under these conditions, despite the fact that the unfolded state has a higher charge than the native state. This suggests that the electrostatic interaction forces in this case are stronger than the otherwise dominating 'excluded volume' forces. The low salt measurements all display the same tendency, decreasing T_m with increasing lysozyme concentration, and this is illustrated in figure 2.7.

At high salt concentration the changes in T_m with protein concentration is depending on the pH of the solution. As seen in figure 2.6 T_m decreases with increasing protein concentration at low pH, whereas T_m increases with increasing protein concentration at high pH. This is illustrated in figure 2.8.

The results of this study can generally be categorised in one of two ways either (i) the apparent unfolding temperature decreases with increasing protein concentration or (ii) the apparent unfolding temperature increases with increasing protein concentration. The former was unanticipated, but the tendencies observed are supported by High Resolution Ultrasonic Spectroscopy (HRUS) measurements (appendix A). The latter is in accordance

Low salt concentration
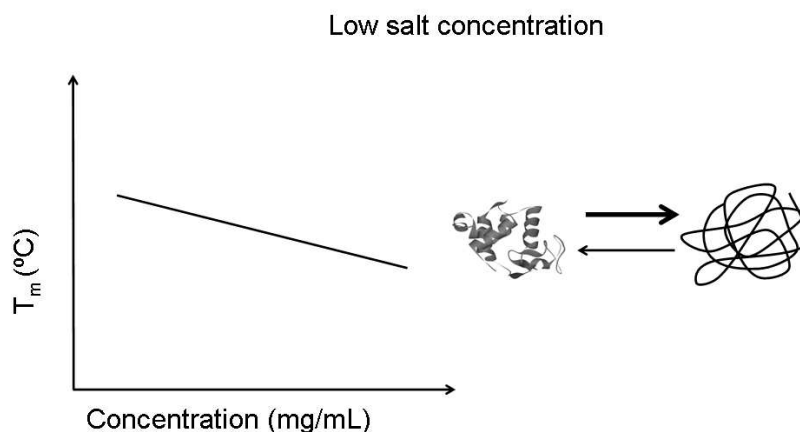
Figure 2.7: For highly concentrated lysozyme solutions at low salt concentration the value of the change in the apparent in T_m with concentration is independent of the pH of the solution. T_m decreases with increasing protein concentration at all pH values. The figure shows a schematic drawing of the native state and the unfolded state of lysozyme, and illustrates that the equilibrium is shifted towards the unfolded state of the protein.

High salt concentration
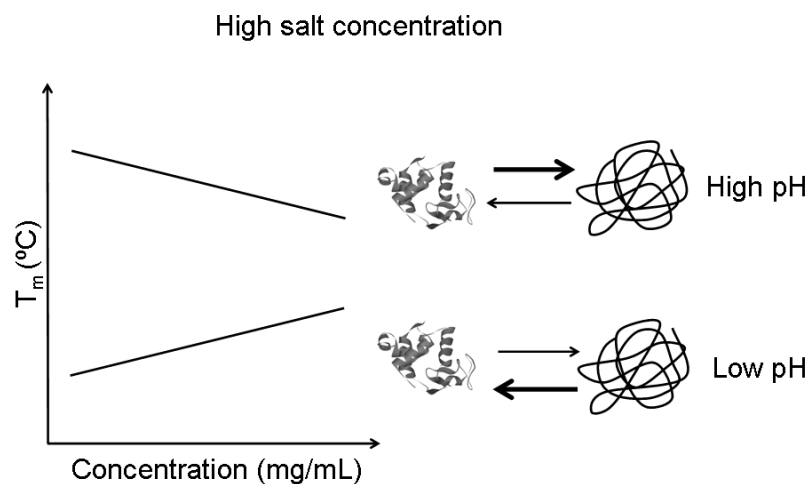
Figure 2.8: For highly concentrated lysozyme solutions at high salt concentration, the value of the apparent T_m is depending on the pH of the solution. T_m decreases with increasing protein concentration at high pH, and T_m increases with increasing protein concentration at low pH. The figure shows a schematic drawing of the native state and the unfolded state of lysozyme. It illustrates that the equilibrium shifts towards the native or the unfolded state depending on the pH of the solution.

with the excluded volume theory stating that the equilibrium between the native and the unfolded state of the protein is shifted towards the native state upon crowding [20, 21]. Harn et al. [9] have investigated the thermal stability of a highly concentrated monoclonal antibody (mAb) solution, and they report a decrease in the apparent unfolding temperature with increasing concentration. They argue, that the decrease in structural stability observed in these studies is probably the result of aggregation or self association of the recombinant mAbs upon heating in crowded solutions and not due to a decrease in the intrinsic structural stability of the mAbs. Due to the high degree of reversibility in the thermal unfolding process (fig.2.1), the decrease in thermal stability of lysozyme does not seem to be a result of aggregation, rather unfolding and subsequent reversible association seems to be the case here.

Guo et al. [8] who have worked with the stability of helix-rich proteins at high concentration including lysozyme argue that the complexity of protein surface and surface related effects could dominate excluded volume phenomena and could make a significant contribution to the stability of the protein. Our results consolidate this argument. Both results emphasise that other phenomena besides conformational stability must be taken under consideration when interpreting data from highly concentrated protein solutions. As the effects on T_m differ with pH and salt concentration, especially the influence of electrostatic interactions must be taken under consideration when the experimental data are interpreted.

The results obtained in this study point to the fact that the native state of a highly charged protein is more likely to be thermally destabilised at high protein concentration, than a protein with a lower surface charge. In this case the thermal stability of the native state of the proteins can be enhanced by adding a sufficient amount of salt to the solution. In addition, the results from the high salt measurements indicate that the addition of salt alters the intermolecular as well as the intramolecular electrostatic interaction. Both illustrated by the increase in T_m with increasing protein concentration. Chi et al. [2] argue that the intramolecular charge-charge interactions affect the conformational stability of the protein, whereas intermolecular electrostatic interactions affect equilibrium and the formation of aggregates. Whether the addition of salt ends up stabilising or destabilising the native state of the protein is thus a balance between various mechanisms, and is influenced by the interactions between the salt and the protein itself as well as the effect of salt on the protein-protein interactions.

2.4 Conclusion

From the results obtained it is concluded, that the apparent unfolding temperature, T_m, of highly concentrated lysozyme dissolved in an aqueous solution with low salt concentration decreases as the protein is exposed to even more crowded environment. According to our studies this is independent of the pH of the solution. At high salt concentration the thermal stability of lysozyme depends on the pH of the aqueous solution. At low pH the thermal stability is shifted towards the native state of the protein, in accordance with the crowding theory. At high pH the thermal stability is shifted towards the unfolded state,

suggesting that electrostatic forces dominate excluded volume phenomena.

Acknowledgements

Part III

PEGylated proteins

3 Effects of PEG size on the structure, function and stability of PEGylated BSA

Bitten Plesner[‡,§], Conan J. Fee[†], Peter Westh[§], Anders D. Nielsen[‡,*]

[§]Department of Science, Roskilde University, P.O. Box 260, Universitetsvej 1, DK-4000 Roskilde, Denmark

[‡]Novo Nordisk A/S, Novo Nordisk Park, DK-2760 Maaloev, Denmark

[†]Biomolecular Interaction Centre and Department of Chemical and Process Engineering, University of Canterbury, Private Bag 4800, Christchurch 8020, New Zealand

[*]Corresponding author. Tel.: +45 30 79 65 75; fax: +45 44 43 40 73

Email address: ADNi@novonordisk.com (A. D. Nielsen).

Abstract

The effects of PEGylation on the structural, thermal and functional stability of Bovine Serum Albumin (BSA) were investigated using BSA and 6 linear, monoPEGylated BSA compounds. The secondary and tertiary structure of BSA measured by Circular Dichroism (CD) was independent of PEGylation. In contrast, the thermal stability of BSA was affected by PEGylation. The apparent unfolding temperature T_m measured by Differential Scanning Calorimetry (DSC) decreased with PEGylation, whereas the temperature of aggregation, T_{agg}, measured by Dynamic Light Scattering (DLS) increased with PEGylation. The unfolding temperature and the temperature of aggregation were both independent of the molecular weight of the PEG chain. Possible functional changes of BSA after PEGylation were measured by Isothermal Titration Calorimetry (ITC), where the binding of Sodium Dodecyl Sulphate (SDS) to BSA and PEGylated BSA was analysed. At 25 °C two distinct classes of binding sites (high affinity and low affinity) for BSA and one class of binding site (low affinity) for PEGylated BSA were identified. The binding isotherm was modelled assuming independence and thermodynamic equivalence of the sites within each class. From the present biophysical characterisation it is concluded that after PEGylation BSA appears to be unaffected structurally (secondary and tertiary structure), slightly destabilised thermally (unfolding temperature), stabilised kinetically (temperature of aggregation) and has an altered functionality (binding profile). These

biophysical characteristics are all independent of the molecular weight of the attached polymer chain.

3.1   Introduction

Modification of pharmaceutical proteins with hydrophilic polymers such as poly-ethylene-glycol (PEGylation) is an established method for prolonging the circulatory half-life of proteins, reducing self-aggregation, increasing water solubility and decreasing antibody recognition, and it has been used successfully in several marketed proteins [50, 51]. Most of the benefits of PEGylated proteins reflect the properties of the PEG polymer itself [60]. The PEG polymer is heavily hydrated and consequently it has a large excluded volume which, among other things, inhibits the approach of other macromolecules, resulting in reduced immunogenicity and decreased antibody recognition [117]. Generally, the hydration of the PEG chain determines the overall hydrodynamic properties of a PEG bioconjugate [59], and the increased molecular size is one of the most important properties of a PEG-ylated protein, resulting for example in a prolonged circulation time due to low rates of clearance from the liver and kidney [117]. Other than increasing the hydrodynamic volume of the protein upon PEGylation, the conformation, physical properties and electrostatics of a PEG-conjugated protein may be altered compared with the unmodified protein [59]. Possible changes include conformational changes of both PEG and protein, altered binding properties resulting from changes in local pI, pKa, hydrophobicity and hydrophilicity of the protein. However, most studies report an unchanged secondary and tertiary structure [65, 88, 90], a retained thermodynamic stability [91] and an increased temperature of aggregation [65] of the protein upon PEGylation, whereas the protein's biological activity is not necessarily preserved [49, 62, 65]. Studies regarding the stability, thermal and structural, as well as the bioactivity of the protein are among the most fundamental when developing pharmaceutical proteins and the ideal pharmaceutical protein should have a long shelf-life and a high bioavailability.

Bovine Serum Albumin (BSA) is a transport protein with a molecular weight of 66400 Da [102]. BSA has one free sulfhydryl group, cysteine 34, which does not form a disulfide bond with another cysteine in the polypeptide backbone [86]. Furthermore, BSA binds several ligands, and it is possible to monitor the function of BSA in vitro with different binding assays. This makes BSA a suitable model protein when investigating the effect of protein PEGylation. Binding mPEG-maleimide (mPEG-MA) to the free cysteine of BSA ensures both mono-PEGylation and site-specific PEGylation.

The relationship between biophysical characteristics and functional properties of proteins and their PEGylated analogues are widely reported but to our knowledge only a few studies have actually investigated these hypotheses experimentally [65, 91, 93, 104]. We have investigated the effect of PEGylation with 6 linear PEG polymers ranging from 5 kDa to 60 kDa, providing us with a unique model system for studying the effect of PEG polymer chain length on the structure, function, thermal and kinetic stability of PEGylated BSA. Various biophysical characterisation tools, including Circular Dichroism (CD), Differential

Scanning Calorimetry (DSC) and Dynamic Light Scattering (DLS), were used to study possible changes in the secondary and tertiary structure as well as the thermodynamic stability of BSA upon PEGylation. Binding of SDS was used to study functional changes of BSA upon PEGylation.

3.2   Materials and Methods

PEGylation reaction

Batch PEG grafting was carried out for each protein individually. All solutions were made up in 10 mM phosphate buffered saline (PBS, Sigma, St. Louis, MO), at pH 7.4. Bovine serum albumin (98 % pure by PAGE) from bovine plasma (Gibco Invitrogen, NZ), was used without further purification. The maleimodo-reactants (Mono-methoxy poly (ethylene glycol) maleimido-propionamide) were of nominal molecular weights 5000, 10000, 20000, 30000, 40000 and 60000 Da, and were a kind gift from Dr Reddy's UK (former Dow Pharma). 1.2 mole of solid mPEG-MA reagent was added per mole of protein to 5 mL of 20 mg/mL native bovine serum albumin and the protein solution was mixed with the PEG reagent and left stirring in an open 10 mL beaker at room temperature overnight. Samples were acidified with one drop of 0.1 M HCl to stop the reaction.

The samples, including a non-PEGylated native BSA sample as a control, were separated individually by ion exchange chromatography (IEC) using a HiPrep 16/10 QFF Anion Exchange column (Amersham Bioscience, Uppsala, Sweden), preparing the column first with 5 CV of 10 mM PBS pH 7.4, 1M NaCl and then 5 CV of 10 mM PBS pH 7.4. 5 mL samples were then injected onto the IEC column and the proteins were eluted with a 15 CV linear gradient to 10 mM PBS, 1 M NaCl at 5 mL/min. The protein elution profile was monitored by UV absorbance at 280 nm and collected in 2 mL fractions. Fractions were analysed by SDS-PAGE, and fractions containing >80 % monoPEGylated BSA monomer, detected by SDS-PAGE, were pooled. These fractions were then polished by injecting 6 mL samples onto a Size Exclusion Chromatography, (SEC) HiPrep 16/60 Sephacryl S-200 column (Amersham Bioscience, Uppsala, Sweden), with PBS running buffer at 1 mL/min. The protein elution profile was monitored by UV absorbance and fractions containing >90 % monoPEGylated BSA monomer, as subsequently detected by SDS-PAGE, were pooled. The purification was carried out on an AKTAexplorer 10$^{\mathrm{TM}}$ liquid chromatography system with an A-900 autosampler and detected by a differential refractometer detector (model RID-10A from Shimadzu, Tokyo, Japan). The chromatography system was operated using Unicorn software, version 4.0, (Amersham Bioscience, Uppsala, Sweden). The protein samples were frozen in liquid nitrogen and lyophilised in a Labconco Freezone 2.5 Total Lab system freeze dryer (Kansas City, MO) overnight at 3.0 Pa -49 ℃. The lyophilised protein samples were kept at -20 ℃ until use. Prior to the experiments, all native BSA and PEGylated BSA solutions were dissolved in PBS buffer and then dialysed intensively against PBS. The dialysate was used as reference. The purity of the BSA and PEGylated BSA samples was tested by SDS-PAGE (see fig 4.2), and revealed that the individual PEGylated BSA samples contained all > 90 % PEGylated BSA and approximately 5 %

native BSA monomer and 4 % native BSA dimer, respectively.

Isothermal Titration Calorimetry (ITC)

The calorimetric measurements were made with a VP-ITC instrument from MicroCal (Northhampton, MA). Before the loading the solutions into the cell and syringe, respectively, the solutions were degassed by stirring under vacuum. The protein concentration was kept in the range 18-25 μM and determined using a Nanodrop spectrophotometer (Thermo Scientific Wilmington, DE). The concentration of SDS was 2.4 mM. The protein solution was loaded into the cell and titrated 40 times with aliquots of 5 μl surfactant solution at 25 °C. The raw ITC data were analyzed using the Origin software package from Microcal. The heat of dilution, defined by the plateau level when the binding is fully saturated was subtracted from the data also using the analysis software package from Microcal. The concentration of SDS used here is slightly above the critical micellar concentration (CMC) (measured in a separate experiment, see [118]) and a small fraction of the surfactant will thus be delivered in a micellar form. The accompanying heat of demicellization was subtracted as described earlier [99].

Circular Dichroism (CD) Spectroscopy

Spectra of BSA in the far-UV region (180-260 nm) were recorded on a Jasco J-810 CD Spectropolarimeter. The light path of the cuvette was 0.1 mm and a protein concentration of 0.8 mg/mL was used. The spectra were recorded at room temperature. Each spectrum is an average of 5 scans. All spectra were background-corrected, smoothed and transformed into molar ellipticity (Θ cm^2 dmol^{-1}). A value of 114 g/mol was used as a mean residue weight for BSA.

Spectra of BSA in the near-UV region (250-350 nm) were recorded on the same spectropolarimeter. The light path of the cuvette was 10 mm and a protein concentration of 0.8 mg/mL was used. The spectra were recorded at room temperature. Each spectrum is an average of 5 scans. All spectra were background-corrected, smoothed and transformed into molar ellipticity (Θ cm^2 dmol^{-1}).

Differential Scanning Calorimetry (DSC)

DSC experiments were performed with a MicroCal VP-DSC (Northhampton, MA). Prior to scanning, all solutions were degassed by stirring under vacuum. A pressure of 2 atm was applied over the cells during scanning, and a scan rate of 1 °C/min was used. The concentration of BSA was 0.8 mg/mL and buffer scans were subtracted from BSA scans. DSC data was analysed using the Origin software from MicroCal Inc., supplied with the instrument. A baseline was subtracted prior to analysis. The apparent unfolding temperature (T_m) values were determined as the temperature corresponding to the maximum C_p, and the errors are determined by repeatable experiments. The enthalpy is calculated from the area under the peak bound by the baseline and the errors are based on the adjustment of this baseline.

Dynamic Light Scattering (DLS)

The DLS experiments were performed with a Wyatt DynaPro Titan (Santa Barbara, CA) which employs a 829 nm laser and collects scattering intensity data at a fixed angle of 90 ℃. Cuvette temperature was controlled using a thermoelectric solid-state heating module (Peltier heat pump). Solutions were examined in a quartz cuvette with 12 μL cell volume containing glass viewing windows for in situ scattering measurements. Samples were centrifuged at 10.000 rpm for 10 minutes prior to analysis. The scan rate for was 1 ℃/min and 10 minutes was allowed for temperature calibration prior to each experiment.

3.3 Results

Isothermal Titration Calorimetry

ITC was used to measure the binding between BSA and the ligand SDS. The enthalpogram for the binding of SDS to native BSA shows two clear inflection points separating three plateaus (figure 3.1).

Figure 3.1: Enthalpograms showing the binding of SDS to native BSA and the 6 PEG-ylated BSA compounds. The ordinate shows the observed enthalpy change ΔH_{obs} in kJ per mol SDS injected, and the abscissa is the concentration of SDS expressed by the surfactant: protein molar ratio. Visually and thermodynamically, there is a significant difference between the binding profiles of the native BSA compared to the PEGylated BSA species. The enthalpogram for native BSA show two inflection points and three plateaus are found, whereas the PEGylated BSA species all have only one inflection point and two plateaus. This indicates that SDS binds differently to native BSA compared to PEGylated BSA. The insert shows an enthalpogram for the binding of 8 kDa PEG to native BSA. As seen on the figure no binding of PEG to BSA is found.

ITC data for the binding to the two classes of independent sites is modelled as described in Nielsen et al. [99]. Briefly, it is assumed that the native BSA molecule has two classes of sites, which can bind the same type of ligand. These sites are thermodynamically similar and can be characterised by a binding constant (K), an enthalpy of binding (ΔH) and a number of binding sites (N). These 6 values are found by a non-linear, least square minimisation routine giving a maximum likelihood value (figure 3.1 and table 3.1.)

	N	ΔH (kJ/mol)	K (M^{-1})	T ΔS (J/mol)
	Low affinity sites			
BSA	5.8±0.1	-23.9 ±0.4	3.4(±0.5)·10^4	7.8
BSA[a]	5.3±0.03	-28.1±1.0	3.7(±0.6)·10^5	2.0±3
5 kDa-PEG BSA	5.3±0.06	-22.6 ±0.3	3.7(±0.6)·10^5	9.3
10 kDa PEG-BSA	4.8±0.05	-21.7±0.3	4.4(±0.6)·10^5	10.5
20 kDa PEG-BSA	5.6±0.06	-22.2±0.3	4.7(±0.8)·10^5	10.0
30 kDa PEG-BSA	4.7±0.05	-22.6±0.3	3.4(±0.4)·10^5	7.0
40 kDa PEG-BSA	3.9±0.04	-22.6±0.3	4.4(± 0.6)·10^5	9.48
60 kDa PEG-BSA	4.9±0.04	-22.2±0.2	4.8(±0.4)·10^5	10.3

	N	ΔH (kJ/mol)	K (M^{-1})	T ΔS (J/mol)
	High affinity sites			
BSA	1.7 ±0.1	-34.3±0.8	3.4(±2.1) ·10^7	8.8
BSA[b]	2.9 ±0.1	-35.5±1.1	3.3 ·10^7	7.4±3
5 kDa PEG-BSA	-	-	-	-
10 kDa PEG-BSA	-	-	-	-
20 kDa PEG-BSA	-	-	-	-
30 kDa PEG-BSA	-	-	-	-
40 kDa PEG-BSA	-	-	-	-
60 kDa PEG-BSA	-	-	-	-

[a] data from [99]
[b] data from [99]

Table 3.1: Summary of thermodynamic and stoichiometric parameters of the binding of SDS to BSA and PEGylated BSA at T= 25 ℃.

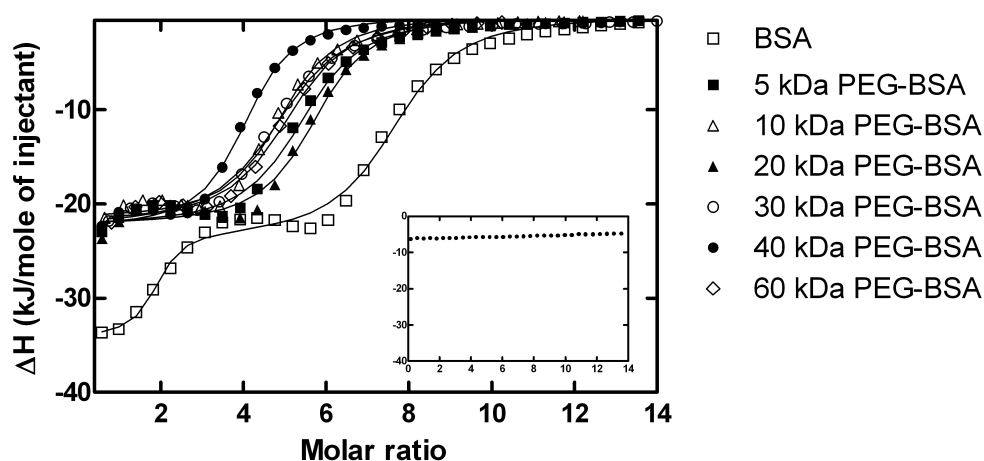The enthalpogram for the binding of SDS to native BSA shows two clear inflexion points separating three plateaus (figure 3.1). This is in accordance with previously reported results ([99, 119]) and indicates that a reasonable simplification of the multiple binding processes is a picture of SDS associating with two classes of independent binding sites (high affinity/low affinity) for the native BSA. Due to a small amount of available PEGylated BSA the ITC measurements and DSC measurements were only performed twice, but as

the results were very alike we have only used one of each measurement.

The enthalpograms for the binding of SDS to PEGylated BSA species show a different course than that of native BSA, namely one clear inflection point separating two horizontal regions (figure 3.1). It seems reasonable to assume that the PEGylated BSA molecule contains only low-affinity binding sites, as the plateaus are found around the enthalpy values -20 kJ/mol and 0 kJ/mol. These values are of the same magnitude as the low-affinity sites of native BSA, supporting the conclusion that only low-affinity binding sites are found on PEGylated BSA. This class of binding site includes several sites that are thermodynamically similar [99, 119] and has been modelled as a one-site model wherefrom 3 parameters are found, the binding constant (K), an enthalpy of binding (ΔH) and a number of binding sites (N). ITC data for the binding to one class of independent sites are readily modelled, see table 3.1. From the results of the modelling it is suggested that the total number of binding sites is reduced upon PEGylation.

Circular Dichroism

The secondary and tertiary structures of PEGylated BSA were investigated by far-UV and near-UV Circular Dichroism.
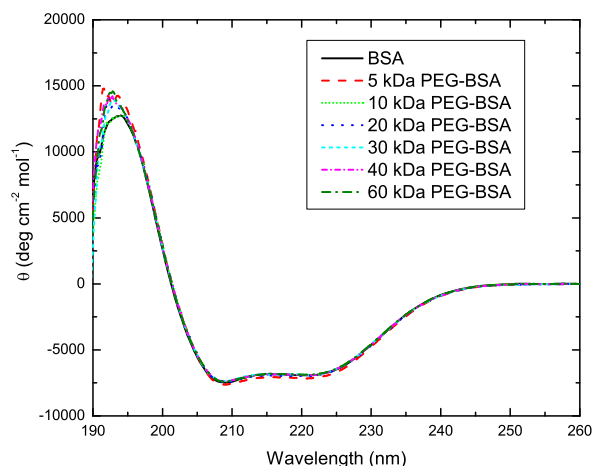
Figure 3.2: Far-UV CD scans of native BSA and 6 PEGylated BSA species. The secondary structure of BSA is maintained upon PEGylation. There is no significant difference between the secondary structure of native BSA and the secondary structure of the 6 PEGylated BSA compounds.

Figure 3.2 shows the far-UV CD scans for the native BSA and the 6 PEGylated BSA compounds. The scans show that the secondary structure of the PEGylated BSA compounds

lines up with the secondary structure of native BSA. Also, there is no significant change in the secondary structure between the various PEGylated BSA species.
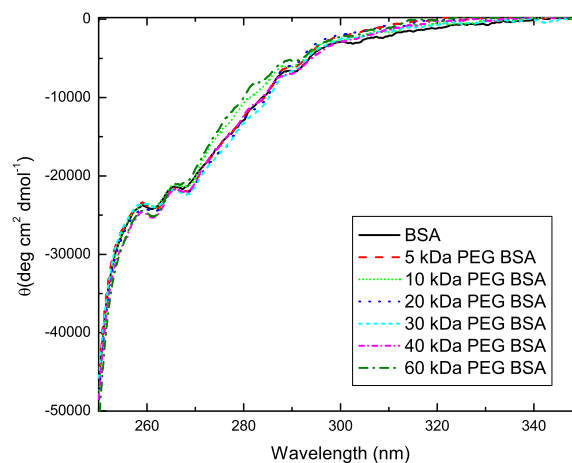

Figure 3.3: Near-UV CD scans of native BSA and 6 PEGylated BSA species. The tertiary structure of BSA and the 6 PEGylated BSA species is practically unaffected by PEGylation, and does not change with the attached PEG chain length. The small differences in the CD scans found around 270-300 nm for 10 kDa PEGylated BSA and 60 kDa PEGylated BSA compared to native BSA and the other PEGylated BSA compounds are probably due to very small changes in the mobility and nature (polarisability, H-bonding) of specific aromatic amino acids, most likely tyrosine.

Figure 3.3 shows the near-UV CD scans of the native BSA and the PEGylated species. The tertiary structure of BSA did not change upon PEGylation. There are small but non systematic differences in the overlaid spectra around 280 nm, are considered being insignificant.

Differential Scanning Calorimetry

The thermal stability of PEGylated BSA was investigated by DSC. The native BSA and the 6 PEGylated BSA compounds were measured separately, showing that the apparent unfolding temperature, T_m, was affected by PEGylation but not by the PEG molecular weight (figure 3.4). The apparent T_m was lower for the PEGylated BSA than for the native BSA, 82.5 ± 0.7 ℃ for native BSA and approximately 2 ℃ lower for the PEGylated BSA compounds (table 3.2). A DSC scan of pure 40 kDa PEG was also performed. This showed that the thermal transition of PEG was above 100 ℃ (data not shown). It is hence unlikely that the PEG polymer itself does contribute to the DSC thermogram in the investigated temperature range. Even though the native BSA thermogram does not

show clear signs of aggregation behaviour (exothermal signal), the native BSA solution was milk-white upon heating whereas the solutions of the PEGylated BSA compounds were transparent.
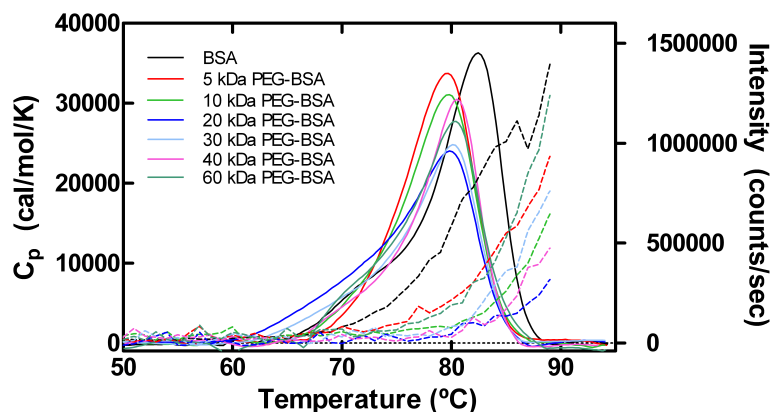

Figure 3.4: DSC scan and DLS measurements of BSA and the 6 PEGylated BSA species with various covalently attached linear PEGs. The DSC scans reveal that PEGylation slightly decreases the apparent unfolding temperature, T_m. The DLS measurements are plotted with the DSC scans, and as expected, the aggregation temperature, T_{agg}, increases with PEGylation.

Dynamic Light Scattering

The thermodynamic stabilities of BSA and PEGylated BSA were measured by DLS in 7 separate experiments. The intensity is plotted as a function of temperature in figure 3.4. The temperature of aggregation, T_{agg} is estimated by reading off the intersection of the intensity curves with three intensity threshold values $1 \cdot 10^6$, $2 \cdot 10^6$ and $3 \cdot 10^6$ counts/sec. As the temperature of aggregation change linearly with the intensity threshold values in the investigated intensity range, we choose the temperature at the lowest intensity $(1 \cdot 10^6)$ as the temperature of aggregation.

The raw DSC scan and the DLS intensity data are plotted in the same figure to illustrate the difference between the changes in the unfolding temperature and the aggregation temperature. The apparent unfolding temperature, the temperature of aggregation and the difference between these two characteristic temperatures are given in table 3.2. The temperatures listed in table 3.2 show that PEGylation increases the aggregation temperature of the protein relative to the unfolding temperature of the protein.

	T_m (°C)	ΔH (kJ/mol)	T_{agg} (°C)	(T_m-T_{agg})
BSA	82.5 ± 0.2	1250 ± 150	71	11.5 ± 0.2
5 kDa PEG BSA	79.7 ± 0.2	1000 ± 100	75	4.7 ± 0.2
10 kDa PEG BSA	79.8 ± 0.2	1060 ± 150	81	-1.2 ± 0.2
20 kDa PEG BSA	79.8 ± 0.2	1030 ± 100	82	-2.2 ± 0.2
30 kDa PEG BSA	80.1 ± 0.2	930 ± 130	81	-0.9 ± 0.2
40 kDa PEG BSA	80.5 ± 0.2	950 ± 150	82	-1.5 ± 0.2
60 kDa PEG BSA	80.4 ± 0.2	980 ± 100	77	3.4 ± 0.2

Table 3.2: Table 2. The apparent unfolding temperature, T_m, and the unfolding enthalpy (ΔH) measured by DSC, the aggregation temperature, T_{agg}, measured by DLS and the difference between T_m and T_{agg}.

3.4 Discussion

Most of the available literature on the effect of PEGylation on the structure, stability and function of proteins has only investigated one non-modified protein and one PEGylated protein, and these studies have focused on the effect of PEGylation [51, 93, 104]. This study expands the concepts of PEGylation by investigating the effect of varying the PEG chain length on the structure, stability and function of BSA.

The structural information obtained with far-UV CD scan show that the secondary structure of BSA is maintained upon PEGylation, and that the far-UV CD scan obtained in this work is in accordance with those reported in the literature previously [120]. In addition, the near-UV CD scans shows that the tertiary structure of BSA is maintained upon PEGylation. Both the secondary and tertiary structure of the various PEGylated BSA species does not change with PEG chain length. The small differences in the CD scans found around 270-300 nm for 10 kDa PEGylated BSA and 60 kDa PEGylated BSA compared to native BSA and the other PEGylated BSA compounds could be due to small changes in the properties (mobility, polarisability, H-bonding) of specific aromatic amino acids, most likely tyrosine. However, the overall tertiary structure of 10 kDa PEGylated BSA and 60 kDa PEGylated BSA is still considered to be essentially identical to that of the native BSA and the other PEGylated BSA compounds.

The thermal stability of BSA and PEGylated BSA was measured by DSC, and the unfolding temperature and related unfolding enthalpy are presented in Table 3.2. There is a range of unfolding temperatures of BSA reported in the literature, based on studies where the ionic strength, the pH or the concentration of anionic surfactants have been changed [121–124]. Our unfolding temperature values are in the high end of the range of those reported in the literature. The enthalpies are generally of the same order of magnitude as those obtained in the literature [122, 124]. The unfolding enthalpies are lower for the PEGylated BSA compounds than the native BSA, but the unfolding enthalpies are alike for all the PEGylated BSA compounds. The bimodal appearance of the DSC scans is especially pronounced for native BSA, and can be correlated to the domain structure of

BSA [124]. The PEGylated BSA compounds with the smaller PEGs attached (5 kDa to 30 kDa) does not seem to have this distinct bimodal appearance, however the peaks are broadened. The broadening of DSC peaks of BSA has been reported in the literature previously [121, 125, 126]. The PEG molecular weight dependence on the appearance of the DSC scan may be related the fact that the molecular weight of the attached PEG has different impacts on the stability of the two domains of BSA.

From the results presented in figure 3.4 it is evident that the apparent unfolding temperature, T_m, for native BSA is slightly lower than that of the PEGylated BSA species. Dhalluin et al. found a slight increase in T_m with PEGylation using interferon-alpha (2a) [91]. How PEGylation affects the apparent unfolding temperature of a certain protein depends on several factors including the degree of PEGylation, the location of the polymer chain, the buffer composition and the specific local environment [127]. A slight decrease in T_m with PEGylation may be found for some proteins, whereas a slight increase may be found for other proteins. The results obtained in this study also reveal that there is no difference in the thermal stability, measured by T_m, between a 5 kDa PEGylated BSA and a 60 kDa PEGylated BSA. Thus, a longer PEG chain length does not contribute more to the stability of the protein than a short PEG chain. Rather, it appears that the thermal stability is independent of the molecular weight of the attached PEG polymer.

In analogy to the effect of PEGylation on the apparent unfolding temperature, the temperature of aggregation, T_{agg}, depends on PEGylation but is relatively insensitive to the size of the attached PEG polymer. The data in table 3.2 shows that under the investigated conditions, aggregation can be detected about 11 °C below T_m for the unmodified protein. In this case T_{agg} practically coincides with the first endothermic deflection in the DSC signal in Fig 3.4. These observations suggest that the thermally unfolded form of (unmodified) BSA has a very poor colloidal stability and thus aggregates immediately upon its formation during heating. Aggregation of the PEGylated form of BSA begins at a temperature much closer to T_m when an appreciable fraction of the protein is denatured (c.f. Figure 3.4). This behaviour may be rationalized along the lines of the Lumry-Eyring model for irreversible protein denaturation [94] which stipulates that an irreversible transition (such as aggregation) is preceded by a reversible denaturation step.

$$N \underset{k_2}{\overset{k_1}{\rightleftharpoons}} D \overset{k_3}{\rightarrow} A \qquad K = \frac{k_1}{k_2}$$
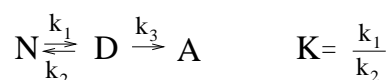
Figure 3.5: The Lumry Eyring model, N is the native protein, D is the denatured protein and A is the aggregated protein.

Thus we suggest that PEGylation of BSA slightly increases the equilibrium constant K (lowers T_m) but has a stronger, reducing effect on k_3, so that the aggregation of the denatured (D) is slowed down. This is illustrated by the difference between T_m and T_{agg} in table 3.2, where there is a large difference between T_m and T_{agg} for the unmodified BSA

but a only a small difference (positive or negative) between T_m and T_{agg} for the PEGylated BSA compounds. The general suppression of protein aggregation by PEG observed here is in accord with earlier reports [65, 95] and the suggestion that this is mainly due to changes in k_3 (and not K) has also been put forward before [65]. Steric hindrance of favourable peptide-peptide contacts appears to be a likely course for the effect of PEG on k_3, but the lack of a correlation of PEG size and T_{agg} suggests that other as of yet unidentified factors may be involved in the PEG induced increase of the colloidal stability.

The ligand binding properties of BSA were investigated with ITC. Previous studies of the binding of serum albumins have reported, that the thermodynamics and stoichiometry of binding fatty acids (FA) to BSA is similar to that of binding Sodium Dodecyl Sulphate (SDS) [99–101]. Because of the major experimental challenges in working with FA binding due to their insolubility, tendency to aggregate and adsorb to surfaces, we used the binding of a single sulfonic (instead of a carboxylic) acid anion to BSA. Sodium dodecyl sulphate, a sulfonic acid, forms stable micellar aggregates that are easily handled experimentally. The binding of SDS to BSA and PEGylated compounds of BSA reflects the functional properties of BSA so the effect of PEGylation on the function of BSA can be monitored. The type of binding sites and their thermodynamic characteristics such as the binding enthalpies, the binding constants and the number of binding sites are listed in table 3.1.The values obtained by modelling the binding of SDS to PEGylated BSA are similar to the low affinity binding site found for the native BSA. Compared with the shape of the actual enthalpogram in figure 3.1 this suggests that the PEGylated BSA molecule contains only one type of binding site. The number of binding sites, high affinity as well as low affinity, is slightly lower than reported previously [99, 119] but of the same order of magnitude. There is surprisingly little variation within the parameters characterising the low affinity sites of the 6 PEGylated BSA compounds. The function of PEGylated BSA seems to be the same whether a small PEG polymer chain or a long PEG polymer chain is attached. Crystallographic and thermodynamic investigations of the these sites on structurally similar serum albumin have revealed that the binding sites for negatively charged ligands with large acyl chains can be roughly divided into two classes: high affinity and low affinity, and that within each class the binding parameters are similar [99, 102, 103]. It has been suggested that the hydrophobic regions of PEG would interact with the hydrophobic clusters on the protein surface, resulting in a structure of the PEG-protein complex, where PEG is coiled on the protein surface [104]. This may explain the change in the binding properties of BSA upon PEGylation. The PEG polymer could compete with SDS for interaction sites on the protein surface and thus weaken SDS-BSA affinities, but control ITC experiments in which an 8 kDa PEG polymer was titrated to unmodified BSA failed to show direct binding (Fig. 3.1).

In the protein screening process that is often performed early in the protein drug development process, one of the goals is to find out whether certain protein modifications affect the structure, stability and function of a potential pharmaceutical protein. Biophysical characterisation screening tools often include techniques such as DLS, DSC and CD, all of which complement one another in determining possible changes to the structure, ki-

netic and thermodynamic stability of the protein. However, this study suggests that even though the protein appears to be structurally unaffected by PEGylation, its function is significantly altered. In fact, the high-affinity sites, which are the physiologically relevant [102, 128], appear to be completely inactivated by the PEGylation. Based on a comprehensive analysis of crystallographic data of HSA, it has previously been reported that only one of the 35 cysteines in HSA is not a part of an S-S bridge, and this residue is not close to any binding site [102, 119]. As BSA and HSA are structurally similar and comparable, and the distance from the cleavage in HSA, where most of the high affinity binding sites for SDS are found, to cysteine 34 is approximately 45 Å, it seems reasonable to assume that the cysteine 34 onto which the PEG is attached is not close to any of the binding site. For this reason the differences in the binding properties of BSA and PEGylated BSA cannot be explained by the PEG being located close to a binding site and in this way sterically hindering the binding of SDS to the high affinity sites of BSA.

3.5 Conclusion

BSA was monoPEGylated with 6 different linear PEG polymers ranging from 5 kDa to 60 kDa in molecular weight. The results from the CD scans suggested that the secondary and tertiary structure of BSA is unaltered upon PEGylation. From the DSC measurements it was evident that the thermodynamic stability of the protein is slightly decreased by the covalently attached PEG, but independent of the PEG molecular weight. The aggregation temperature, derived from DLS measurements, increases with PEGylation, but is independent of the size of the attached PEG. The binding of SDS to BSA and PEGylated BSA reveals that the function of BSA as a transport protein may be changed significantly when the protein is PEGylated. Of the two high-affinity binding sites and six low-affinity binding sites found on native BSA, only five of the low-affinity binding sites are retained on the PEGylated BSA species, and this change was found to be independent of the PEG chain length. Thus, PEGylation may leave a protein structurally unaffected but profoundly changed in terms of function.

Acknowledgements

56

4 The binding kinetics of PEGylated BSA

4.1 Introduction

Modification of pharmaceutical proteins with hydrophilic polymers such as poly-ethylene-glycol (PEGylation) is an established method for prolonging the circulatory half-life of proteins, reducing self-aggregation, increasing water solubility and decreasing antibody recognition, and it has been used successfully in several marketed proteins [50, 51]. Most of the benefits of PEGylated proteins reflect the properties of the PEG polymer itself [60]. The PEG polymer is heavily hydrated and consequently it has a large excluded volume which, among other things, inhibits the approach of other macromolecules, resulting in reduced immunogenicity and decreased antibody recognition [117]. Generally, the hydration of the PEG chain determines the overall hydrodynamic properties of a PEG bioconjugate [59], and the increased molecular size is one of the most important properties of a PEGylated protein, for example resulting in a prolonged circulation time due to low rates of clearance from the liver and kidney [117]. Other than increasing the hydrodynamic volume of the protein upon PEGylation, the conformation, physical properties and electrostatics of a PEG-conjugated protein may be altered compared with the unmodified protein [59]. Possible changes include conformational changes of both PEG and protein, altered binding properties resulting from changes in local pI, pKa, hydrophobicity and hydrophilicity of the protein. However, most studies report an unchanged secondary and tertiary structure [65, 88, 90], a retained thermodynamic stability [91] and an increased temperature of aggregation of the protein upon PEGylation [65], whereas the protein's biological activity is not necessarily preserved [49, 62, 65].

SPR has been widely used during the past decades to obtain detailed information on the binding properties of different biomolecular interactions [129–135]. SPR is mainly used to obtain detailed information about the binding kinetics and binding affinities of a variety of biomolecular interactions. The key advantage of SPR is the use of biosensors which allow real-time analysis of reactions without labelling requirements (radioactive or fluorescent). Fundamentally the SPR sensor consists of a thin metal film in contact with the fluid medium to be analysed. Light passes through the fluid and is reflected from the metal film. At specific wavelengths or angles a part of the incident light couples into a surface plasmon wave travelling along the interface of the fluid medium and the metal, resulting in a sharp attenuation in reflectivity. This is known as the surface plasmon effect. The wavelengths and angles of this occurrence depend strongly on the refractive index (RI) of the fluid

medium. SPR biosensors measure only relative changes in the molecular mass attached to the sensor surface from the beginning of the interaction being studied [136]. Despite the fact that SPR has been extensively used during the past decades investigations regarding the properties of PEGylated proteins by SPR are still a new discipline. However, a few studies have shown how the binding affinity determined by the association, dissociation and hence equilibrium constant changes as a protein is modified by PEGylation [96, 137]. The most common commercially available SPR-based biosensors are Biacore 2000 and 3000 systems, which are equipped with a four flow-cell fluidic system [136]. For this study a ProteOn™ XPR36 Protein Interaction Array System from Bio Rad was used. The instrument is characterised by having the capability of measuring 36 protein interactions in a single injection cycle [138].

Bovine Serum Albumin (BSA) is a transport protein with a molecular weight of 66400 Da [102]. BSA has one free sulfhydryl group, cysteine 34, which does not form a disulfide bond with another cysteine in the polypeptide backbone [86]. Furthermore, BSA binds several ligands including fatty acids, and it is possible to monitor the function of BSA in vitro with different binding assays. This makes BSA a suitable model protein when investigating the effect of protein PEGylation. Binding mPEG-maleimide (mPEG-MA) to the free cysteine of BSA ensures both mono-PEGylation and site-specific PEGylation.

We have investigated the effect of monoPEGylation with 6 linear PEG polymers ranging from 5 kDa to 60 kDa, providing us with a unique model system for studying the effect of PEG polymer chain length on the binding kinetics of BSA and PEGylated BSA. From the results presented in chapter 3 we concluded that the binding of SDS to BSA changed upon PEGylation but was independent of the molecular weight of the PEG chain. To further investigate the possible altered binding properties of BSA due to PEGylation, we have used Surface Plasmon Resonance (SPR) to measure the binding between anti-BSA and BSA or PEGylated BSA[1]. The purpose of the present study is to investigate how the binding of BSA and various PEGylated BSA (the analyte) species to immobilised anti-BSA (the ligand) changes with PEGylation as well as PEG molecular weight. Additionally BSA and the PEGylated BSA species are immobilised on the chip and anti-BSA is run over as an analyte. This makes it possible to compare two independent ways of measuring the binding between anti-BSA and BSA or PEGylated BSA.

Binding kinetics

The SPR detector is a continuous, real time detector, which makes it possible to estimate the kinetics of a given reaction. Consider the case where an immobilised protein (the ligand) will forma complex with the soluble counterpart (the analyte). In the case of a 1:1 reaction the complex-conformation rate can then be written as [139, 140]:

$$\frac{d[LA]}{dt} = k_a[L]_t[A]_t - k_d[LA]_t \tag{4.1}$$

---

[1] All experiments were carried out at University of Canterbury, New Zealand.

where k_a is the association rate constant, k_d is the dissociation rate constant. $[L]_t$ can be substituted by $[L]_0$-$[LA]_t$, where $[L]_0$ is the total concentration of ligands on the surface of the chip and $[LA]]_t$ is the concentration of complexes, and then

$$\frac{d[LA]}{dt} = k_a[A]_t([L]_0 - [LA]_t) - k_d[LA]_t \tag{4.2}$$

As the signal observed, R, will be proportional to the formation of the LA complex, and R_{max} will be proportional to the surface concentration of active ligands on the surface, equation 4.2 can be rewritten to:

$$\frac{dR}{dt} = k_a C_A (R_{max} - R) - k_d R \tag{4.3}$$

$$= k_a C_A R_{max} - (k_a C_A + k_d)R \tag{4.4}$$

Here $\frac{dR}{dt}$ is the formation rate of surface associated complexes and C_A is the constant concentration of analyte in the solution. Solving this differential equation gives:

$$R_t = \frac{k_a(C_A)R_{max}[1 - \exp(-C_A k_a + k_d)t]}{C_A k_a + k_d} \tag{4.5}$$

The concentration of analyte in the solution is, in this case, much larger than the concentration of immobilised ligand which is why it can be considered as a constant. R_{max} is the maximum signal, equivalent to surface concentration of ligand, $[L]_0$, if all the immobilised ligands have bound an analyte. (R_{max} - R_t) expresses the number of vacant analytes on the surface of the chip, expressed in response units. The SPR data in the present study are fitted to the Langmuir model, a simple 1:1 biomolecular interaction, which is the most common kinetic fit model used for SPR data analysis [138]. The Langmuir model is based on a scenario, where the reaction occurs between the ligand immobilized to the chip surface and the analyte that is flowed across it. As the analyte interacts with the ligand, a complex is formed following pseudo first-order kinetics. When the analyte is washed away from the chip, the two molecules dissociate. It is assumed that the binding is equivalent and independent for all binding sites, and that the reaction is not limited by mass transport.

SPR measurements

A SPR experiment consists primarily of 4 steps, immobilisation, association, dissociation and regeneration, three of these steps are shown on figure 4.1. In the immobilisation step the ligand is bound to the surface of the SPR chip, in the association step the analyte solution is flowing across the surface of the chip and binds to the immobilised ligand. In the dissociation step buffer is flowing across the surface of the chip, removing most of the bound analytes. The regeneration step 'cleans' the chip, removes excess analytes and primes the chip for the next experiment.
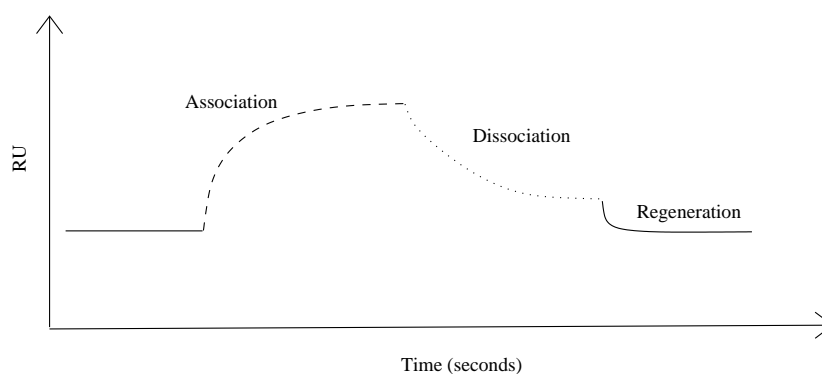
Figure 4.1: T sketch of the SPR response as a function of time. The association rate constant, k_a, is related to the association process, stippled line, and the dissociation rate constant, k_d, is related to the association process, dotted line. The regeneration step follows the dissociation.

All analysed samples were concomitant with the binding experiments injected onto an un-coated reference channel. The data were evaluated with the ProteOn™ software (version 2.1.0.36), applying the simple 1:1 Langmuir binding model. The obtained sensorgrams were group fitted over the whole concentration range as association and dissociation are considered being concentration independent. The association rate constants, k_a, the dissociation constants, k_d, and the maximum response, R_{max}, were determined for each sample. The equilibrium constants were then calculated from the association constant and the dissociation constant ($k_d/k_a=K_D$).

4.2   Materials and Methods

PEGylation reaction

Batch PEG grafting was carried out for each protein individually as described in section 3.2. Briefly, all solutions were made up in 10 mM phosphate buffered saline (PBS, Sigma, St. Louis, MO), at pH 7.4. Bovine serum albumin (98 % pure by SDS-PAGE) from bovine plasma (Gibco Invitrogen, NZ), was used without further purification. The maleimodo-reactants (Mono-methoxy poly (ethylene glycol) maleimido-propionamide) were of nominal molecular weights 5000, 10000, 20000, 30000, 40000 and 60000 Da, and were a kind gift from Dow Pharma, UK. 1.2 mole of solid mPEG-MA reagent was added per mole of protein to 5 mL of 20 mg/mL native bovine serum albumin and the protein solution was mixed with the PEG reagent and left stirring in an open 10 mL beaker at room temperature overnight. Samples were acidified with one drop of 0.1 M HCl to stop the reaction.

The samples, including a non-PEGylated native BSA sample as a control, were separated individually by ion exchange chromatography (IEC) using a HiPrep 16/10 QFF Anion Exchange column (Amersham Bioscience, Uppsala, Sweden), preparing the column first

with 5 column volumes (CV) of 10 mM PBS pH 7.4, 1M NaCl and then 5 CV of 10 mM
PBS pH 7.4. 5 mL samples were then injected onto the IEC column and the proteins
were eluted with a 15 CV linear gradient to 10 mM PBS, 1 M NaCl at 5 mL/min. The
protein elution profile was monitored by UV absorbance at 280 nm and collected in 2
mL fractions. Fractions were analysed by SDS-PAGE, and fractions containing >80 %
monoPEGylated BSA monomer, detected by SDS-PAGE, were pooled. These fractions
were then polished by injecting 6 mL samples onto a Size Exclusion Chromatography,
(SEC) HiPrep 16/60 Sephacryl S-200 column (Amersham Bioscience, Uppsala, Sweden),
with PBS running buffer at 1 mL/min. The protein elution profile was monitored by
UV absorbance and fractions containing >90 % monoPEGylated BSA monomer, as sub-
sequently detected by SDS-PAGE, were pooled. The purification was carried out on an
AKTAexplorer 10™ liquid chromatography system with an A-900 autosampler and de-
tected by a differential refractometer detector (model RID-10A from Shimadzu, Tokyo,
Japan). The chromatography system was operated using Unicorn software, version 4.0,
(Amersham Bioscience, Uppsala, Sweden). The purity of the PEGylated BSA solutions
was investigated by gel electrophoresis. SDS-PAGE analysis was carried out using a 12 %
Bis-Tris gel from Invitrogen. The gels were loaded with an average of 5 μg (10 μL load
volume) per well and run at 120 mA constant current per gel. The running buffer was
MES running buffer. The gel was washed in 150 mL 0.1 M perchloric acid for 15 minutes
until 40 mL 5 % barium chloride solution and 15 mL 0.1 M iodine solution were added to
detect protein bands containing PEG compounds, as described in [141]. After discolour-
ing in water, the gel was coloured with Coomassie blue. From figure 4.2 it is evident that
PEGylated proteins are not behaving like non-PEGylated proteins when analysed by gel
electrophoresis. It would be natural to anticipate that a 66 kDa protein with a 20 kDa
PEG attached would show a band around 86 kDa, but due to the high hydration of the
PEG, the 20 kDa PEGylated 66 kDa protein shows a band at 106 kDa (fig. 4.2).

The PEG-staining gel technique is based on the complex formation between PEG and
barium iodide, and the PEG-stained gel (4.2b) reveal that only lane 2-5 contain PEG-
compounds. It has previously been shown, that PEG binds to SDS micelles [142] and that
PEGylation decreases the mobility of the protein [141, 143]. For this reason the molecular
weight of a PEGylated protein on a SDS gel will not correspond to the actual molecular
weight of the PEGylated protein. Due to the low mobility of the PEGylated protein, the
location of a PEGylated protein on a SDS gel corresponds to the molecular weight of the
protein added twice the molecular weight of the attached PEG polymer.

BSA or PEGylated BSA as analyte

The GLC SPR chip was activated by a mixture of 130 μL 4 M 1-ethyl-3-(3-dimethylamino-
propyl) carbodiimide hydrochloride (EDAC) and 130 μL 1 M N-hydroxysulfosuccinimide
(NHS). Polyclonal anti-BSA molecules were immobilised on the chip at a flow rate of
30 μL/min and a contact time of 300 seconds. The remaining carboxyl groups were
deactivated by ethanol amine hydrochloride. Measurements were carried out at 25 °C,
using a flow rate of 100 μL/min with an association phase of 60 sec after injection, followed
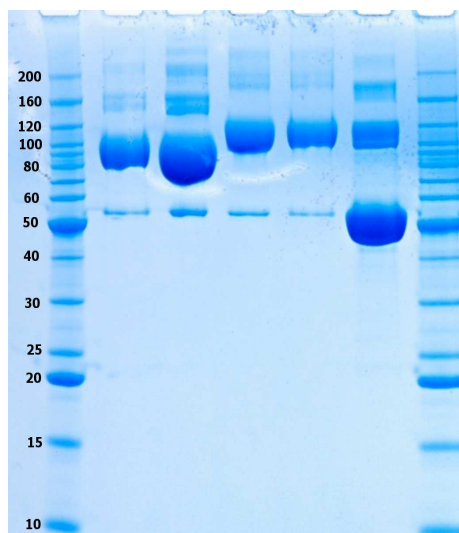
(a) SDS PAGE of PEGylated BSA. The numbers on the left side are the molecular marker in kDa.
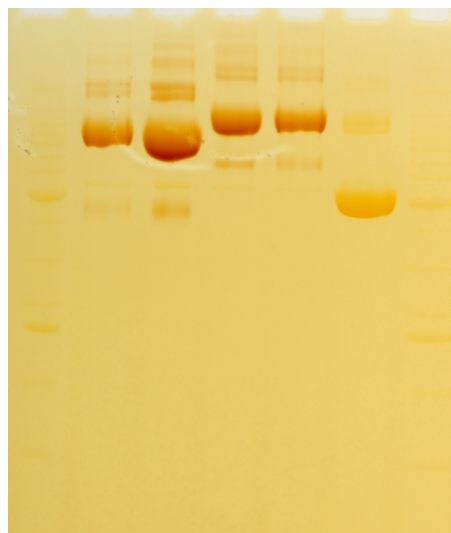
(b)   A so-called PEG stained gel.   The gel is stained with iodide as described in [141].The bonds refer to the 20 kDa PEGylated BSA and the 30 kDa PEGylated BSA, respectively. The vague colored band corresponding to the native BSA is some minor, non-specific staining of protein by the iodide.

Figure 4.2:
Lane 1 and 7, bench mark protein ladder.
Lane 2 and 3, 20 kDa PEGylated BSA.
Lane 4 and 5, 30 kDa PEGylated BSA.
Lane 6 native BSA.
The location of the PEGylated species on the gel reveals that a 20 kDa PEGylated BSA is located at $66+2 \cdot 20$ ~106 kDa and a 30 kDa PEGylated BSA is located at $66+2 \cdot 30$ ~126 kDa. Analysis of the gel on figure 4.2a reveals a ~5 % of native BSA within the PEGylated BSA samples after purification. The purity of 5 kDa, 10 kDa, 40 kDa and 60 kDa are similar (data not shown).

by a dissociation phase of 600 sec. The proteins and antibodies were diluted in PBS buffer, filtered, and the BSA and PEGylated BSA solutions were injected at concentrations between 0.01 mg/mL and 0.625 μg/mL. The binding process is illustrated in figure 4.3.
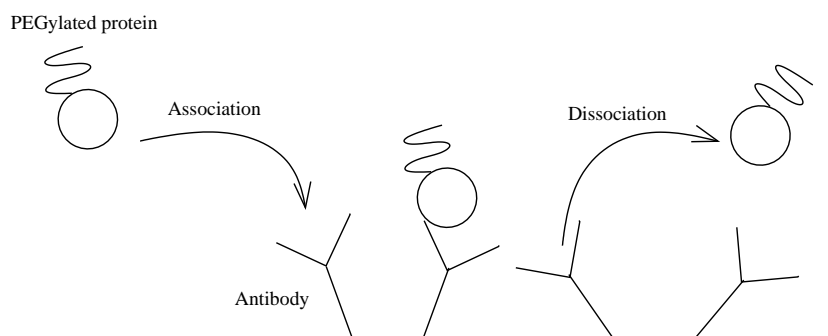

Figure 4.3: The binding of a PEGylated BSA molecule to the immobilised anti-BSA (Y-shaped).

Anti-BSA as analyte

The GLC SPR chip was activated by a mixture of 130 μL 0.4 mM 1-ethyl-3-(3-dimethylamino-propyl)carbodiimide hydrochloride (EDAC) and 130 μL 0.1 mM N-hydroxysulfosuccinimide (NHS). BSA and the various PEGylated BSA species were immobilised on the chip in different channels at a flow rate of 30 μL/min and a contact time of 867 seconds. The remaining carboxyl groups were deactivated by ethanol amine hydrochloride. Measurements were carried out at 25 °C, using a flow rate of 50 μL/min with an association phase of 500 sec after injection, followed by a dissociation phase of 600 sec. The proteins and antibodies were diluted in PBS buffer, filtered, and the antibody solutions were injected at concentrations between 0.025 mg/mL and 1.56 μg/mL. The binding process is illustrated in figure 4.4.

Figure 4.4: The binding of anti-BSA (Y-shaped) to the immobilised PEGylated BSA molecule.

For this instrument the working ranges are $3 \cdot 10^3$-$3 \cdot 10^6$ $M^{-1}s^{-1}$ for k_a, $5 \cdot 10^{-5}$-$6 \cdot 10^{-1}$ s^{-1} for k_d and $2 \cdot 10^{-4}$- $1.6 \cdot 10^{-11}$ M for K_D [138]. For subtraction of bulk effects caused by changes in the buffer composition or nonspecific binding, a subtraction of a reference channel is performed.

4.3 Results

BSA or PEGylated BSA as analyte

The SPR response of the binding of BSA or PEGylated BSA to the immobilised anti-BSA is found in figure 4.5. From the data shown in this figure it is evident, that the RU from the binding of the unmodified BSA is much larger than that of the PEGylated BSA compounds. The RU from the binding of the PEGylated BSA compounds to anti-BSA appears to be independent of the molecular weight of the attached PEG.
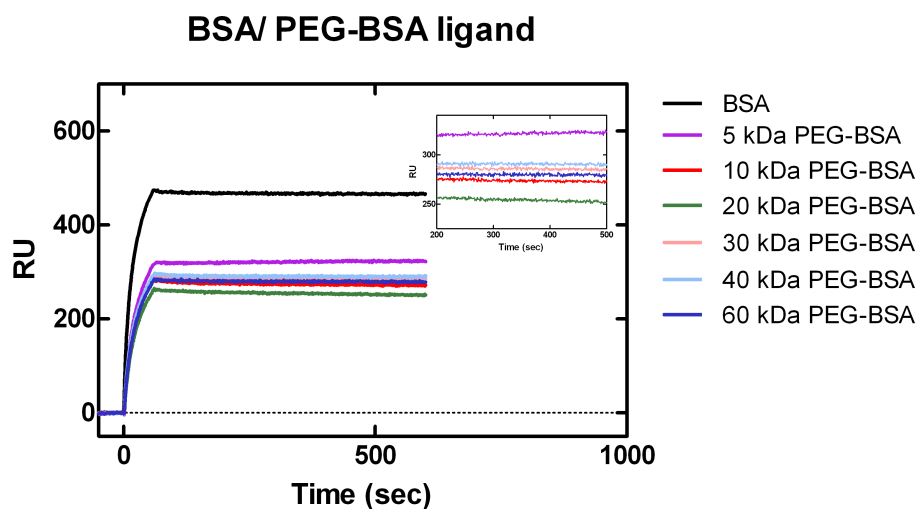

Figure 4.5: The raw data for the association and dissociation of BSA and PEGylated BSA to immobilised anti-BSA.

The results shown in figure 4.5 were modelled by using the Langmuir 1:1 model and a family of curves at different, known concentrations for the same species. One curve from each of those families is shown in figure 4.5. From the modelling the association rate constants of BSA and the PEGylated BSA compounds to the immobilised anti-BSA are found, see figure 4.6a. The association rate constants of BSA and PEGylated BSA to anti-BSA are of the same order of magnitude, but k_a for 5 kDa PEGylated BSA is lower than that of the native protein but k_a increases almost linearly with the molecular weight of the attached PEG. The dissociation rate constants of BSA and the PEGylated BSA

compounds from anti-BSA are shown in figure 4.6b. Those constants are also found by using the Langmuir 1:1 model and a family of curves at different, known concentrations for the same species. The dissociation rate constants are very low, especially k_d for 40 kDa PEG-BSA and 60 kDa PEG-BSA, which are outside the detection ranges given on page 64. However, generally the k_d values seem to depend on PEGylation and on the molecular weight of the attached PEG, and the rates of dissociation are of the same order of magnitude. The equilibrium constants, $K_D = k_d/k_a$, as a function of PEG molecular weight are plotted in figure 4.6c. The equilibrium constant for the binding of BSA or PEGylated BSA to immobilised anti-BSA illustrate the same tendency as the dissociation constant; a slight dependence on PEGylation and on the molecular weight of the attached PEG.
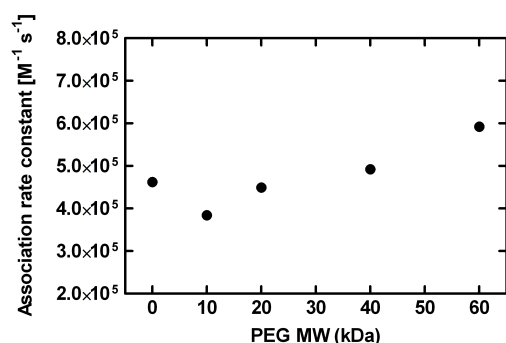
(a) The association rate constants as a function of PEG molecular weight.
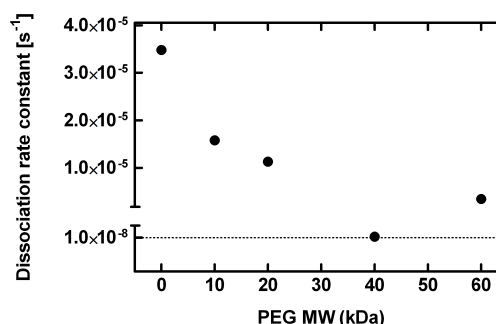
(b) The dissociation rate constant as a function of PEG molecular weight.
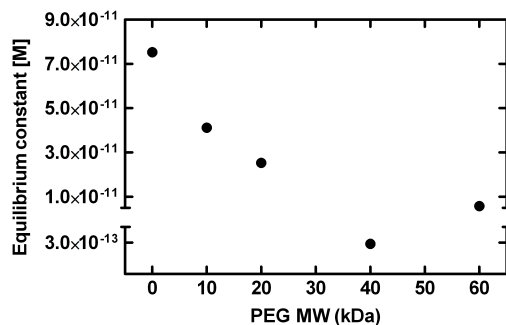
(c) The equilibrium constant as a function of PEG molecular weight.

Figure 4.6: Association rate constants, dissociation rate constants and the resulting equilibrium constant of the binding of BSA or PEGylated BSA to the immobilised anti-BSA as a function of the molecular weight of the PEG polymer attached to the immobilised BSA molecules. The k_a, k_d and K_D of unmodified BSA to immobilised anti-BSA is located at PEG molecular weight zero. The error bars are too small to be shown.

The results are summarised in table 4.1.

Analyte	k_a (M^{-1}s^{-1})	k_d (s^{-1})	K_D (M)
BSA	$4.6 \cdot 10^5 \pm 3.2 \cdot 10^3$	$3.5 \cdot 10^{-5} \pm 7.7 \cdot 10^{-7}$	$7.5 \cdot 10^{-11}$
10 kDa PEG-BSA	$3.8 \cdot 10^5 \pm 2.4 \cdot 10^3$	$1.6 \cdot 10^{-5} \pm 6.7 \cdot 10^{-7}$	$4.1 \cdot 10^{-11}$
20 kDa PEG-BSA	$4.5 \cdot 10^5 \pm 2.8 \cdot 10^3$	$1.1 \cdot 10^{-5} \pm 6.8 \cdot 10^{-7}$	$2.5 \cdot 10^{-11}$
40 kDa PEG-BSA	$4.9 \cdot 10^5 \pm 3.3 \cdot 10^3$	$1.4 \cdot 10^{-7} \pm 6.9 \cdot 10^{-7}$	$2.9 \cdot 10^{-13}$
60 kDa PEG-BSA	$5.9 \cdot 10^5 \pm 4.3 \cdot 10^3$	$3.5 \cdot 10^{-6} \pm 7.4 \cdot 10^{-7}$	$5.8 \cdot 10^{-12}$

Table 4.1:   The association rate constant, the dissociation rate constant and the equilibrium constant of the binding of BSA and PEGylated BSA compounds to immobilised anti-BSA.

Anti-BSA as analyte

The raw SPR data for the binding of anti-BSA to immobilised BSA or PEGylated BSA compounds are found in figure 4.7.
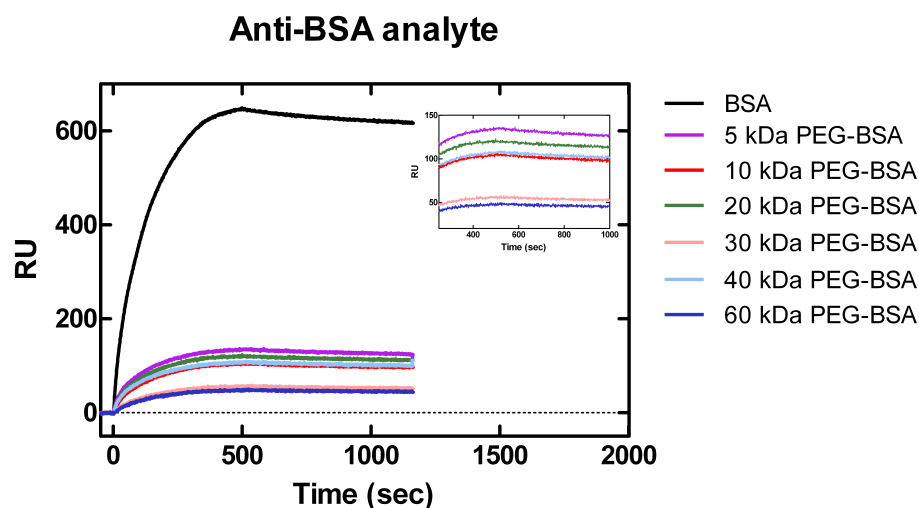
Figure 4.7: The raw SPR data for the association and dissociation of anti-BSA to tethered BSA or PEGylated BSA. The insert shows the order of the PEGylated BSA compounds.

The SPR response is much higher for the binding of anti-BSA to tethered BSA compared to the binding to PEG-BSA. The SPR data are fitted to the 1:1 binding model, and the fitting results for two selected data set are shown in figure 4.8, and from the results it is evident that the model parameters fits the SPR data quite well.

Figure 4.8: The fitted data for the binding of anti-BSA to BSA and 30 kDa PEGylated BSA. The other experiments are fitted in the same manner and the fit are of similar quality as those shown.
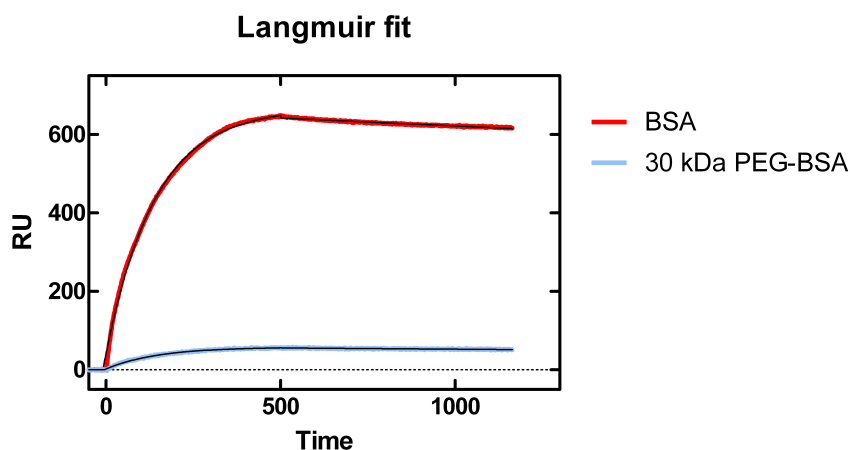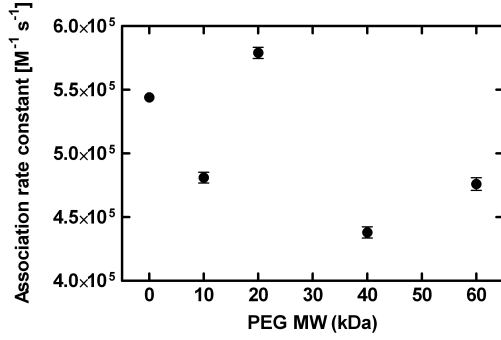
From the Langmuir fitting model, the association rate constants of anti-BSA to the immobilised BSA and PEGylated BSA compounds are found, and the association rate constants are plotted as a function of the PEG molecular weight in figure 4.9a. As with the reversed assay orientation experiment, the dissociation rate constants of anti-BSA to BSA and its PEGylated compounds appear to be independent of PEGylation and molecular weight of the PEG polymer, see figure 4.9b. The dissociation rate constants depends slightly on PEGylation, but all the values are of the same order of magnitude. Again, there appears to be no dependence on the molecular weight of the attached PEG. The equilibrium constants for the binding of anti-BSA to the immobilised BSA or PEGylated BSA compounds reflect the tendency of the dissociation constants, and seems to depend slightly on whether the protein is PEGylated or not, but it does not seem to depend on the molecular weight of the attached PEG polymer, see figure 4.9c.
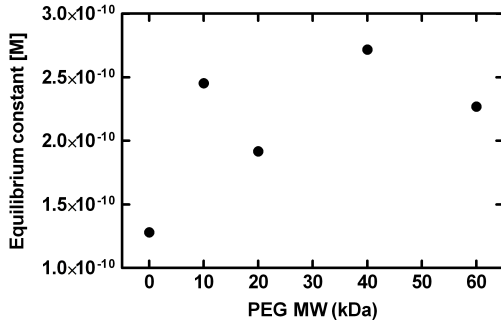
The results are summarised in table 4.2.

(a) The association rate constants as a function of PEG molecular weight.
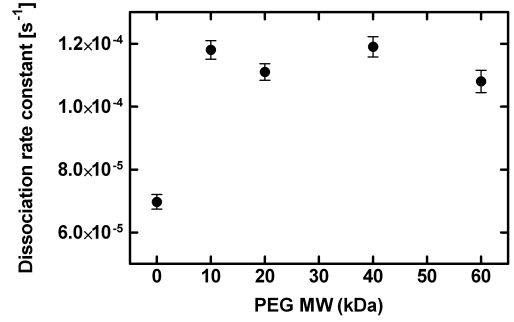
(b) The dissociation rate constant as a function of PEG molecular weight.

(c) The equilibrium constant as a function of PEG molecular weight.

Figure 4.9: Association rate constants, dissociation rate constants and the resulting equilibrium constant of the binding of anti-BSA to the immobilised BSA and PEGylated BSA as a function of the molecular weight of the PEG polymer attached to the immobilised BSA molecules. The k_a, k_d and K_D of anti-BSA to immobilised unmodified BSA is located at PEG molecular weight zero. The error bars are too small to be shown.

Ligand	k_a (M^{-1} s^{-1})	k_d (s^{-1})	K_D (M)
BSA	$5.4 \cdot 10^5 \pm 3.8 \cdot 10^3$	$7.0 \cdot 10^{-5} \pm 2.3 \cdot 10^{-6}$	$1.3 \cdot 10^{-10}$
10 kDa PEG-BSA	$4.8 \cdot 10^5 \pm 4.2 \cdot 10^3$	$1.2 \cdot 10^{-4} \pm 2.9 \cdot 10^{-6}$	$2.5 \cdot 10^{-10}$
20 kDa PEG-BSA	$5.8 \cdot 10^5 \pm 4.4 \cdot 10^3$	$1.1 \cdot 10^{-4} \pm 2.7 \cdot 10^{-6}$	$1.9 \cdot 10^{-10}$
40 kDa PEG-BSA	$4.4 \cdot 10^5 \pm 4.4 \cdot 10^3$	$1.2 \cdot 10^{-4} \pm 3.3 \cdot 10^{-6}$	$2.7 \cdot 10^{-10}$
60 kDa PEG-BSA	$4.8 \cdot 10^5 \pm 5.0 \cdot 10^3$	$1.0 \cdot 10^{-4} \pm 3.6 \cdot 10^{-6}$	$2.3 \cdot 10^{-10}$

Table 4.2: The association rate constant, the dissociation rate constant and the equilibrium constant of the binding of anti-BSA to the immobilised BSA and PEGylated BSA compounds.

4.4 Discussion

The binding kinetics of BSA and PEGylated BSA to anti-BSA was investigated using SPR with two identical but reversed assay orientations as illustrated in figure 4.3 and figure 4.4. The study was intended to provide knowledge on possible changes in the binding between BSA and anti-BSA, including information on how the association rate constant, the dissociation rate constant and the equilibrium constant might change with PEGylation and with the molecular mass of the attached PEG polymer. The association constant is describing how fast the analyte-ligand complex is formed, whereas the dissociation constant is describing how fast the formed complex is broken. Both constants can be affected by the mass transfer (or transport) effects. However if the flow rate across the SPR chip is sufficiently high, this effect can be minimised. Several experiments with varying flow rates were conducted and no differences were found in either the association or the dissociation constants (data not shown).

The SPR response to the binding of BSA or PEGylated BSA to anti-BSA is depending significantly on PEGylation, and it applies to both assay orientations that the binding between anti-BSA and unmodified BSA results in the largest SPR response compared to the binding between anti-BSA and the PEGylated BSA compounds. The SPR response seems to be independent on the molecular weight of the grafted PEG moiety. This is surprising as we expected using a PEGylated BSA with a high molecular weight PEG would lead to a higher response due to the higher total molecular weight of the PEG-protein complex. However the lower SPR response from both experiments could be due to a lower number of interactions between PEGylated BSA and anti-BSA compared to unmodified BSA and anti-BSA. The anti-BSA used is polyclonal, and conclusions regarding binding of anti-BSA to specific epitopes on BSA and possible steric hindrance from the attached PEG cannot be drawn. This problem could be solved by using a monoclonal antibody but we did not succeed in finding one commercially available. However for the BSA or PEGylated BSA ligand experiment an explanation of the lower RU for the binding of anti-BSA to the PEGylated BSA could be found in a lower number of immobilised PEG-protein molecules. The latter hypothesis is further developed in appendix B, where a model of the conformation of a PEGylated BSA molecule on the SPR chip is put forward.

From the fitting results obtained in this study it appears as though the association rate constants are independent of PEGylation and also independent of the molecular weight of the attached PEG polymer. The complex formation between anti-BSA and BSA or PEGylated BSA happens at the same rate regardless of which protein is ligand and which serves as analyte. The association rate constants are up to a factor 100 higher than similar studies of the binding of PEGylated proteins reported in the literature [66, 96]. Yang et al. [66] found association rate constants from $1.0 \cdot 10^3$-$4.6 \cdot 10^4$ M^{-1} s^{-1} and Kubetzko et al. [96] found k_a values from $6.1 \cdot 10^4$-$9.8 \cdot 10^5$ M^{-1} s^{-1}. This could indicate that the binding between anti-BSA and BSA is particularly fast. It is noticeable that the association rate constants are not affected by PEGylation. We expected using a PEGylated BSA with a high molecular weight PEG would lead to a slower binding (lower k_a) due to more steric hindrance. But even when attaching a PEG polymer of similar molecular weight as the

protein, there appears to be no difference in the association between BSA or PEGylated BSA and anti-BSA.

While there does not seem to be any change in the association with PEGylation or with assay orientation and hence the initial binding itself, the dissociation process appears to give a somewhat different picture. From the raw SPR data in figure 4.5 and figure 4.7 it is evident that the dissociation curve is nearly straight, indicating a very slow dissociation. Even though the data fit on figure 4.8 show that the Langmuir model fits nicely, the actual values for k_d for both experiments are hard to interpret. The interpretation of the value of the dissociation constant and the way it changes with PEGylation and PEG molecular weight should be done carefully and is not unambiguous. In general our k_d results are approximately lower than those obtained in the two comparable studies of the dissociation of PEGylated proteins from immobilised antibodies [66, 96]. Here Yang et al. [66] found dissociation rate constants from $2.6 \cdot 10^{-4}$ to $6.8 \cdot 10^{-4}$ s^{-1} and Kubetzko et al. [96] found k_d values from $2.6 \cdot 10^{-5}$ to $5.0 \cdot 10^{-5}$ s^{-1}. The dissociation rate constants describing the dissociation of PEGylated BSA from the immobilised anti-BSA are outside the measurable range of the instrument, which in itself indicate that the interpretations of the modelling results can only be guiding. Still, overall the dissociation rate constants obtained in our experiments are of similar values and the dissociation rate constants do not appear to be affected significantly by the orientation of the assay, by PEGylation or by the molecular weight of the attached PEG polymer.

The equilibrium dissociation constant, K_D, calculated from k_d/k_a, is the inverse of the binding constant, and can for this reason be used as a measure for the binding strength; a strong binding equals a low equilibrium constant, whereas a weak binding equals a higher equilibrium constant. The equilibrium dissociation results reported in this study are subject to uncertainty, as K_D is calculated from k_d. However from the K_D results summarised in table 4.1 and table 4.2 it is seen that the obtained equilibrium dissociation constants are of the same order of magnitude for all interactions. Hence PEGylation, molecular weight of the grafted PEG moiety and orientation of the assay do not seem to influence the binding kinetics of the current study significantly.

To our knowledge there are only a few comparable experiments in the literature, where the binding between antibodies and PEGylated proteins have been measured with SPR [66, 67, 96]. In two of these studies ([66, 96]) the authors refrain from commenting on the large reduction in SPR response with PEGylation, which we have also observed. We have investigated whether this observation could have to do with the difference between the refractive index of the BSA and the PEGylated BSA solutions and have treated more closely in appendix C. The authors mostly reflect on the variations in the association and dissociation rate constants, and they all observe that the association rate constant is reduced upon PEGylation, but the dissociation rate constant is practically independent of PEGylation. Briefly, Yang et al. [66] report SPR studies on single-chain antibodies and 3 PEGylated compounds hereof with 5 kDa, 20 kDa and 40 kDa PEG polymers attached. Yang et al. report a trend toward slower association rate constants with increasing mass of the attached PEG polymer, whereas the dissociation rate constants of the PEGylated

species did not differ significantly from the unmodified protein to the PEGylated compounds. They argue that the association is altered due to the physical hindrance by the bulky and mobile PEG moiety, and that this hindrance does not affect the dissociation rate constants. Kubetzko et al. [96] report SPR studies on site-specifically 20 kDa PEGylated variants of anti-p185(HER-2) antibody fragments, and they have experimentally determined, that the observed association rate constants of the PEGylated monomer are 5.4-fold slower than that of the unmodified monomer, led to approximately a 5-fold reduction in apparent affinity. Kubetzko et al. conclude that neither a reduction in the function antibody concentration nor a slower diffusion seems to be responsible for the decrease in the observed association rate constants. Kubetzko et al. argue that it appears to be a combination of intramolecular and intermolecular blocking mechanisms, which cause the alteration in the kinetic and equilibrium binding of the PEGylated proteins. Clark et al. [67] have investigated a 5 kDa PEGylated derivatives of human growth hormone (hGH), and report that increasing the level of PEG modification linearly reduced the affinity of hGH for its receptor. Clark et al. measured a relative decrease in binding affinity and association rate constants and a relative increase in dissociation rate constants by comparing the unmodified hGH to the PEGylated compound.

There are examples in the literature of measurements of the binding of BSA to anti-BSA including work done by Kausaite et al. [140] and Chiem and Harrison [144]. Kausaite et al. did SPR measurements and Chiem and Harrison did affinity capillary electrophoresis measurements with monoclonal anti-BSA. Both equilibrium constants are larger than the ones obtained in this study, see table 4.3.

Sample	k_a (M^{-1} s^{-1})	k_d (s^{-1})	K_D (M)
BSA analyte			
BSA	$4.6 \cdot 10^5 \pm 3.2 \cdot 10^3$	$3.5 \cdot 10^{-5} \pm 7.7 \cdot 10^{-7}$	$7.5 \cdot 10^{-11}$
BSA [140]	$9.63 \cdot 10^3$	$7.85 \cdot 10^{-3}$	$8.2 \cdot 10^{-7}$
Anti-BSA analyte			
BSA	$5.4 \cdot 10^5 \pm 3.8 \cdot 10^3$	$7.0 \cdot 10^{-5} \pm 2.3 \cdot 10^{-6}$	$1.3 \cdot 10^{-10}$
BSA [144]			$2.68 \cdot 10^{-8}$

Table 4.3: Association rate constants and dissociation rate constants for the binding of BSA to anti-BSA.

These differences may be explained by the fact that Kausaite et al. and Chiem and Harrison have used other anti-BSA antibodies than we have. Also our equilibrium constants are based on the dissociation rate constants obtained by Langmuir modelling, which were very slow and with high deviations. The inverse of the equilibrium constant, the binding constant, can be found by the use of ITC. Studies have shown that binding constants obtained by ITC are comparable in size to those obtained by SPR [145]. However, measuring the binding between anti-BSA and BSA/PEGylated BSA with ITC was beyond the scope of

this particular study.

4.5   Conclusion

The binding of BSA and PEGylated BSA to anti-BSA was measured by SPR using two similar, but reversed orientation assays. The SPR response was fitted using 1:1 biomolecular interaction model, yielding the association rate constant, the dissociation rate constant and the equilibrium dissociation constant of the binding reaction. The SPR response was markedly affected by PEGylation, and the response decreased significantly when reflecting the binding between anti-BSA and PEGylated BSA as compared to the anti-BSA/BSA binding. From the present study it is concluded, that the association rate constants are unaffected by PEGylation, molecular weight of the attached PEG polymer as well as assay orientation. These k_a results are not in accordance with those previously reported in the literature and might be explained by the use of a polyclonal antibody. From SPR response it was evident, that the dissociation rate constants were very low, and the subsequent modelling revealed that K_d in some of the experiment were too low for the instrument to model. But overall k_d appeared to be slightly depending on PEGylation, but independent of the molecular weight of the attached PEG polymer and of the orientation of the assay. The equilibrium dissociation constant reflected the variations in the dissociation rate constant, and was also slightly dependent on PEGylation, but unaffected by the molecular weight of the PEG polymer as well as the assay orientation.

5 Biophysical Characterisation of GlycoPEGylated human rFVIIa

Bitten Plesner[a,b], Peter Westh[a], Anders D. Nielsen[b,†]
[a]Department of Science, Roskilde University, P.O. Box 260, Universitetsvej 1, DK-4000 Roskilde, Denmark
[b]Novo Nordisk A/S, Novo Nordisk Park, DK-2760 Maaloev, Denmark

[†]Corresponding author. Tel.: +45 30 79 65 75; fax: +45 44 43 40 73
Email address: ADNi@novonordisk.com (A. D. Nielsen).

Abstract

The effects of GlycoPEGylation on the structural, kinetic and thermal stability of recombinant human rFVIIa were investigated using rFVIIa and linear 10 kDa and branched 40 kDa GlycoPEGylated recombinant human FVIIa derivatives. The secondary and tertiary structure of rFVIIa measured by Circular Dichroism (CD) was maintained upon PEGylation. In contrast, the thermal and kinetic stability of rFVIIa was affected by GlycoPEGylation, as the apparent unfolding temperature T_m measured by Differential Scanning Calorimetry (DSC) and the temperature of aggregation, T_{agg}, measured by Light Scattering (LS) both increased with GlycoPEGylation. Both T_m and T_{agg} were independent of the molecular weight and the shape of the PEG chain. From the present biophysical characterisation it is concluded that after GlycoPEGylation, rFVIIa appears to be unaffected structurally (secondary and tertiary structure), slightly stabilised thermally (unfolding temperature) and stabilised kinetically (temperature of aggregation).

Keywords: GlycoPEGylation, rFVIIa, Circular Dichroism, Differential Scanning Calorimetry, Light Scattering, stability.

5.1 Introduction

Coagulation factor VIIa (FVIIa) is a trypsin-like serine protease, which in the presence of calcium initiates the blood coagulation when associated with its cofactor tissue factor (TF) which is exposed upon vascular injury [146, 147]. TF-bound FVIIa activates factor IX and factor X resulting in a burst of thrombin, fibrin deposition and the formation of a

haemostatic plug on the surface of activated platelets [146]. Deficiencies in the coagulation system due to partial or complete deficiency of FVIII or FIX, haemophilia A or haemophilia B respectively can lead to severe morbidity or mortality if the bleeding is left untreated.

A safe and efficient way to prevent bleeds and joint destruction in haemophilia is pro-phylactically by dosing factor (F) FVIII or FIX 2-4 times weekly [148], and recent stud-ies have shown that prophylactic treatment with rFVIIa (NovoSeven®) of haemophilia patients with inhibitors reduces the frequency of bleedings significantly as compared to conventional on-demand haemostatic therapy [149]. However rFVIIa has a short circula-tion time (2-4 hours in humans), and it is assumed that rFVIIa should be administered daily if used for long-term prevention [149, 150]. Hence, development of rFVIIa deriva-tives with longer circulation time could result in both fewer administrations and better patience compliance. Modification of pharmaceutical proteins with hydrophilic polymers such as poly-ethylene-glycol (PEGylation) is an established method for prolonging circu-latory half-life of proteins, reducing self-aggregation, increase water solubility and increase stability [82, 117]. PEGylation has been used successfully in several marketed proteins including Pegasys® (40 kDa PEG Interferon alpha-2a,Roche), Oncaspar® (5 kDa PEG-L-aspariginase, Enzon), Cimzia® (40 kDa PEG Anti-TNFα, UCB Pharma) and Neulasta® (20 kDa PEG G-CSF, AMGEN) [50–52]. Due to the risk of losing activity of FVIIa because of the numerous interactions with the cell surface, TF, FIX and FX there is a limitation in the unspecific chemical modification of this protein. For this reason a novel strategy for site-directed PEGylation using glycosyltransferases to attach PEG to glycan residues, the enzyme based GlycoPEGylation™ technology, is used to covalently attach either a linear 10 kDa or a branched 40 kDa PEG polymer to rFVIIa. The site of PEG attachment to rFVIIa is demonstrated to be one of the two N-linked glycans of rFVIIa (Asn145 or Asn322) located on the light chain and heavy chain, respectively [64].

The most important property of a PEGylated protein is the increased molecular size re-sulting form the large hydrodynamic volume of the PEG [61]. The underlying mechanisms for the effect of PEG is not fully understood, but it is evident that the hydrodynamic ra-dius is significantly increased by PEG leading to reduced renal clearance, especially of smaller proteins [50, 63]. Most of the benefits of PEGylated proteins reflect the properties of the PEG polymer itself [60]. The PEG polymer is heavily hydrated and consequently it has a large excluded volume which among other things inhibits the approach of another molecule, this could in theory result in reduced immunogenicity and decreased antibody recognition [82, 151]. The favourable properties as postponed or prevented aggregation and thermal stabilisation are caused by the heavily hydrated PEG polymer, and the prop-erties of the PEG polymer are transferred to the PEGylated compounds [59]. Favourable pharmacokinetic and pharmacodynamic profiles are also a consequence of the improved hydrodynamic properties [82]. Other than increasing the hydrodynamic volume of the protein upon PEGylation, the conformation, physical properties and electrostatics of a PEG-conjugated protein may be altered compared with the unmodified protein [59], and the protein's biological activity is not necessarily preserved [49, 62, 65]. However most studies report an unchanged secondary and tertiary structure [65, 88, 90, 152, 153], an

increased thermal stability [91] and an increased temperature of aggregation [65, 152] of the protein upon PEGylation. Studies regarding the stability, both thermal and structural, as well as the bioactivity of the protein are among the most fundamental when developing pharmaceutical proteins and the ideal pharmaceutical protein should have a long shelf-life and a high bioavailability. Also, the physical stability of a pharmaceutical protein has a significant impact on the ability to design a suitable liquid protein drug, as insoluble aggregates can increase immunogenic responses and are not biologically active. We study the effect of GlycoPEGylation on the thermal, kinetic and structural stability of rFVIIa with one linear 10 kDa and one branched 40 kDa PEG polymer. This provides us with a relevant pharmaceutical model system for investigating the biophysical effects of PEGylation. Biophysical characterisation tools, including Circular Dichroism (CD), Differential Scanning Calorimetry (DSC) and Light Scattering (LS), were used to study possible changes in the secondary and tertiary structure as well as the thermal and kinetic stability of rFVIIa upon GlycoPEGylation. To our knowledge no study has yet been published on a highly relevant pharmaceutical protein which combines investigations of the effect of GlycoPEGylation on the structural, thermal and kinetic stability using both linear and branched PEG polymers. This study contributes to the further understanding of the basic biophysical properties of PEGylated pharmaceutical proteins.

5.2   Materials and Methods

Materials

rFVIIa, 10 kDa GlycoPEGylated rFVIIa and 40 kDa GlycoPEGylated rFVIIa was produced by Novo Nordisk A/S, Denmark, as described in [64]. L-Histidine was purchased from Aijonomoto AminoScience (Raleigh, N.C.), calciumchloride-dihydrate from Merck (Germany), Barium Chloride 20 w/w from Ampliqon (Denmark), 0.1 N iodine solution from Sigma-Aldrich (Germany), 70 % perchloric acid from Merck (Germany), LDS sample buffer and MES SDS running buffer and Simple Blue Safe Stain all from Invitrogen (Carlsbad, CA). All protein solutions were dialysed in Slide-A-Lyzer^{TM} 30.000 MWCO dialyse cassettes against 10 mM histidine, 10 mM CaCl$_2$, pH 5.75

SDS-PAGE

SDS-PAGE analysis was carried out using a 12 % Bis-Tris gel from Invitrogen. The gels were loaded with an average of 5 μg per well and run at 120 mA constant current per gel. The running buffer was MES running buffer. The gel was washed in 150 mL 0.1 M perchloric acid for 15 minutes until 40 mL 5 % barium chloride solution and 15 mL 0.1 M iodine solution were added to detect protein bands containing PEG compounds, as described in [141]. After discolouring in water, the gel was coloured with Coomassie blue.

MALDI-TOF MS

Mass spectrometric analysis was performed on a Bruker Daltonics Microflex MALDI-TOF instrument equipped with a nitrogen laser (337 nm). The instrument was operated in linear

mode with delayed extraction, and the accelerating voltage in the ion source was 25kV. Sample preparation was done as follows: 1 μl sample-solution was mixed with 10 μl matrix-solution (alphacyano-cinnamic acid dissolved in a 5:4:1 mixture of acetonitrile:water:3% TFA) and 1 μl of this mixture was deposited on the sample plate and allowed to dry before insertion into the mass spectrometer. Calibration was performed using external standards (a range of standard proteins) and the resulting accuracy of the mass determinations is within 0.1%.

Circular Dichrosim (CD) Spectroscopy

Spectra of rFVIIa in the far-UV region (180-260 nm) were recorded on a Jasco J-810 CD Spectropolarimeter. The light path of the cuvette was 0.05 mm and a protein concentration of 2.4 mg/mL was used. The spectra were recorded at room temperature. Each spectrum is an average of 5 scans. All spectra were background-corrected, smoothed and transformed into molar ellipticity (Θ cm^2 dmol^{-1}). A value of 114 g/mol was used as a mean residue weight for rFVIIa. Spectra of rFVIIa in the near-UV region (250-350 nm) were recorded on the same Spectropolarimeter. The light path of the cuvette was 10 mm and a protein concentration of 2.4 mg/mL was used. The spectra were recorded at room temperature. Spectra at selected temperatures in the range 10 ℃ - 80 ℃ spectra were obtained in a 2 mm cuvette. Each spectrum is an average of 5 scans. All spectra were background-corrected, smoothed and transformed into molar ellipticity (Θ cm^2 dmol^{-1}).

Differential Scanning Calorimetry (DSC)

DSC experiments were performed with a MicroCal VP-DSC (Northhampton, MA). Prior to scanning, all solutions were degassed by stirring under vacuum. A pressure of 2 atm was applied over the cells during scanning, and a scan rate of 1 ℃/min was used. The concentration of rFVIIa was 2-2.4 mg/mL, and buffer scans were subtracted from protein scans. DSC data was analysed using the Origin software from MicroCal Inc., supplied with the instrument. A baseline was subtracted prior to analysis. The apparent denaturation temperatures (T_m) values were determined as the temperature corresponding to the maximum C_p.

Light Scattering (LS)

The LS experiments were performed with a Wyatt DynaPro Titan (Santa Barbara, CA) which employs a 829 nm laser and collects scattering intensity data at a fixed angle of 90 ℃. Cuvette temperature is controlled using a thermoelectric solid-state heating module (Peltier heat pump). Solutions are examined in a quartz cuvette with 12 μL cell volume containing glass viewing windows for in situ scattering measurements. The concentration of rFVIIa was 1-2 mg/mL. 200 μL samples volumes are centrifuged at 10.000 RPM for 10 minutes prior to analysis. A scan rate of 1 ℃/min was used.

5.3   Results

After dialysis the purity of the protein solutions were determined by SDS-PAGE and by MALDI-TOF MS. SDS-PAGE has often been used to characterise the distribution of PEGylated proteins [154]. It is assumed that the higher molecular weight gel band ladders represented the mono- or di-GlycoPEGylated rFVIIa compounds (fig. 5.1).
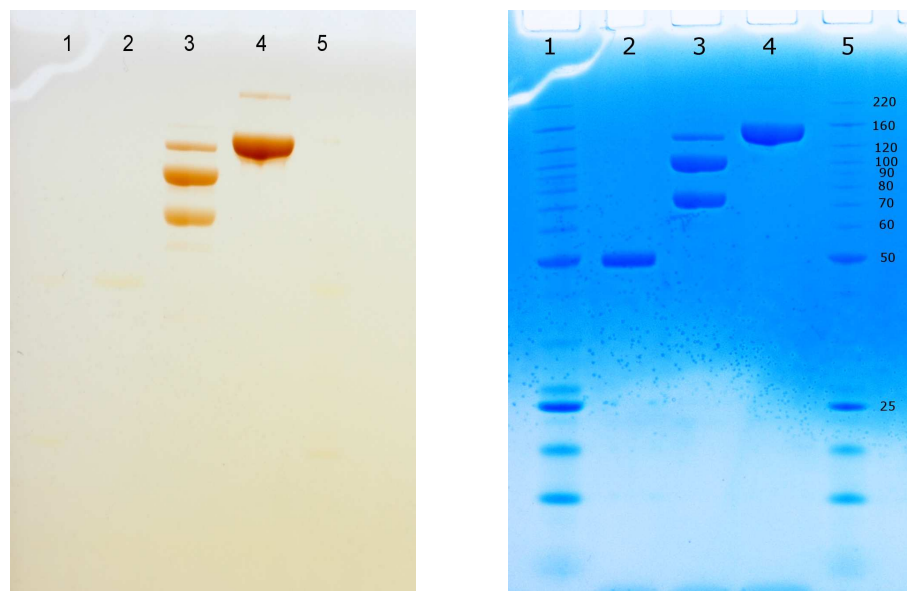
(a) A PEG stained gel.   The gel is stained with iodide as described in [141].

(b) SDS PAGE of rFVIIa and Glyco-PEGylated rFVIIa.

Figure 5.1:
Lane 1 and 5, bench mark protein ladder.
Lane 2: rFVIIa.
Lane 3: 10 kDa PEG-rFVIIa.
Lane 4: 40 kDa PEG-rFVIIa.
The gel is stained with iodine (fig. 5.1a), discoloured in water and subsequently stained with Coomassie blue (fig. 5.1b).

The PEG-staining gel technique is based on the complex formation between PEG and barium iodide, and the PEG-stained gel (figure 5.1a) reveal that only lane 3 and lane 4 contain PEG-compounds. It has previously been shown, that PEG binds to SDS micelles [142] and that PEGylation decreases the mobility of the protein [141, 143]. For this reason the molecular weight of a PEGylated protein on a SDS gel will not correspond to the actual molecular weight of the PEGylated protein. Due to the low mobility of the PEGylated protein, the location of a PEGylated protein on a SDS gel corresponds to the molecular weight of the protein added approximately 2.5 times the molecular weight of the attached PEG polymer. Comparing the results in the PEG-stained gel with the very same gel,

only now Coomassie blue stained, it is evident, that the three bands in lane 3 (10 kDa PEG-rFVIIa) and the two bands in lane 4 (40 kDa PEG-rFVIIa) are GlycoPEGylated compounds of rFVIIa. From the results on the SDS-PAGE gel (fig 5.1) it is shown that the rFVIIa sample was pure and contained only rFVIIa with a molecular mass of 50 kDa. The third lane reveals that 10 kDa PEG-rFVIIa is not only mono-GlycoPEGylated. There are 3 different GlycoPEGylated species in this protein solution. These compounds have apparent molecular weights of 75 kDa, 110 kDa and 125 kDa, respectively. This corresponds to mono-GlycoPEGylated 10 kDa PEG-rFVIIa (50 kDa + 2.5 x 10 kDa) $\sim$ 75 kDa, di-GlycoPEGylated 10 kDa PEG-rFVIIa (50 kDa + 2.5 x 2 x 10 kDa) $\sim$ 110 kDa and tri-GlycoPEGylated rFVIIa (50 kDa + 2.5 x 3 x 10 kDa) $\sim$ 125 kDa. The fourth lane contains mainly mono-GlycoPEGylated 40 kDa PEG-rFVIIa with a molecular weight of (50 kDa + 2.5 x 40 kDa) $\sim$ 160 kDa but also a small amount of di-GlycoPEGylated 40 kDa PEGylated rFVIIa at (50 kDa + 2.5 x 2 x 40 kDa) $\sim$ 250 kDa.

The results of the MALDI-TOF MS spectra of rFVIIa, 10 kDa PEG-rFVIIa and 40 kDa PEG-rFVIIa are shown in figure 5.2.
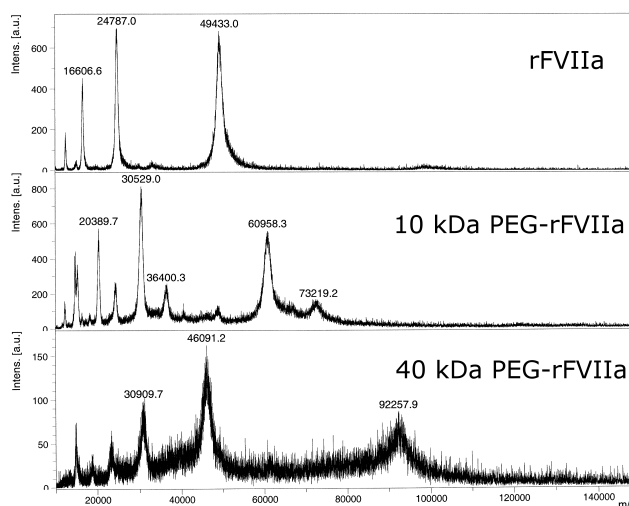

Figure 5.2: MALDI-TOF spectra of rFVIIa, 10 kDa PEG-rFVIIa and 40 kDa PEG-rFVIIa, see text for further details.

The MS spectra show that the rFVIIa solution only contains a 50 kDa protein, and the peak pattern corresponds to different charges (16606 Da peak corresponds to triple charged rFVIIa, 24787 corresponds to double charged rFVIIa and 49433 corresponds to single charged). The 10 kDa PEG-rFVIIa solution contains a mono-GlycoPEGylated, 60 kDa, and smaller amounts of a di-GlycoPEGylated compound, at 70 kDa, of 10 kDa PEG-rFVIIa. The peak at 36400 corresponds to double charged di-GlycoPEGylated rFVIIa, and the 30529 and 20389 are double and triple charged mono-GlycoPEGylated rFVIIa, respectively. The 40 kDa PEG-rFVIIa solution contains mono-GlycoPEGylated 40 kDa PEG-rFVIIa, which is reflected at the 92 kDa peak. Peaks at 46 and 31 kDa are as-

signed to double and triple charged mono-GlycoPEGylated 40 kDa PEG-rFVIIa. The tri-GlycoPEGylated 10 kDa rFVIIa compound and the di-GlycoPEGylated 40 kDa rFVIIa compound are not detectable with MS.

Structural Stability

The secondary structure of rFVIIa and GlycoPEGylated rFVIIa is investigated by far-UV CD in order to study the effect of GlycoPEGylation. The far-UV CD scan reflecting the secondary structure of rFVIIa, 10 kDa PEG-rFVIIa and 40 kDa PEG-rFVIIa are practically inseparable, however there is a small deviation in the far-UV signal at very low wavelength between the 10 kDa PEG-rFVIIa and the two other rFVIIa compounds. The near-UV CD scans show no change in the tertiary structure of rFVIIa upon GlycoPEGylation. The near-UV CD scan show two characteristic peaks around 286 nm and 292 nm most likely corresponding to signals from the tryptophan residues.
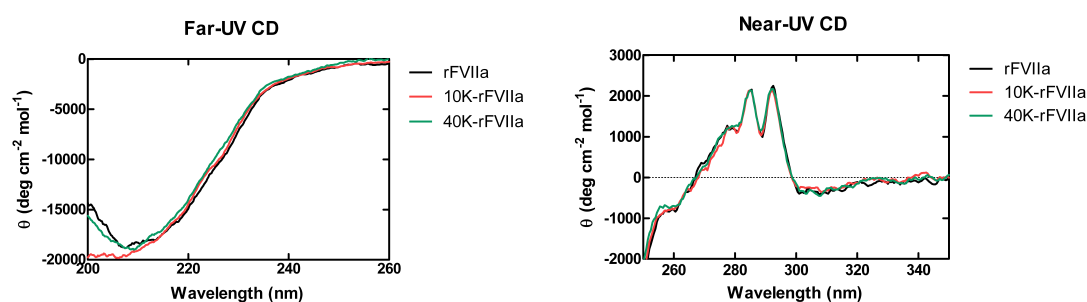

Figure 5.3: Far-UV CD scan and near-UV CD scan of rFVIIa, 10 kDa PEG-rFVIIa and 40 kDa PEG-rFVIIa. The far-UV CD scans show only little variation between the spectrum of 10 kDa PEG-rFVIIa and the two spectrums of rFVIIa and 40 kDa PEG-rFVIIa, and the near-UV CD scans show that GlycoPEGylation has no notable effect on the tertiary structure (near-UV CD) of rFVIIa.

Thermal, kinetic and structural stability

The thermal stability is investigated by three different complementing techniques: DSC, LS and CD. From the CD scans it is evident that the GlycoPEGylated rFVIIa compounds maintain some residual tertiary structure at high temperatures (> 70 ℃) (fig 5.4). The appearance of the near-UV CD heating scan is different from the unmodified protein to the two GlycoPEGylated protein compounds. It is evident that the tertiary structure of the GlycoPEGylated rFVIIa molecules is less affected by the increase in temperature than the unmodified protein.

We chose to follow one characteristic wavelength, 286 nm, throughout the CD heating scan (fig. 5.5). This wavelength was chosen as the CD signal at this specific wavelength
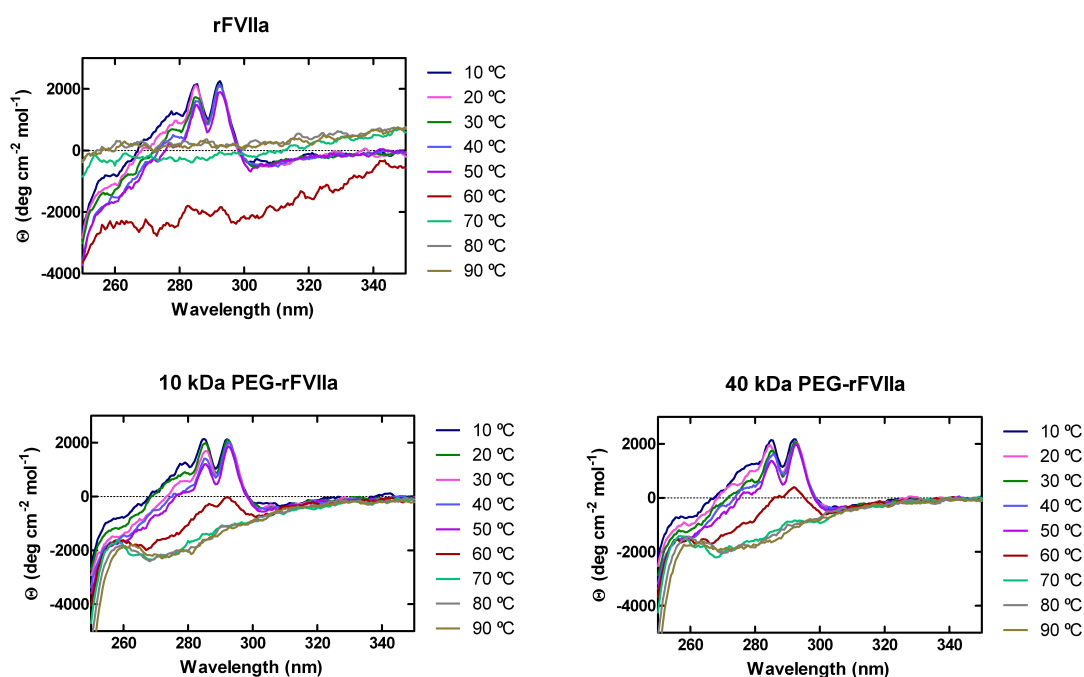
Figure 5.4: Near-UV CD at different temperatures (see legends) of rFVIIa, 10 kDa PEG-rFVIIa and 40 kDa PEG-rFVIIa. The spectra show that the unfolding process differs from the non-modified protein to the GlycoPEGylated proteins. The GlycoPEGylated proteins maintain some residual tertiary structure at 70 °C and above, whereas CD signal from the unmodified protein is showing no tertiary structural characteristics at these temperatures. The native rFVIIa solution was milk-white upon heating whereas the solutions of the GlycoPEGylated rFVIIa compounds were transparent.

changes significantly upon heating, as illustrated in figure 5.4, and corresponds to the first of the two characteristic peaks.

The overall CD signal at 286 nm is different for the unmodified protein compared to the GlycoPEGylated protein compounds. The low temperature range CD signal for all the three compounds is around 2000 deg cm^{-2} mol^{-1} and decreases slowly until 50 °C where the CD signal decreases significantly for all the three compounds to around -1000 deg cm^{-2} mol^{-1}. For rFVIIa there is a drop in the CD signal around T_m, whereupon the signal increases and stabilises around 0 deg cm^{-2} mol^{-1}. The GlycoPEGylated rFVIIa compounds, on the other hand, demonstrate a more continuous course and stabilises around -1500 deg cm^{-2} mol^{-1}. The CD signals were differentiated with respect to the temperature in order to obtain the transition midpoint (T_m) value, which is defined as the point where the tangent has the largest slope, see table 5.1.
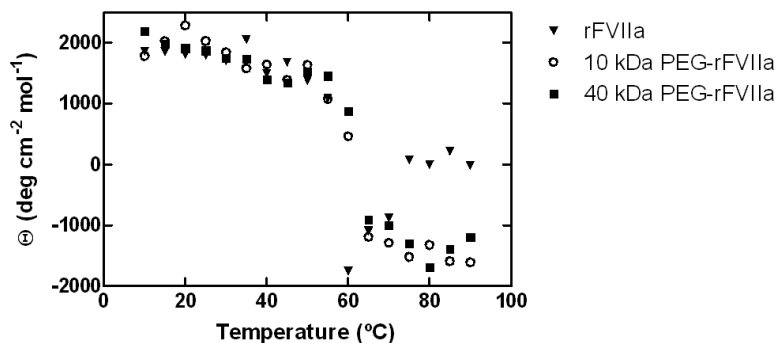
Figure 5.5: Near-UV CD signals of rFVIIa, 10 kDa PEG-rFVIIa and 40 kDa PEG-rFVIIa versus temperature at 286 nm. Triangles, circles and squares are chosen in favour of solid lines to clearly illustrate the differences around 60 ℃, and the error bars are hidden under the symbols. From the results represented in this figure it is clear that the temperature dependent CD signal at 286 nm is different from the unmodified protein to the GlycoPEGylated proteins. The two GlycoPEGylated proteins are alike.

The DSC thermograms and the LS intensity data are plotted in the same figure (figure 5.6) to illustrate the difference between the thermal and kinetic changes. Three different characteristic temperatures are found from figure 5.6. The onset temperature, T_{onset}, corresponding to the temperature where the unfolding of the unmodified rFVIIa or Glyco-PEGylated rFVIIa initiates. The apparent unfolding temperature, T_m, where half of the unmodified rFVIIa or GlycoPEGylated rFVIIa molecules are folded, the other half unfolded theoretically, and the temperature of aggregation, T_{agg}, the aggregation onset temperature. There is a clear difference between the appearance of the DSC scan of the unmodified rFVIIa and the GlycoPEGylated rFVIIa compounds as the former is showing signs of aggregation identified by a sharp drop in C_p and large, immeasurably aggregates in the LS experiment. The aggregation of the two GlycoPEGylated compounds appears to happen at a slower rate, detectable by LS.

The DSC thermograms reveal that GlycoPEGylation increases the apparent unfolding temperature, T_m. The temperature of aggregation, T_{agg} is found by differentiating the intensity of the LS signal with respect to the temperature. Linear regression was performed on this last part of the curve, where the intensity increases due to formation of aggregates. The calculated intercept with the x-axis, where the scattering intensity is zero, is named T_{agg}, temperature of aggregation in the following. The LS measurements demonstrate that the aggregation temperature, T_{agg}, increases with GlycoPEGylation (table 5.1).
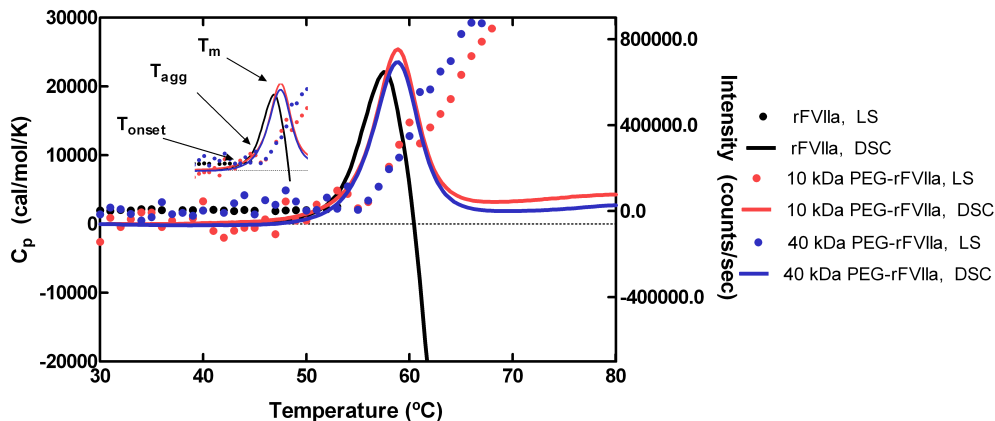
Figure 5.6: DSC thermograms and LS intensity measurements of rFVIIa, 10 kDa PEG-rFVIIa and 40 kDa PEG-rFVIIa as a function of temperature. The dotted line correspond to the LS intensity (the error bars are hidden under the symbols), the solid line correspond to the DSC thermogram. The insert illustrate where the onset temperature, T_{onset}, the temperature of aggregation, T_{agg}, and the apparent unfolding temperature, T_m, are found. The rFVIIa aggregates formed close to T_{agg} were too large for the LS detector to measure, and continuous intensity measurements as a function of temperature were impossible after 53 ℃ for rFVIIa.

	T_m (℃) (CD)	T_{onset} (℃) (DSC)	T_m (℃) (DSC)	ΔH (kJ/mol) (DSC)	T_{agg} (℃) (LS)	(T_{onset}-T_{agg})
rFVIIa	60.3±0.2	50.9±0.2	57.7±0.2	NA	50.8±0.4	0.1
10 kDa PEG-rFVIIa	59.9±0.2	53.3±0.1	59.0±0.2	140	57.1±0.2	-3.8
40 kDa PEG-rFVIIa	60.7±0.2	52.9±0.1	59.0±0.2	134	57.9±0.9	-5

Table 5.1: The unfolding temperature measured by CD, the onset temperature of the peaks in the DSC heating scan, the apparent unfolding temperature, T_m, measured by DSC, the aggregation temperature, T_{agg}, measured by LS and the difference between T_{onset} and T_{agg}. The extraction of the enthalpy of unfolding of rFVIIa is not possible due to the irreversibility of the denaturation process.

5.4   Discussion

The structural information obtained with far-UV and near UV-CD scans shows that both the secondary and the tertiary structure of rFVIIa are maintained upon GlycoPEGylation and the structures do not change with PEG chain length nor with the PEG conformation (linear or branched). Minor differences in the CD scans are observed around 210-200 nm for the 10 kDa GlycoPEGylated rFVIIa compound compared to the 40 kDa GlycoPEGylated rFVIIa compound and the unmodified rFVIIa, the origin of this small difference is not known but it could reflect changes in β-turns [127].

Structural, kinetic and thermal stability

The DSC, LS and CD heat scans were all performed at the same scan rate, which makes it possible to compare the kinetics. The three different measurement types are complementary and they illustrate each different aspects of the unfolding or aggregation processes. The unfolding and aggregation pathway can be described by a model put forward by Lumry and Eyring in 1954 [94]. According to the Lumry Eyring model, irreversible protein denaturation involves at least two steps. The first step is the reversible unfolding of the native protein (N), characterised by the rate constants, k_1 and k_2. This step is followed by an irreversible change of the unfolded protein (D), into an inactivated, irreversible aggregate (A), characterised by the rate constant k_3. The unfolded state, D, is characterised by having some tertiary structure.

$$N \underset{k_2}{\overset{k_1}{\rightleftharpoons}} D \overset{k_3}{\rightarrow} A \qquad K = \frac{k_1}{k_2}$$
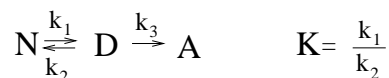
Figure 5.7: The Lumry Eyring model, N is the native protein, D is the unfolded protein and A is the aggregated protein.

From our experimental results it is suggested that the covalent attachment of a PEG polymer to rFVIIa influences at least two of the three rate constants mentioned above. The aggregation of the protein depends on the unfolding of the protein to occur first. The aggregation is measured by LS; the unfolding is measured by CD, whereas DSC measures unfolding, an endothermic event, as well as aggregation, which here is an exothermic event. There is an equilibrium between the native (N) and the unfolded (D) state, which shifts towards unfolding as the temperature increases. This process is followed by the irreversible step from unfolding (D) to aggregation (A), which is also promoted with increasing temperature.

From the results shown in figure 5.6 it is evident that the apparent unfolding temperature, T_m, of the GlycoPEGylated rFVIIa compounds is slightly higher than that of rFVIIa. This is in accordance with previous studies, which have reported that PEGylation can increase the apparent unfolding temperature, T_m, compared to the unmodified protein [63, 91]. For rFVIIa it seems as though a longer, and branched, PEG chain does not contribute

more to the thermal stability than a shorter, linear PEG chain. Taking a closer look at the DSC thermograms and the LS intensities for the GlycoPEGylated rFVIIa compounds (fig. 5.6) it is evident that GlycoPEGylation delays the thermally induced aggregation of rFVIIa, and that the thermally induced aggregation event begins while endothermic processes dominates. The formation of aggregates will contribute exothermally to the total heat signal. As the heat measured by DSC is the total contribution from both unfolding and aggregation, an extensive formation of aggregates beginning shortly after T_{onset} may shift the location of the peak in the thermogram towards a lower temperature. Thus GlycoPEGylation may not directly stabilise rFVIIa thermally, but could affect the value of T_m indirectly by postponing the formation of the thermally induced aggregates. The hypothesis that GlycoPEGylation prevents or postpones the aggregation of rFVIIa is supported by the results of the CD heating scans. The changes in the CD signal at 286 nm in the heating scan (fig. 5.5) indicate that the non-modified rFVIIa undergo a conformational change in the tertiary structure around the apparent unfolding temperature and no tertiary structure can be detected at higher temperature. As the physical appearance of the rFVIIa solution upon heating was milk-white, the non-detectable tertiary structure above 70 ℃ could be a sign of aggregation and precipitation. The GlycoPEGylated rFVIIa compounds, on the other hand, do maintain some non-native residual tertiary structure upon unfolding, even at 90 ℃, as the CD signal stabilises around 1500 deg cm^{-2} mol^{-1} (fig. 5.5). These observations support the general conception that PEGylation may not necessarily prevent the protein from unfolding [91, 152], but it hinders protein-protein interactions, which can lead to aggregation and precipitating.

Nielsen and Rischel have investigated the thermal stability of rFVIIa and 40 kDa PEG-rFVIIa with DSC and High Resolution Ultra Sonic Spectroscopy (HR-US) [152]. On the basis of the DSC measurements they conclude, that the denaturation of rFVIIa is irreversible. In contrast they find that the unfolding of 40 kDa PEG-rFVIIa is characterised by being partly reversible, as approximately 60 % reversibility is observed after heating to 60 ℃. Based on HR-US experiments they report that the post-denaturation aggregation process is delayed upon GlycoPEGylation. In addition it is suggested, that the Glyco-PEGylated protein demonstrate a less pronounced aggregation. All these conclusions are supported by the results obtained in this study.

Based on the results obtained in this study it seems reasonable to assume that the equilibrium constant k_1/k_2, reflecting the equilibrium between the native and the unfolded protein, is independent of GlycoPEGylation, since unfolding process for rFVIIa seems to be similar, whether the protein is GlycoPEGylated or not. The rate constant k_3, on the other hand, describing the step from unfolding to aggregation, decreases when the protein is GlycoPEGylated. The thermally induced rFVIIa aggregates formed close to T_{agg} were too large for the LS detector to measure, and continuous intensity measurements as a function of temperature were impossible after 53 ℃ for rFVIIa. As the light scattering increases with the sizes of the formed aggregates [155], a high intensity count most likely corresponds to large aggregates. The increase in the LS intensity is much slower for the GlycoPEGylated rFVIIa compounds, thus the formation of aggregates is reduced and

happens at a lower rate. The fact that PEGylating a protein postpones the aggregation has also been reported previously [65, 95, 152]. By comparing the difference between the onset of unfolding, T_{onset}, with the onset of aggregation, T_{agg}, (figure 5.6 and table 5.1), it is evident that (T_{agg} - T_{onset}) is of the same order of magnitude for both for 10 kDa PEG-rFVIIa and 40 kDa PEG-rFVIIa. Given that both GlycoPEGylated compounds postpone the aggregation behaviour of rFVIIa, but not the thermally induced unfolding, indicates that PEGylating a protein may affect the aggregation properties of a protein but not through thermal stabilisation of the protein. This is in agreement with previously reported studies on insulin [65].

It is noticeable that the PEG molecular weight and shape has no effect on the thermal, the structural or the kinetic stability of rFVIIa. All of the results obtained in this study indicate that attaching a PEG moiety of similar size as rFVIIa appears to have the same effect as attaching a smaller 10 kDa PEG to rFVIIa. From a pharmaceutical formulation point of view these results indicate that the decision of what shape and size of PEG to use for GlycoPEGylation of rFVIIa depends on other factors than those currently investigated. Instead, the size and shape PEG should be chosen as that which gives the best biological effect.

Favourable properties, such as postponed or prevented aggregation and thermal stabilisation are caused by the heavily hydrated PEG polymer, and the properties of the PEG polymer are transferred to the GlycoPEGylated compounds. In particular, the postponed and decreased aggregation is crucial in protein drugs as this increases the stability of the protein.

5.5 Conclusion

Recombinant human Factor VII was mono-GlycoPEGylated with two different PEG polymers, a 10 kDa linear PEG and a 40 kDa branched PEG. The CD measurements suggest that the secondary and tertiary structure of rFVIIa is maintained upon GlycoPEGylation. The DSC and LS measurements suggests that GlycoPEGylation delays the thermally induced aggregation, and slightly increases the unfolding temperature of the protein (increase from $57.7 \pm 0.2\,°C$ to $59.0 \pm 0.2\,°C$), both of which are independent of the molecular weight and size of the attached PEG polymer. From the biophysical characterisation of rFVIIa and GlycoPEGylated rFVIIa in the present study it is concluded, that rFVIIa after GlycoPEGylation appears to be unaffected structurally (secondary and tertiary structure), slightly stabilised thermally (unfolding temperature), and stabilised kinetically (temperature of aggregation).

Acknowledgements

6 The effect of CaCl$_2$ on the stability of GlycoPEGylated rFVIIa

Bitten Plesner[a,b], Peter Westh[a], Anders D. Nielsen[b,†]
[a]Department of Science, Roskilde University, P.O. Box 260, Universitetsvej 1, DK-4000 Roskilde, Denmark
[b]Novo Nordisk A/S, Novo Nordisk Park, DK-2760 Maaloev, Denmark

[†]Corresponding author. Tel.: +45 30 79 65 75; fax: +45 44 43 40 73
Email address: ADNi@novonordisk.com (A. D. Nielsen).

Abstract

The effects of calcium chloride on the structural, kinetic and thermal stability of recombinant human Factor VIIa (rFVIIa) were investigated using rFVIIa and two GlycoPEGylated recombinant human FVIIa derivatives, a linear 10 kDa PEG and a branched 40 kDa PEG, respectively. Three different CaCl$_2$ concentrations were used; 10 mM, 35 mM and 100 mM. The secondary and tertiary structure of rFVIIa at 25 ℃, measured by Circular Dichroism (CD), was maintained upon GlycoPEGylation as well as CaCl$_2$ content. In contrast the thermal stability of the three rFVIIa compounds, measured by Differential Scanning Calorimetry (DSC) and Circular Dichroism (CD), and aggregation behaviour, measured by Light Scattering (LS), was affected by the increasing calcium concentration. Increasing the CaCl$_2$ concentration from 10 mM to 35 mM resulted in a decrease in the apparent unfolding temperature, T$_m$, of rFVIIa, whereas the concentration of CaCl$_2$ has to be raised to 100 mM in order to see the same effect on the GlycoPEGylated rFVIIa compounds. The temperature of aggregation of rFVIIa, T$_{agg}$, increased as the CaCl$_2$ concentration increased from 35 mM to 100 mM, while T$_{agg}$ for the GlycoPEGylated rFVIIa compounds was practically independent of the CaCl$_2$ concentration. From the obtained results it is concluded that GlycoPEGylation postpones the calcium induced thermal destabilisation of rFVIIa, and a much higher calcium concentration also post-

pones the thermally induced aggregation of rFVIIa. The thermally induced aggregation of the GlycoPEGylated rFVIIa compounds is unaffected by an increasing calcium chloride concentration.

Keywords: rFVIIa, GlycoPEGylation, protein aggregation, protein unfolding, salt effects, Ca^{2+}.

6.1   Introduction

For blood coagulation factor VIIa (FVIIa) the presence of calcium ions is vital, as these ions assist in initiating the blood coagulation cascade including the association of tissue factor (TF), and following the activation of factor IX and factor X resulting in a burst of thrombin, fibrin deposition and the formation of a haemostatic plug on the platelet surface [146]. Deficiencies in the coagulation system due to partial or complete deficiency of FVIII or FIX, haemophilia A or haemophilia B respectively, can lead to severe morbidity or mortality if the bleeding is left untreated.

A safe and efficient way to prevent bleeds and joint destruction in haemophilia is with the use of prophylaxis giving FVIII or FIX 2-4 times weekly [148]. Recent studies have shown that prophylactic treatment with recombinant FVIIa (rFVIIa, NovoSeven®) in haemophilia patients with inhibitors against FVIII or FVIX reduces the frequency of bleedings significantly as compared to conventional on-demand haemostatic therapy [149]. However, based on the half-life and circulation time of rFVIIa (2-4 h), it is assumed that rFVIIa should be administered daily if used for long-term prevention [149, 150]. Hence, development of rFVIIa derivatives with longer circulation time could result in both fewer administrations and better patient compliance. Modification of pharmaceutical proteins with hydrophilic polymers such as poly-ethylene-glycol (PEGylation) is an established method for prolonging circulatory half-life, reducing self-aggregation, increase water solubility and increase stability [82, 117]. Due to the risk of losing activity of FVIIa because of the numerous interactions with the cell surface, TF, FIX and FX there is a limitation in the unspecific chemical modification of this protein. For this reason a novel strategy for site-directed PEGylation using glycosyltransferases to attach PEG to glycan residues, the enzyme based GlycoPEGylation™ technology is used to covalently attach either a linear 10 kDa or a branched 40 kDa PEG polymer to rFVIIa, a technique originally described by DeFrees et al. [79]. The site of PEG attachment to rFVIIa is demonstrated to be one of the two N-linked glycans of rFVIIa (Asn145 or Asn322) located on the light chain and heavy chain, respectively [64]. It is assumed that the specific location of the GlycoPEGylation site and presence of small amounts of di-GlycoPEGylated species are irrelevant in relation to the overall interpretation of the obtained results.

From a pharmaceutical formulation point of view altering the salt concentration in the protein buffer is of interest in relation to its effect on the protein stability. Addition of electrolytes to proteins in solution can have complex effects on the physical stability of the protein. Electrolytes can modify the conformational stability, the equilibrium solubility (e.g. salting-in and salting-out) and the formation of aggregates [2]. Salts can interact with the unpaired charged side chains of proteins and stabilise or destabilise the native

state of the protein. The former is a result of the binding of mainly multivalent ions to the unpaired charged surface available side chains, which can lead to cross-linking between the charges and thus stabilisation. The latter is found e.g. if the ions bind more strongly to the unfolded state of the protein than to the native state [2]. A number of physical properties of aqueous salt solutions follow the rank order of the Hofmeister series, which arrange solutes according to their ability to act as kosmotrope (salting-out) or chaotrope (salting-in) agents [156, 157]

In this study the effect of $CaCl_2$ on the thermal, kinetic and structural stability of rFVIIa and GlycoPEGylated rFVIIa compounds is investigated. Ca^{2+} binding is an important stabiliser for a number of proteins, and structural aspects of the specific Ca^{2+} binding to rFVIIa are of great importance for understanding its physiological function [158]. There are a total of 9 specific binding sites for Ca^{2+} in three distinct regions on rFVIIa, and they all have different affinities [159, 160]. The binding of these 9 Ca^{2+} ions are vital for the initiation of the blood coagulation cascade, as the binding of Ca^{2+} is a prerequisite for the high-affinity binding of rFVIIa to TF [160–162]. All the Ca^{2+} binding sites are saturated when the calcium buffer concentration exceeds 10 mM [159]. In the present study we have used three $CaCl_2$ concentrations ranging from 10 mM to 100 mM to make sure all the specific binding sites of rFVIIa are saturated, and hence focus the study on the effect of low affinity binding of Ca^{2+}. The physical stability of liquid protein drugs is an important property to investigate as insoluble aggregates may increase immunogenic responses and are not biologically active. $CaCl_2$ is a potential salting in agent, which interacts more strongly with the unfolded form than with the native form, consequently shifting the equilibrium towards the unfolding reaction [157]. This behaviour is pronounced at concentrations around 100 mM [157, 163]. Investigating the stability of rFVIIa and GlycoPEGylated rFVIIa in higher concentrations of $CaCl_2$ than 10 mM is of relevance in relation to the pharmaceutical development, purification and formulation processes, during which the protein concentration often exceeds 1 mg/mL (1 mg/mL NovoSeven® contains 10 mM $CaCl_2$). When concentrating rFVIIa an addition of $CaCl_2$ is needed in order to keep rFVIIa in solution. In contrast, the absence of visual precipitate suggests that GlycoPEGylated rFVIIa stays in solution in 10 mM $CaCl_2$ even at high concentration (> 10 mg/mL).

The effect on the physical stability rFVIIa of increasing the $CaCl_2$ concentration is investigated by using rFVIIa, and two GlycoPEGylated rFVIIa compounds, a 10 kDa linear kDa and 40 kDa branched PEG. This provides us with a relevant pharmaceutical model system for studying the effect of an increasing Ca^{2+} concentration on both a native protein and its two GlycoPEGylated compounds. Biophysical characterisation tools, including Circular Dichroism (CD), Differential Scanning Calorimetry (DSC) and Light Scattering (LS), were used to study possible changes in the secondary and tertiary structure as well as the thermal and kinetic stability of rFVIIa, 10 kDa PEG-rFVIIa and 40 kDa rFVIIa upon an increase in $CaCl_2$ concentration.

6.2   Materials and Methods

Materials

rFVIIa, 10 kDa GlycoPEGylated rFVIIa and 40 kDa GlycoPEGylated rFVIIa was produced by Novo Nordisk A/S, Denmark, as described in [64]. L-Histidine was purchased from Aijonomoto AminoScience (Raleigh, N.C.), calciumchlorid-dihydrate from Merck (Germany), Barium Chloride 20 w/w from Ampliqon (Denmark), 0.1 N iodine solution from Sigma-Aldrich (Germany), 70 % perchloric acid from Merck (Germany), LDS sample buffer and MES SDS running buffer and Simple Blue Safe Stain all from Invitrogen (Carlsbad, CA). All protein solutions were dialysed in Slide-A-Lyzer^{TM} 30.000 MWCO dialyse cassettes against the desired buffer. Three different buffers were used, only varying in CaCl$_2$ content. Buffer 1 contained 10 mM Histidine (HIS), 10 mM CaCl$_2$. Buffer 2 contained 10 mM HIS and 35 mM CaCl$_2$. Buffer 3 contained 10 mM HIS and 100 mM CaCl$_2$. All buffers were adjusted to pH 5.75

SDS-PAGE

SDS-PAGE analysis was carried out using a 12 % Bis-Tris gel from Invitrogen. The gels were loaded with an average of 5 μg protein per well and run at 120 mA constant current per gel. The running buffer was MES running buffer. The gel was washed in 150 mL 0.1 M perchloric acid for 15 minutes until 40 mL 5 % barium chloride solution and 15 mL 0.1 M iodine solution were added to detect protein bands containing PEG compounds, as described in [141]. After discolouring in water, the gel was coloured with Coomassie blue.

MALDI-TOF MS

Mass spectrometric analysis was performed on a Bruker Daltonics Microflex MALDI-TOF (Billerica, MA) equipped with a nitrogen laser (337 nm). The instrument was operated in linear mode with delayed extraction, and the accelerating voltage in the ion source was 25kV. 1 μl sample-solution was mixed with 10 μl matrix-solution (alphacyano-cinnamic acid dissolved in a 5:4:1 mixture of acetonitrile:water:3% TFA) and 1 μl of this mixture was deposited on the sample plate and allowed to dry before insertion into the mass spectrometer. Calibration was performed using external standards (a range of standard proteins) and the resulting accuracy of the mass determinations is within 0.1%.

Circular Dichrosim (CD) Spectroscopy

Spectra of rFVIIa in the far-UV region (180-260 nm) were recorded on a Jasco J-810 CD Spectropolarimeter (JASCO International Co. Ltd., Hachioji City, Japan). The light path of the cuvette was 0.05 mm and a protein concentration of 2.4 mg/mL was used. The spectra were recorded at room temperature. Each spectrum is an average of 5 scans. A value of 114 g/mol was used as a mean residue weight for rFVIIa. Spectra of rFVIIa in the near-UV region (250-350 nm) were recorded on the same Spectropolarimeter. The light path of the cuvette was 10 mm and a protein concentration of 2.4 mg/mL was used. The spectra were recorded at room temperature. Spectra at selected temperatures in the

range 10 ℃-80 ℃ spectra were obtained in a 2 mm cuvette. Each spectrum is an average of 5 scans. All spectra were background-corrected, smoothed and transformed into molar ellipticity (Θ cm^2 dmol^{-1}) as described in [127].

Differential Scanning Calorimetry (DSC)

DSC experiments were performed with a MicroCal VP-DSC (Northhampton, MA). Prior to scanning, all solutions were degassed by stirring under vacuum. A pressure of 2 atm was applied over the cells during scanning, and a scan rate of 1 ℃/min was used. The concentration of rFVIIa was 2-2.4 mg/mL, and buffer scans were subtracted from protein scans. DSC data was analysed using the Origin software from MicroCal Inc., supplied with the instrument. A baseline was subtracted prior to analysis. The apparent denaturation temperatures (T_m) values were determined as the temperature corresponding to the maximum C_p, the errors are determined by repeatable experiments. The enthalpy is calculated from the area under the peak bound by the baseline, and the errors are based on the adjustment of this baseline.

Light Scattering (LS)

The LS experiments were performed with a Wyatt DynaPro Titan (Santa Barbara, CA) which employs a 829 nm laser and collects scattering intensity data at a fixed angle of 90 ℃. Cuvette temperature is controlled using a thermoelectric solid-state heating module (Peltier heat pump). Solutions are examined in a quartz cuvette with 12 μL cell volume containing glass viewing windows for in situ scattering measurements. The concentration of rFVIIa was 1-2 mg/mL. 200 μL samples volumes are centrifuged at 10.000 RPM for 10 minutes prior to analysis. A scan rate of 1 ℃/min was used.

6.3   Results

Purity

After dialysis the purity of the protein solutions were determined by SDS-PAGE and by MALDI-TOF MS as described and published in Plesner et al. [164]. Briefly, it was shown that the rFVIIa sample was pure and contained only rFVIIa with a molecular mass of 50 kDa. The 10 kDa PEG-rFVIIa solution contains a mono-GlycoPEGylated, 60 kDa, and smaller amounts of a di-GlycoPEGylated compound, at 70 kDa, of 10 kDa PEG-rFVIIa. The 40 kDa PEG-rFVIIa solution contains mono-GlycoPEGylated 40 kDa PEG-rFVIIa with a molecular mass of 92 kDa. It is assumed that the specific location of the GlycoPEGylation site and presence of small amounts of di-GlycoPEGylated species are irrelevant in relation to the overall interpretation of the results obtained in this study.

Structural Characteristics

The secondary structure of rFVIIa and GlycoPEGylated rFVIIa is investigated by far-UV CD and the results have been reported previously [164]. From that study it was evident that the far-UV CD scans of rFVIIa and 40 kDa PEG-rFVIIa are inseparable, and there

is only a small variation in the far-UV signal at very low wavelength between the native rFVIIa and the 40 kDa PEG-rFVIIa compared to the 10 kDa GlycoPEGylated rFVIIa compound. The near-UV CD scans show no change in the tertiary structure of rFVIIa upon GlycoPEGylation. Due to the high absorbance of Cl$^-$ ions below 200 nm [127], it was not possible to measure far-UV CD scans on samples containing 35 mM and 100 mM CaCl$_2$.
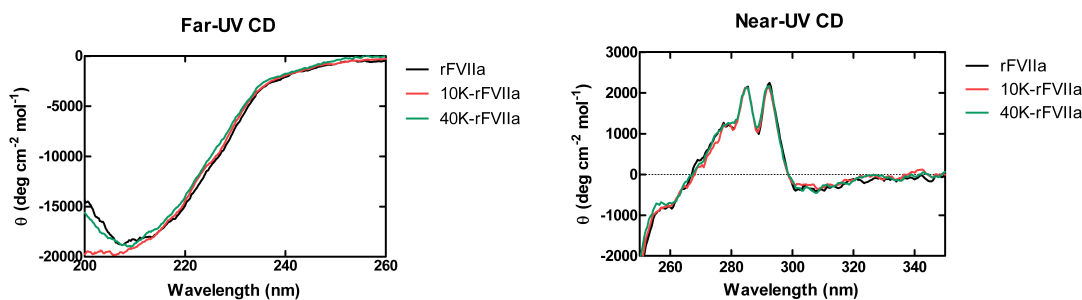

Figure 6.1: Far-UV CD scan and near-UV CD scan of rFVIIa, 10 kDa PEG-rFVIIa and 40 kDa PEG-rFVIIa in 10 mM HIS, 10 mM CaCl$_2$, pH 5.75. The far-UV CD scans show only little variation between the spectrum of 10 kDa PEG-rFVIIa and the two spectrums of rFVIIa and 40 kDa PEG-rFVIIa, and the near-UV CD scans show that GlycoPEGylation has no notable effect on the tertiary structure (near-UV CD) of rFVIIa. Results adapted from [164].

Thermal, kinetic and structural stability

The effect of increasing the CaCl$_2$ buffer content on the thermal, kinetic and structural stability of rFVIIa and GlycoPEGylated rFVIIa is investigated by three different complementary techniques: DSC, LS and CD. From the CD scans it is evident that there is no difference between the thermally induced structural changes upon an increase in CaCl$_2$ in rFVIIa and GlycoPEGylated rFVIIa, respectively (figure 6.2).

We chose to follow one characteristic wavelength, 286 nm, throughout the CD heating scan. This wavelength was chosen as the CD signal at this specific wavelength changes markedly upon heating, see figure 6.3. The CD signal at 286 nm reflects primarily the aromatic amino acids tryptophan (290-305 nm) and tyrosine (275-282 nm) [127].

It is shown in figure 6.3 that from 60 °C and above the change in the 286 nm CD signal is independent of the CaCl$_2$ content, but clearly different from the unmodified rFVIIa to the GlycoPEGylated rFVIIa compounds. For rFVIIa there is a clear drop in the CD signal around T$_m$, whereupon the signal increases and stabilises around 0 deg cm^{-2} mol^{-1}. On the other hand, the GlycoPEGylated rFVIIa compounds demonstrate a more continuous course. Differentiating the CD signal with respect to the temperature gives an estimate of
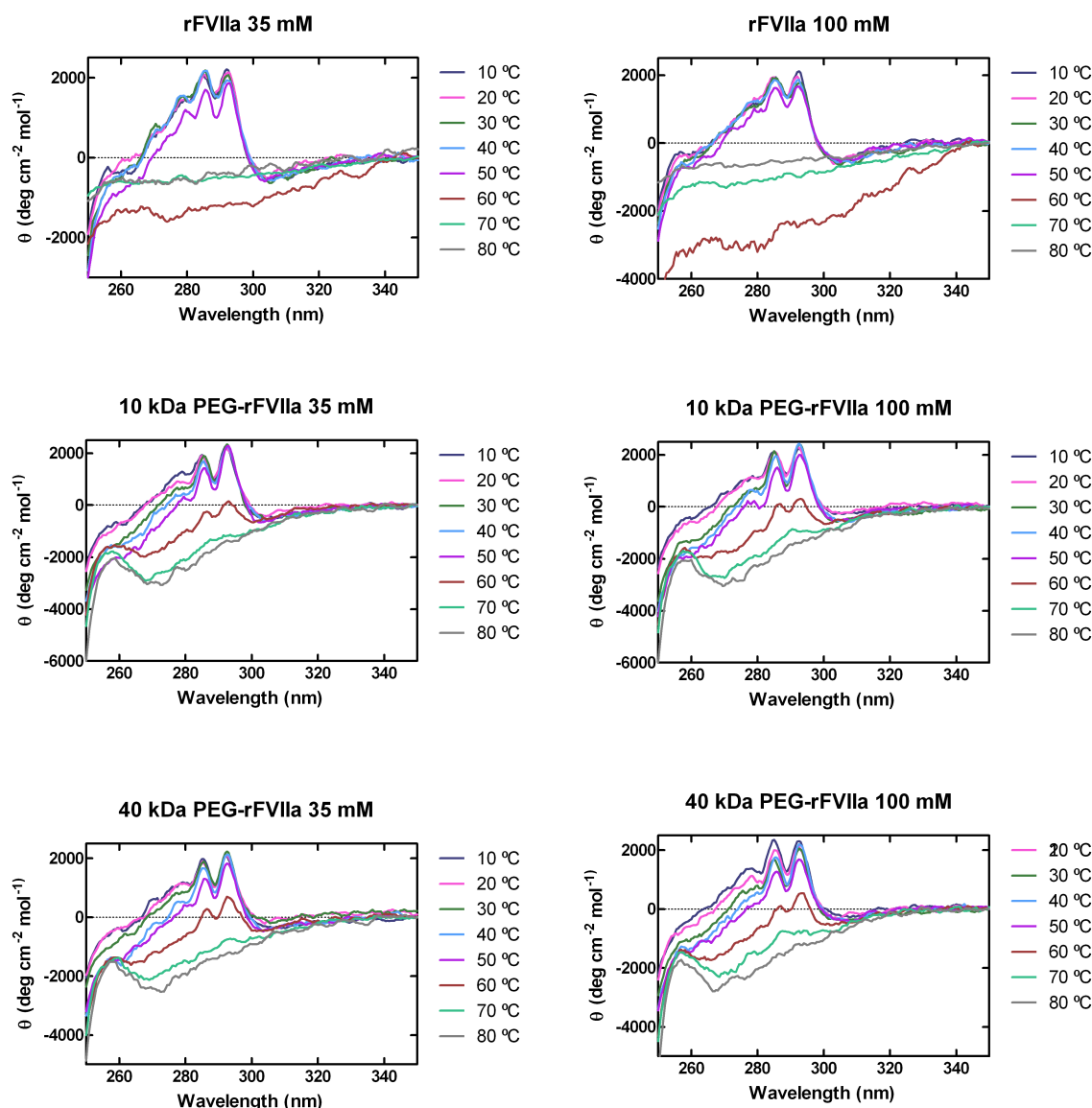
Figure 6.2:   Near-UV CD at different temperatures (see legends) of rFVIIa, 10 kDa PEG-rFVIIa and 40 kDa PEG-rFVIIa. The left panels show results obtained in 10 mM HIS, 35 mM CaCl$_2$, pH 5.75 and the right panels show results obtained in 10 mM HIS, 100 mM CaCl$_2$, pH 5.75. The spectra in both panels are similar, indicating that there are no or very small differences in the thermally induced unfolding due to increasing CaCl$_2$ content. Both panels also show spectra which indicate that the thermally induced unfolding process differs from the non-modified protein to the GlycoPEGylated proteins. The GlycoPEGylated proteins maintain some residual tertiary structure at 60 °C and above, whereas CD signal from the native protein shows no structural characteristics at these temperatures. The native rFVIIa solution was milk-white upon heating whereas the GlycoPEGylated rFVIIa compounds were transparent. Similar results are found for rFVIIa and its GlycoPEGylated compounds in 10 mM HIS, 10 mM CaCl$_2$, pH 5.75 [164].
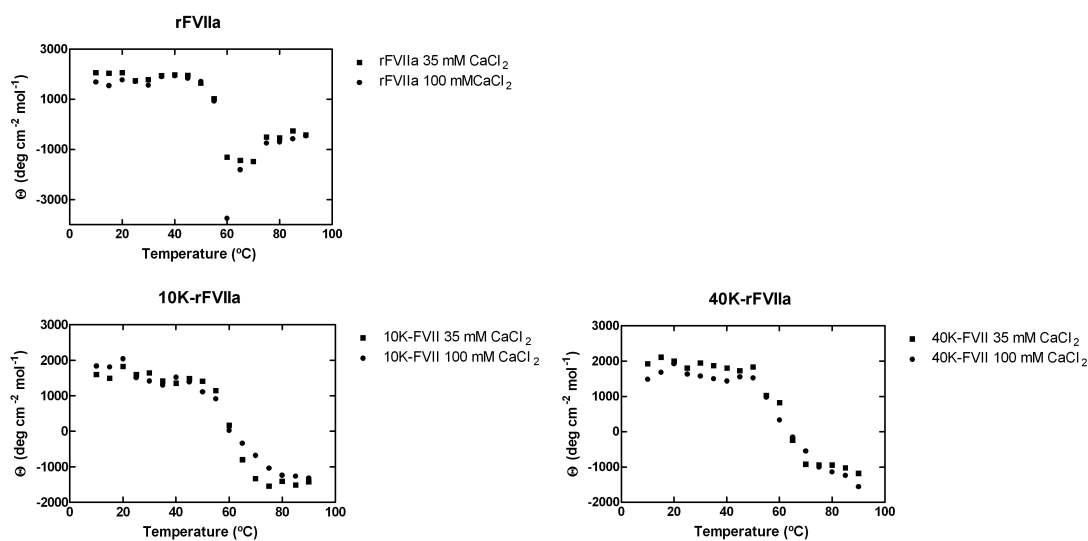
Figure 6.3: Near-UV CD signals of rFVIIa, 10 kDa PEG-rFVIIa and 40 kDa PEG-rFVIIa versus temperature at 286 nm in 10 mM HIS, 35 mM CaCl$_2$, pH 5.75 and 10 mM HIS, 100 mM CaCl$_2$, pH 5.75. The temperature dependent near-UV CD signals appears to be independent of the CaCl$_2$ concentration, but different from the unmodified protein to the GlycoPEGylated proteins. The thermally induced unfolding of the two GlycoPEGylated proteins are alike. Differentiating the CD signal with respect to the temperature gives an estimate of the unfolding temperature, see table 6.1. Similar results are obtained in 10 mM HIS, 10 mM CaCl$_2$, pH 5.75 [164].

the unfolding temperature based on the thermally induced structural changes, see table 6.1.

The DSC thermograms and the LS intensity data are plotted in the same figure (figure 6.4). The effect of CaCl$_2$ on the thermal stability of rFVIIa, 10 kDa PEG-rFVIIa and 40 kDa PEG-rFVIIa is investigated by DSC. From the resulting thermograms it is evident, that the thermal stability of rFVIIa depends on both CaCl$_2$ content and Glyco-PEGylation (figure 6.4). The apparent unfolding temperature of rFVIIa decreases at 35 mM and 100 mM CaCl$_2$ compared to 10 mM CaCl$_2$, whereas 10 kDa PEG-rFVIIa and 40 kDa PEG-rFVIIa are not thermally destabilised until the CaCl$_2$ concentration reaches 100 mM. There is a substantial difference between the appearances of the thermograms after T$_m$ has been reached. From the DSC thermograms and the LS intensities for the GlycoPEGylated rFVIIa compounds (figure 6.4) it appears that GlycoPEGylation delay the thermally induced aggregation of rFVIIa at 10 mM CaCl$_2$ and 35 mM CaCl$_2$. At 100 mM CaCl$_2$ the unmodified rFVIIa and the GlycoPEGylated rFVIIa compounds display similar aggregation behaviour.
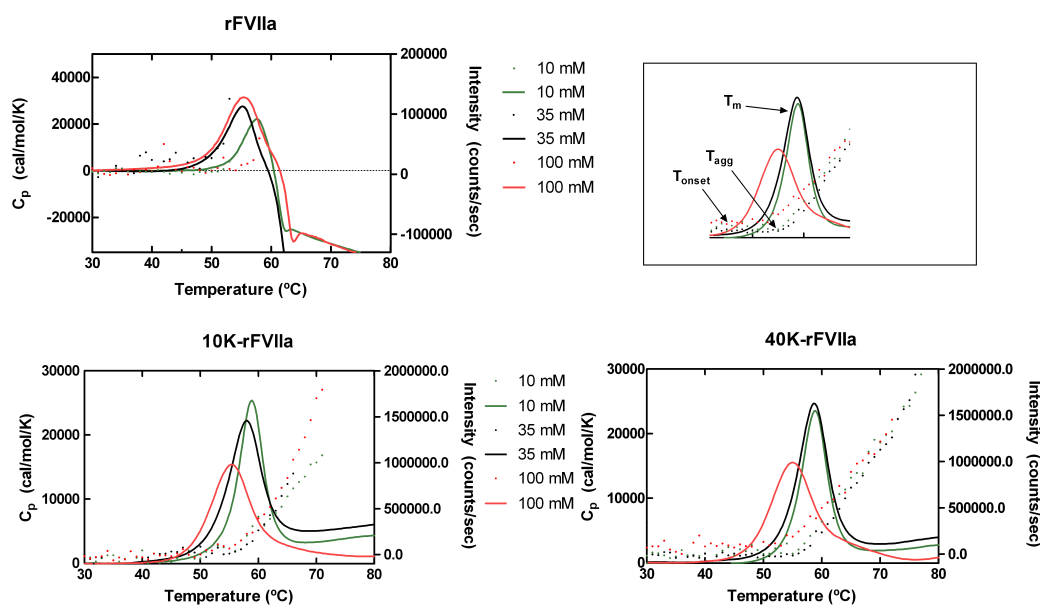
Figure 6.4: DSC thermograms and LS intensity measurements of rFVIIa, 10 kDa PEG-rFVIIa and 40 kDa PEG-rFVIIa as a function of temperature in buffers with 3 different $CaCl_2$ concentrations. The dotted line correspond to the LS intensity, the solid line correspond to the DSC thermogram. The insert illustrate where the onset temperature, T_{onset}, the temperature of aggregation, T_{agg}, and the apparent unfolding temperature, T_m, are found. The rFVIIa aggregates formed close to T_{agg} were too large for the LS detector to measure, and continuous intensity measurements as a function of temperature were impossible after 53 ℃ for rFVIIa. The obtained results at 10 mM HIS, 10 mM $CaCl_2$, pH 5.75 are from [164]

6.4 Discussion

The effect of $CaCl_2$ on the thermal, structural and kinetic stability of rFVIIa was measured by three complementary techniques; DSC, CD and LS. The three different measurement types illustrate each different aspect of the unfolding or aggregation processes. The unfolding and aggregation pathway can be illustrated by a model put forward by Lumry and Eyring in 1954. According to the Lumry Eyring model, irreversible protein denaturation involves at least two steps. The first step is the reversible unfolding of the native protein (N), characterised by the rate constants, k_1 and k_2. This step is followed by an irreversible change of the unfolded protein (D), into an inactivated, irreversible aggregate (A), a step characterised by the rate constant k_3. The unfolded state is characterised by having some non-native residual tertiary structure.

It is our experimental approximation, that the aggregation is measured by LS; the unfolding is measured by CD, whereas DSC measures unfolding, an endothermic event, as well as aggregation, an exothermic event. We hypothesize, that during the heating scan there

	T$_m$ (℃) (CD)	T$_{onset}$ (℃) (DSC)	T$_m$ (℃) (DSC)	ΔH (kJ/mol) (DSC)	T$_{agg}$ (℃) (LS)	(T$_{onset}$-T$_{agg}$)
10 mM CaCl$_2$ [a]						
rFVIIa	60.3±0.2	50.9±0.2	57.7±0.2	NA	50.8±0.4	0.1
10 kDa PEG-rFVIIa	59.9±0.2	53.3±0.1	59.0±0.2	140	57.1±0.2	-3.8
40 kDa PEG-rFVIIa	60.7±0.2	52.9±0.1	59.0±0.2	134	57.9±0.9	-5
35 mM CaCl$_2$						
rFVIIa	59.9±0.2	49.0±0.1	55.2 ±0.2	NA	49.8±0.7	-0.8
10 kDa PEG-rFVIIa	59.3±0.2	51.0± 0.1	58.0 ±0.2	140	56.8±0.3	-5.8
40 kDa PEG-rFVIIa	59.3±0.2	52.3±0.1	58.6±0.2	153	57.7±0.2	-5.4
100 mM CaCl$_2$						
rFVIIa	61.5±0.2	48.3±0.1	55.1±0.2	NA	59.3±0.4	-11
10 kDa PEG-rFVIIa	59.9±0.2	47.6±0.2	55.3±0.2	147	59.2±0.4	-11.6
40 kDa PEG-rFVIIa	59.7±0.2	47.1±0.1	55.0±0.2	156	56.7±0.2	-9.6

[a] From Plesner et al. [164]

Table 6.1: The apparent unfolding temperature, T$_m$, measured by CD, the onset temperature T$_{onset}$, the T$_m$ and corresponding enthalpy measured by DSC, the aggregation temperature, T$_{agg}$, measured by LS and the difference between T$_{onset}$ and T$_{agg}$. The extraction of the enthalpy of unfolding of rFVIIa is not possible due to the irreversibility of the denaturation process.

is an equilibrium between the native (N) and the unfolded (D) state, which shifts towards unfolding as the temperature increases. This process is followed by the irreversible step from unfolding (D) to aggregation (A), which is also temperature driven. Our experimental results show that an increasing CaCl$_2$ influences at least two of the three rate constants mentioned above.

$$N \underset{k_2}{\overset{k_1}{\rightleftharpoons}} D \overset{k_3}{\rightarrow} A \qquad K = \frac{k_1}{k_2}$$

Figure 6.5: The Lumry Eyring model, N is the native protein, D is the denatured protein and A is the aggregated protein.

The thermally induced unfolding of rFVIIa and GlycoPEGylated rFVIIa at three different CaCl$_2$ concentrations is measured by CD (figure 6.2), and is further illustrated by the changes in the CD signal at 286 nm (figure 6.3). The CD heating scans show that the non-modified rFVIIa undergo a conformational change in the tertiary structure around the apparent unfolding temperature and no tertiary structure can be detected at higher

temperature. This trend is observed at all calcium concentrations. As the physical appearance of the rFVIIa solution upon heating was milk-white, the non-detectable tertiary structure above 70 ℃ could be a sign of temperature induced aggregation. The Glyco-PEGylated rFVIIa compounds, on the other hand, seems to maintain some non-native residual tertiary structure upon unfolding as the CD signal stabilises around 5000 Θ cm^{-2} mol^{-1} (figure 6.3).

From the DSC and LS results obtained in 10 mM and 35 mM CaCl$_2$ shown in figure 6.4, it is evident that both the apparent unfolding temperature, T$_m$, and the temperature of aggregation, T$_{agg}$, of the GlycoPEGylated rFVIIa compounds are higher that than of the unmodified protein. There is no notable difference between the 10 kDa GlycoPEGylated rFVIIa and the 40 kDa GlycoPEGylated rFVIIa. The increase in both T$_m$ and T$_{agg}$ with PEGylation is in accordance with previous studies [63, 91, 152]. The combined DSC and LS results in figure 6.4 illustrate that the thermally induced aggregation event for rFVIIa begins while endothermic processes dominates. The formation of aggregates will contribute exothermally to the total heat signal. As the heat measured by DSC is the total contribution from both unfolding and aggregation, an extensive formation of aggregates beginning shortly after T$_{onset}$ may shift the location of the peak in the thermogram towards a lower temperature. Increasing the CaCl$_2$ concentration from 10 mM to 35 mM result in a minor decrease in both T$_m$ (measured by DSC) and T$_{agg}$ for rFVIIa, most pronounced is the decrease in T$_m$. Thus, increasing the CaCl$_2$ concentration appears to result in a decrease in the thermal stability of rFVIIa.

At 100 mM CaCl$_2$ the apparent unfolding temperature measured by DSC is similar for rFVIIa, 10 kDa GlycoPEGylated rFVIIa and 40 kDa GlycoPEGylated rFVIIa. The thermal stability of the GlycoPEGylated rFVIIa compounds increases compared to thermal stability of rFVIIa, when the CaCl$_2$ concentration is increased from 10 mM to 35 mM. The GlycoPEGylated compounds are not thermally destabilised until the concentration of CaCl$_2$ reaches 100 mM. In addition the thermally induced aggregation of all the investigated compounds appears to occur at a higher temperature at 100 mM CaCl$_2$ compared to the lower calcium concentrations.

It is noticeable how both the native rFVIIa and the GlycoPEGylated rFVIIa compounds display different aggregation behaviours at 100 mM CaCl$_2$. At 100 mM CaCl$_2$ the thermally induced aggregation does not only set in at a higher temperature for all the investigate proteins, native and GlycoPEGylated, the difference between T$_{onset}$ and T$_{agg}$ is 10-11 degrees as opposed to 1-5 degrees at lower CaCl$_2$ concentrations. Based on the LS and DSC measurements it is suggested that rFVIIa (unmodified and GlycoPEGylated) in general is stabilised by electrostatic interactions which are weakened by the addition of CaCl$_2$, and that CaCl$_2$ might interact preferentially with the protein in the unfolded state, 'D'. Both effects stabilise the aqueous 'D' state, as the equilibrium constant K increases and the rate constant k$_3$ decreases with increasing calcium concentration, leading to a lower apparent T$_m$ and a higher T$_{agg}$.

Based on the results obtained in this study it seems reasonable to assume that the equilibrium constant K, reflecting the equilibrium between the native and the unfolded protein, is independent of the increase in CaCl$_2$ content from 10 mM to 35 mM as well as independent of GlycoPEGylation, since unfolding process for rFVIIa appears to be similar, whether the protein is GlycoPEGylated or not (fig. 6.3). The rate constant k$_3$, on the other hand, describing the step from unfolding to aggregation, decreases dramatically when the protein is GlycoPEGylated. And k$_3$ of rFVIIa is markedly decreased as the CaCl$_2$ concentration is increased from 35 mM to 100 mM, where T$_{agg}$ increases from $\sim 50\,°C$ at 10 mM and 35 mM CaCl$_2$ to $\sim 59\,°C$ at 100 mM CaCl$_2$. From the LS results in figure 6.4, it is evident, that the formation of aggregates is affected by GlycoPEGylation as well as CaCl$_2$ content. At 10 mM and 35 mM CaCl$_2$ the thermally induced rFVIIa aggregates formed close to T$_{agg}$ were too large for the LS detector to measure, and continuous intensity measurements as a function of temperature were impossible. As the light scattering increases with the sizes of the formed aggregates [155], a high intensity count corresponds to large aggregates. The increase in the LS intensity is much slower for the GlycoPEGylated rFVIIa compounds in general, thus the formation of thermally induced aggregates is reduced and happens at a lower rate. At 100 mM CaCl$_2$ the formation of thermally induced rFVIIa aggregates seems to follow a similar pattern as the GlycoPEGylated rFVIIa compounds. The aggregates are formed slower and to a lower extent compared to the aggregates formed at lower CaCl$_2$ concentration.

6.5   Conclusion

Recombinant human Factor VIIa was GlycoPEGylated with two different PEG polymers, a 10 kDa linear PEG and a 40 kDa branched PEG, and the stability of these compounds was investigated at three different CaCl$_2$ concentrations. The addition of salt, CaCl$_2$, seems to have the same effect on the stability of rFVIIa, regardless of GlycoPEGylation. However, the thermal destabilising effect and postponed aggregation appear to be depending on the concentration of CaCl$_2$ once the protein is GlycoPEGylated. The thermal and kinetic effects of increasing the CaCl$_2$ concentration is found at 35 mM for rFVIIa, whereas the concentration of CaCl$_2$ has to be raised to 100 mM in order to see the same effect on the GlycoPEGylated rFVIIa compounds. Thus GlycoPEGylation postpones the calcium induced thermal destabilisation of rFVIIa, and a sufficiently high calcium concentration also postpones the aggregation of rFVIIa.

Acknowledgements

7   The hydrodynamic volume changes of Factor VIIa due to GlycoPEGylation

Bitten Plesner[a,b], Peter Westh[a], Søren Hvidt[a], Anders D. Nielsen[b,†]
[a]Department of Science, Roskilde University, P.O. Box 260, Universitetsvej 1, DK-4000 Roskilde, Denmark
[b]Novo Nordisk A/S, Novo Nordisk Park, DK-2760 Maaloev, Denmark

[†]Corresponding author. Tel.: +45 30 79 65 75; fax: +45 44 43 40 73
Email address: ADNi@novonordisk.com (A. D. Nielsen).

Abstract

The effects of GlycoPEGylation on the molar hydrodynamic volume of recombinant human rFVIIa were investigated using rFVIIa and two GlycoPEGylated recombinant human FVIIa derivatives, a linear 10 kDa PEG and a branched 40 kDa PEG, respectively. Molar hydrodynamic volumes were determined by capillary viscometry and mass spectrometry. The intrinsic viscosities of rFVIIa, its two GlycoPEGylated compounds, and of linear 8 kDa, 10 kDa, 20 kDa and branched 40 kDa PEG polymers were determined. The measured intrinsic viscosity of rFVIIa is 6.0 mL/g, while the intrinsic viscosities of 10 kDa PEG-rFVIIa and 40 kDa PEG-rFVIIa are 29.5 mL/g and 79.0 mL/g, respectively. The intrinsic viscosities of the linear PEG polymers are 20, 22.6 and 41.4 mL/g for 8, 10, and 20 kDa, respectively, and 61.1 mL/g for the branched 40 kDa PEG. From the results of the intrinsic viscosity and MALDI-TOF measurements it is evident, that the molar hydrodynamic volume of the conjugated protein is not just an addition of the molar hydrodynamic volume of the PEG and the protein. The molar hydrodynamic volume of the GlycoPEGylated protein is larger than the volume of its composites. These results suggest that both the linear and the branched PEG are not wrapped around the surface of rFVIIa but are chains that are significantly stretched out when attached to the protein.

Keywords: GlycoPEGylation, rFVIIa, intrinsic viscosity, molar hydrodynamic volume, capillary viscometry

7.1 Introduction

Coagulation factor VIIa (FVIIa) is a trypsin-like serine protease, which in the presence of calcium initiates the blood coagulation when associated with its cofactor tissue factor (TF) which is exposed upon vascular injury [146, 147]. TF-bound FVIIa activates factor IX and factor X resulting in a burst of thrombin, fibrin deposition and the formation of a haemostatic plug on the surface of activated platelets [146]. Deficiencies in the coagulation system due to partial or complete deficiency of FVIII or FIX, haemophilia A or haemophilia B respectively can lead to severe morbidity or mortality if the bleeding is left untreated. A safe and efficient way to prevent bleeds and joint destruction in haemophilia is with the use of prophylaxis giving FVIII or FIX 2-4 times weekly [148]. Recent studies have shown that prophylactic treatment with recombinant FVIIa (rFVIIa, (NovoSeven®)) of haemophilia patients with inhibitors reduces the frequency of bleedings significantly as compared to conventional on-demand haemostatic therapy [149]. However, based on the half-life and circulation time of rFVIIa (2-4 h), it is assumed that rFVIIa should be administered daily if used for long-term prevention [149, 150]. Hence, development of rFVIIa derivatives with longer circulation time could result in both fewer administrations and better patient compliance. Modification of pharmaceutical proteins with hydrophilic polymers such as poly-ethylene-glycol (PEGylation) is an established method for prolonging circulatory half-life, reducing self-aggregation, increase water solubility and increase stability [82, 117]. Due to the risk of losing activity of FVIIa because of the numerous interactions with the cell surface, TF, FIX and FX there is a limitation in the unspecific chemical modification of this protein. For this reason a novel strategy for site-directed PEGylation using glycosyltransferases to attach PEG to glycan residues, the enzyme based Glyco-PEGylation technology is used to covalently attach either a linear 10 kDa or a branched 40 kDa PEG polymer to rFVIIa. The site of PEG attachment to rFVIIa is demonstrated to be one of the two N-linked glycans of rFVIIa (Asn145 or Asn322) located on the light chain and heavy chain, respectively [64]. It is assumed that the specific location of the GlycoPEGylation site and presence of small amounts of di-GlycoPEGylated species are irrelevant in relation to the overall interpretation of the results obtained in this study. Most of the benefits of PEGylated proteins reflect the properties of the PEG polymer itself [60] and the hydration of the PEG chain determines the overall hydrodynamic properties of PEG bioconjugates [59, 61]. The underlying mechanisms for the effect of PEG is not fully understood, but it is evident that the hydrodynamic radius is significantly increased by PEG leading to reduced clearance, especially of smaller proteins [63].

When developing a pharmaceutical protein solution intended for injection, the viscosity of the solution plays a key role. The final viscosity of an aqueous protein solution can be estimated from knowledge of the intrinsic viscosity or the molar hydrodynamic volume of the protein in question together with the concentration of protein in solution. Investigations regarding possible changes in the molar hydrodynamic volume of rFVIIa upon GlycoPEGylation are of high relevance in the drug development process. The present work examines the change in molar hydrodynamic volume of rFVIIa upon GlycoPEGylation by measuring the intrinsic viscosity and the molar mass of rFVIIa, PEG and GlycoPEGylated rFVIIa.

7.2   Materials and Methods

Materials

rFVIIa, 10 kDa GlycoPEGylated rFVIIa and 40 kDa GlycoPEGylated rFVIIa were produced by Novo Nordisk A/S, Denmark, as described in [64]. L-Histidine was purchased from Aijonomoto AminoScience (Raleigh, N.C.), and calcium chloride-dihdyrat was purchased from Merck (Germany). Barium chloride 20 w/w solution from Ampliqon (Denmark), 0.1 N iodine solution from Sigma-Aldrich (Germany), 70 % perchloric acid from Merck (Germany), LDS sample buffer and MES SDS running buffer and Simple Blue Safe Stain are all from Invitrogen (Carlsbad, CA). All protein solutions were dialysed in Slide-A-Lyzer$^{\mathrm{TM}}$ 30.000 MWCO dialyse cassettes against the 10 mM HIS, 100 mM CaCl$_2$ adjusted to pH 5.75. The PEG-rFVIIa solutions were subsequently concentrated in Amicon cells with 30.000 MWCO, while rFVIIa was concentrated and buffer exchanged with a Tangential Flow Filtration system using a 0.1 m^2 30.000 MWCO membrane. Linear Polyethylene glycol 8 kDa was purchased from Amresco (Solon, OH), polyethyleneglycol 10 kDa and 20 kDa were purchased from Merck (Germany), branched polyethyleneglycol 40 kDa (GL2-400CA) was purchased from NOF Corporation (Japan).

SDS-PAGE

SDS-PAGE analysis was carried out using a 12 % Bis-Tris gel from Invitrogen. The gels were loaded with an average of 5 μg per well and run at 120 mA constant current per gel. The running buffer was MES running buffer. The gel was washed in 150 mL 0.1 M perchloric acid for 15 minutes until 40 mL 5 % barium chloride solution and 15 mL 0.1 M iodine solution were added to detect protein bands containing PEG compounds, as described in [141]. After removal of excess colouring in water, the gel was coloured with Coomassie blue.

MALDI-TOF MS

Mass spectrometric analysis was performed on a Bruker Daltonics Microflex MALDI-TOF (Billerica, MA) instrument equipped with a nitrogen laser (337 nm). The instrument was operated in linear mode with delayed extraction, and the accelerating voltage in the ion source was 25 kV. Sample preparation was done as follows: 1 μL sample-solution was mixed with 10 μL matrix-solution (alphacyano-cinnamic acid dissolved in a 5:4:1 mixture of acetonitrile:water:3% TFA) and 1 μl of this mixture was deposited on the sample plate and allowed to dry before insertion into the mass spectrometer. Calibration was performed using external standards (a range of standard proteins) and the resulting accuracy of the mass determinations is within 0.1%.

Capillary viscometry

The viscosity measurements were performed with a Micro-Ubbelohde Schott 53b 10/l capillary viscometer. The flow times varied from 90 sec to 280 sec, and the reproducibility was $\pm$ 0.2 sec for the pure PEG solutions and $\pm$ 1 sec for the rFVIIa and GlycoPEGylated

rFVIIa solutions. The dimensions of this viscometer are such that the kinetic correction can be neglected [165]. Viscosity measurements were carried out at 25.0 ± 0.1 ℃ in a constant temperature water bath. The viscosity values, η, of the various solutions were determined from the flow times of the solvent (t_s) and of the solutions (t) for low concentrations of the high PEG MW solutions, and higher concentration for short PEG MW solutions. The time was measured with a quartz stopwatch. 5 different concentrations of each solute were measured, and each flow time measurement was repeated three times. The concentrations of the GlycoPEGylated rFVIIa species are all based on the total weight concentration of the complex (protein and PEG).

7.3   Results

After dialysis the purities of the proteins were determined by SDS-PAGE and by MALDI-TOF MS.

SDS-PAGE

The apparent molar mass of GlycoPEGylated proteins was assessed by SDS-PAGE [154]. It is assumed that the higher molecular weight gel bands represent one (or more) molar incremental addition of PEG to the protein.

The PEG-staining gel technique is based on the complex formation between PEG and barium iodide, and the PEG-stained gel (figure 7.1a) reveals that only lanes 3 and 4 contain PEG-compounds. It has previously been shown, that PEG binds to SDS micelles [142] and that PEGylation decreases the mobility of the protein [141, 143]. For this reason the apparent molecular weight of a PEGylated protein on a SDS gel will not correspond to the actual molecular weight of the PEGylated protein. Due to the low mobility of the PEGylated protein, the location of a PEGylated protein on a SDS gel corresponds to the molecular weight of the protein plus 2.5 times the molecular weight of the attached PEG polymer. Comparing the results in the PEG-stained gel with the very same gel, only now Coomassie blue stained, it is evident, that the three bands in lane 3 (10 kDa PEG-rFVIIa) and the two bands in lane 4 (40 kDa PEG-rFVIIa) are GlycoPEGylated compounds of rFVIIa. From the results on the SDS-PAGE gel (figure 7.1b) it is seen that the rFVIIa sample was pure (> 95 %) and contained only rFVIIa with a molecular mass of 50 kDa. The third lane reveals that 10 kDa PEG-rFVIIa is not only mono-GlycoPEGylated. There are 3 different GlycoPEGylated species in this protein solution. These compounds have an apparent molecular weights of 75 kDa, 110 kDa and 125 kDa, respectively. This corresponds to mono-GlycoPEGylated 10 kDa PEG-rFVIIa (50 kDa + 2.5 x 10 kDa) ∼ 75 kDa, di-GlycoPEGylated 10 kDa PEG-rFVIIa (50 kDa + 2.5 x 2 x 10 kDa) ∼ 110 kDa and tri-GlycoPEGylated rFVIIa (50 kDa + 2.5 x 3 x 10 kDa) ∼ 125 kDa. The fourth lane contains mainly mono-GlycoPEGylated 40 kDa PEG-rFVIIa with a molecular weight of (50 kDa + 2.5 x 40 kDa) ∼ 160 kDa but also a very small amount of di-GlycoPEGylated 40 kDa GlycoPEGylated rFVIIa at (50 kDa + 2.5 x 2 x 40 kDa) ∼ 250 kDa.
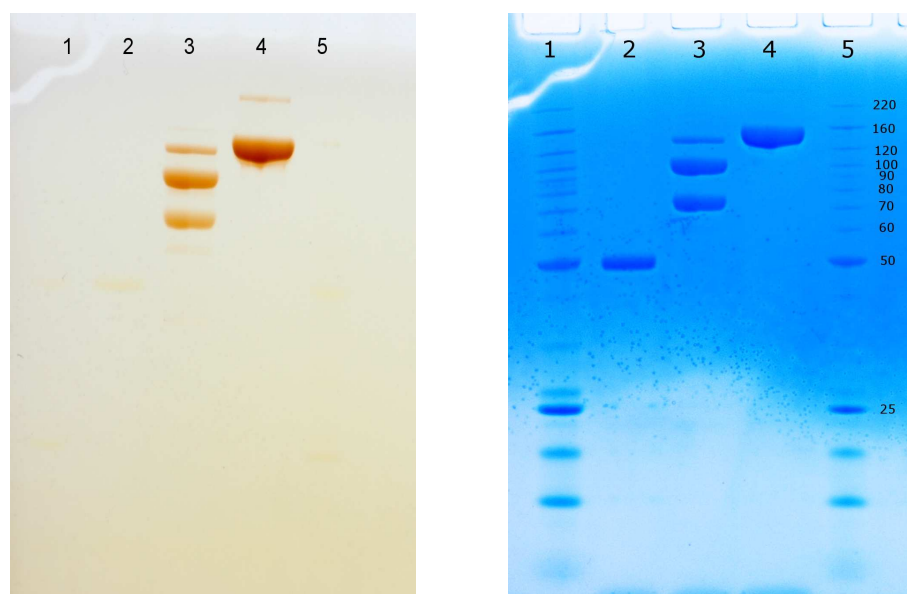
(a) PEG stained gel. The gel is stained with iodide as described in [141].

(b) SDS PAGE of PEGylated rFVIIa.

Figure 7.1:
Lane 1 and 5, bench mark protein ladder.
Lane 2: rFVIIa.
Lane 3: 10 kDa PEG-rFVIIa.
Lane 4: 40 kDa PEG-rFVIIa.
The gel is stained with iodine (fig. 7.1a), discoloured in water and subsequently stained with Coomassie blue (fig. 7.1b).

MALDI-TOF

The results of the MALDI-TOF MS spectra of rFVIIa, 10K-rFVIIa and 40K-rFVIIa are shown in figure 7.2.

The MALDI-TOF MS spectrum of rFVIIa shows one dominating peak, at 49.4 kDa, equivalent to the expected molecular mass of rFVIIa [166]. Its peak pattern corresponds to different charges, e.g. 16606 Da peak corresponds to triple charged rFVIIa, 24787 corresponds to double charged rFVIIa and 49433 corresponds to single charged. The 10 kDa PEG-rFVIIa solution contains a monoPEGylated, 61 kDa, and smaller amounts of a di-GlycoPEGylated compound, at 73 kDa. The peak at 36400 corresponds to double charged di-GlycoPEGylated rFVIIa, and the 30529 and 20389 are double and triple charged mono-GlycoPEGylated rFVIIa, respectively. The 40 kDa PEG-rFVIIa solution contains mono-GlycoPEGylated 40 kDa PEG-rFVIIa, which is seen as the 92 kDa peak. Peaks at 46 and 31 kDa are assigned to double and triple charged mono-GlycoPEGylated 40 kDa PEG-rFVIIa.
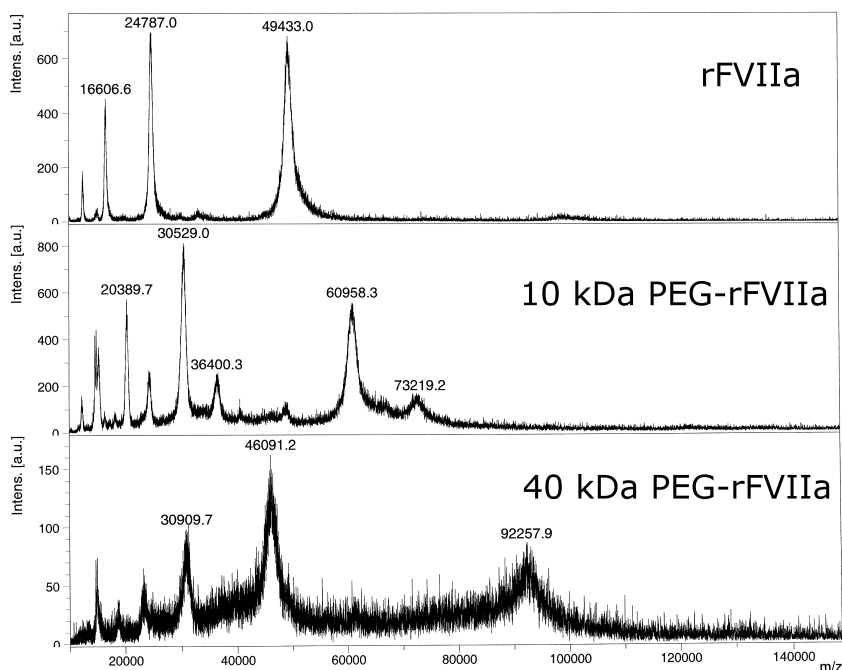
Figure 7.2: MALDI-TOF spectra of rFVIIa, 10 kDa PEG-rFVIIa and 40 kDa PEG-rFVIIa, see text for further details.

The MS spectrum of 10 kDa PEG-rFVIIa shows two peaks, one at 61 kDa, corresponding to a mono-GlycoPEGylated 10 kDa PEG-rFVIIa, and a smaller peak at 73 kDa corresponding to a di-GlycoPEGylated 10 kDa PEG-rFVIIa. The MS spectrum of 40 kDa PEG-rFVIIa illustrates, that only mono-GlycoPEGylated 40 kDa rFVIIa can be detected. The amount of di-GlycoPEGylated 40 kDa PEG-rFVIIa is too small to be detected by MS.

MALDI-TOF spectra for pure PEG samples are summarised in table 7.1 (data not shown).

Intrinsic Viscosity

The intrinsic viscosity of samples of pure PEG, rFVIIa and GlycoPEGylated rFVIIa compounds was measured with an Ubbelohde Capillary viscometer. Values of the intrinsic viscosity, $[\eta]$, were found by plotting the measured reduced viscosities according to the Huggins method [167]:

$$\frac{\eta_{\text{sp}}}{\text{c}} = [\eta] + \text{k}_1[\eta]^2\text{c} \tag{7.1}$$

and also by plotting the inherent viscosities according to the Kraemer method [168]:

$$\frac{\ln \eta_{\text{r}}}{\text{c}} = [\eta] + \text{k}_1[\eta]^2\text{c} \tag{7.2}$$

where $\eta_{\mathrm{sp}} = \frac{\eta - \eta_{\mathrm{s}}}{\eta}$, $\eta_{\mathrm{r}} = \frac{\eta}{\eta_{\mathrm{s}}}$, η is the viscosity of the solution, and η_{s} is the viscosity of the solvent, respectively. The Huggins and Kraemer constant are k_1 and k_2, respectively. Kraemer and Huggins plot were made from the measured solution viscosities at different concentrations, and the common intercept is the intrinsic viscosity $[\eta]$. The results obtained for rFVIIa and 40 kDa GlycoPEGylated rFVIIa solutions are seen in figure 7.3.
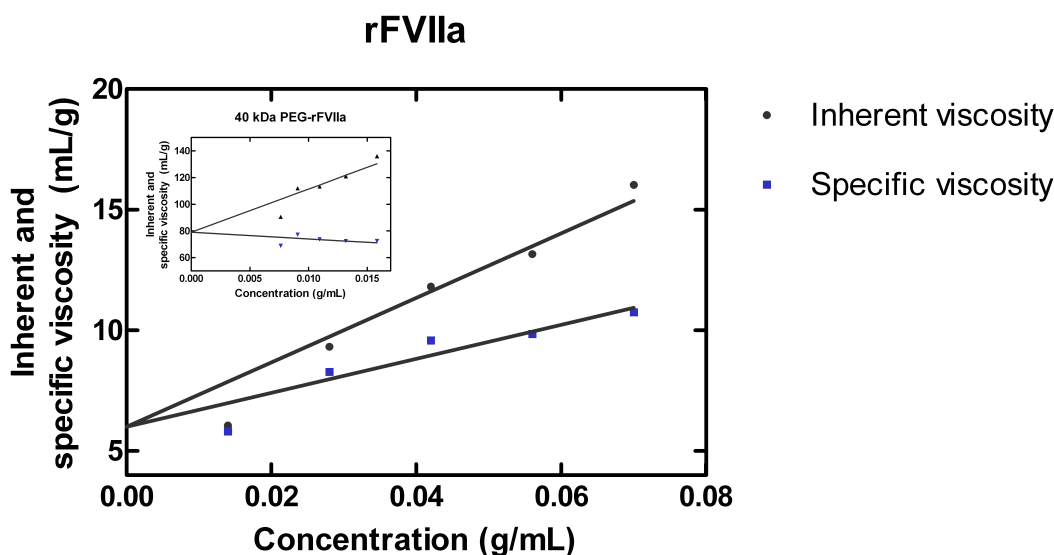
Figure 7.3: The measured viscosity is plotted as a function of concentration of rFVIIa. The insert shows the viscosities of 40 kDa PEGylated rFVIIa. Kraemer and Huggins plot were made from the measured solution viscosities at different concentrations, and the common intercept is $[\eta]$. Note the different y-axis ranges.

The intrinsic viscosities were determined for rFVIIa, 10 and 40 kDa GlycoPEGylated rFVIIa and the pure PEG samples of similar molecular weight; see table 7.1 and figure 7.4. The intrinsic viscosities, $[\eta]$, were found by the common intercepts from the Kraemer and Huggins plot and are an average of two intercepts. The deviations in the determination of the molar hydrodynamic volume are based on the deviations in the determination of the intrinsic viscosities. The molecular mass multiplied with the intrinsic viscosity gives the molar hydrodynamic volume.

From the results in table 7.1 it is evident, that the molar hydrodynamic volume (V_{H}) of the conjugated protein is not just an additio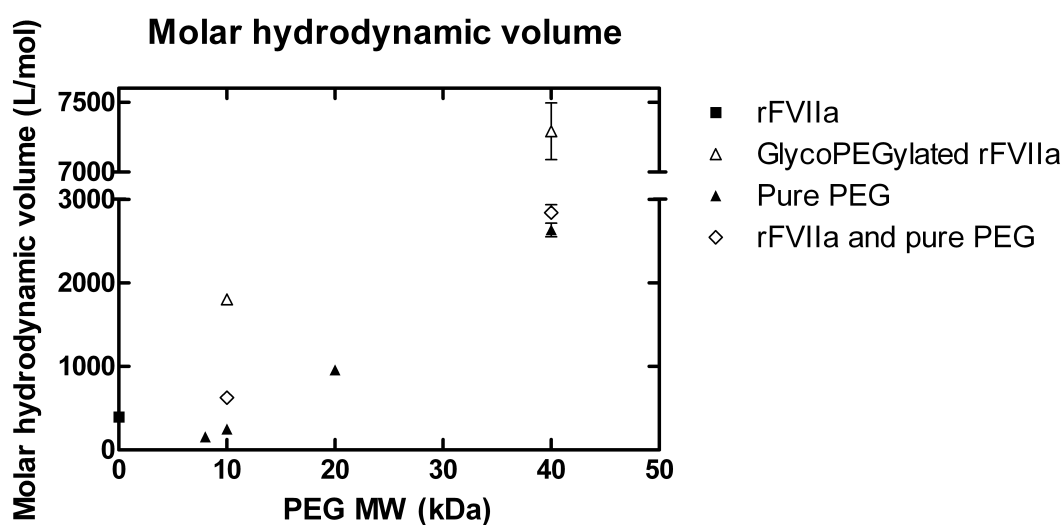n of the molar hydrodynamic volume of the PEG polymer and the protein. In figure 7.4 the molar hydrodynamic volume of rFVIIa, the two GlycoPEGylated rFVIIa compounds and pure PEG are plotted as a function of PEG molecular weight, zero molecular weight corresponds to the non-modified rFVIIa.

	MW (kDa)	$[\eta]$(mL/g)	V_H (L/mol)
8 kDa linear PEG	8	19.8 ± 0.15	160
10 kDa linear PEG	10	22.8 ± 0.8	228
20 kDa linear PEG	20	41.5 ± 0.5	827
40 kDa branched PEG	40	61.1 ± 1.9	2442
rFVIIa	50	6.0 ± 0.3	301
10 kDa PEG-rFVIIa	60	29.5 ± 0.9	1770
40 kDa PEG-rFVIIa	90	79.0 ± 2.2	7111

Table 7.1: The molecular weight, the intrinsic viscosity and the corresponding molar hydrodynamic volume of pure PEG (linear and branched), rFVIIa and GlycoPEGylated rFVIIa. The molecular mass multiplied with the intrinsic viscosity gives the molar hydrodynamic volume.

Figure 7.4: The molar hydrodynamic volume of rFVIIa, the two GlycoPEGylated rFVIIa compounds and pure PEG polymers are plotted as a function of the PEG molar mass. The native protein is placed at PEG molar mass zero. The diamonds are the total molar hydrodynamic volume of rFVIIa and pure PEG. The error bars are generally so small that they are hidden behind the symbols.

The molar hydrodynamic volumes, V_H, plotted in figure 7.4 illustrate that V_H of the GlycoPEGylated rFVIIa is larger than the total V_H of its composites. The molar hydrodynamic volume of the protein-PEG complex is approximately 2.5 times larger than the sum of its two components.

7.4 Discussion

From the intrinsic viscosity and the molar mass measured by MALDI-TOF, the molar hydrodynamic volume was calculated. The molar hydrodynamic volume of rFVIIa increases markedly with GlycoPEGylation, and the molar hydrodynamic volume of 40 kDa PEG-rFVIIa is larger than that of 10 kDa PEG-rFVIIa. When dissolving a PEG polymer or a protein in an aqueous solution, the molecule occupies a certain hydrodynamic volume determined by the molecular weight and the intrinsic viscosity of the molecule. By covalently attaching a PEG moiety to the protein the molar hydrodynamic volume of the protein itself will increase unavoidably. Our intrinsic viscosity and MALDI-TOF data indicate that the molar hydrodynamic volume is not just an addition of the molar hydrodynamic volume of PEG and protein, respectively. This observation is in accordance with studies done on PEGylated haemoglobin [169]. From table 7.1 it is evident that the V_H of both 10 kDa PEG-rFVIIa and 40 kDa PEG-rFVIIa is more than 2.5 times larger than the total V_H of rFVIIa and linear 10 kDa PEG or branched 40 kDa, respectively.

One of the basic characteristics of the PEG polymer is its ability to bind two to three water molecules per ethylene glycol unit [170]. These properties are transferred to the protein-PEG complex upon PEGylation, leading to a molecule with an effective molar hydrodynamic volume that increases up to 2-3 times in this study. We suggest that this significant increase in molar hydrodynamic volume indicates that the grafted PEG polymer is not wrapped around the protein; on the contrary it appears as though it is stretched out from the protein to which it is attached. This hypothesis is illustrated in figure 7.5. If the very hydrophilic PEG was wrapped around the protein, then it would have only little effect on the total molar hydrodynamic volume of the PEGylated protein. On the other hand, if the PEG polymer was located as a 'polymer cloud' next to the protein and thus stretched out from the protein, then the polymer would contribute significantly to the intrinsic viscosity.

The increase in molar hydrodynamic volume of rFVIIa upon GlycoPEGylation seems to be independent of the shape of the PEG polymer as the molar hydrodynamic volumes of both GlycoPEGylated species appear to be approximately 2.5 times larger than its composites.

To illustrate the change in viscosity of rFVIIa with GlycoPEGylation, the viscosity of rFVIIa, GlycoPEGylated rFVIIa (10 kDa and 40 kDa) and pure PEG at 10 mg/mL are plotted as a function of PEG molar mass (fig. 7.6). The viscosity at 10 mg/mL based on the experimental measurements (Huggins and Kraemer constants) described in the section 7.2, Materials and Methods.

rFVIIa

10 kDa linear PEG
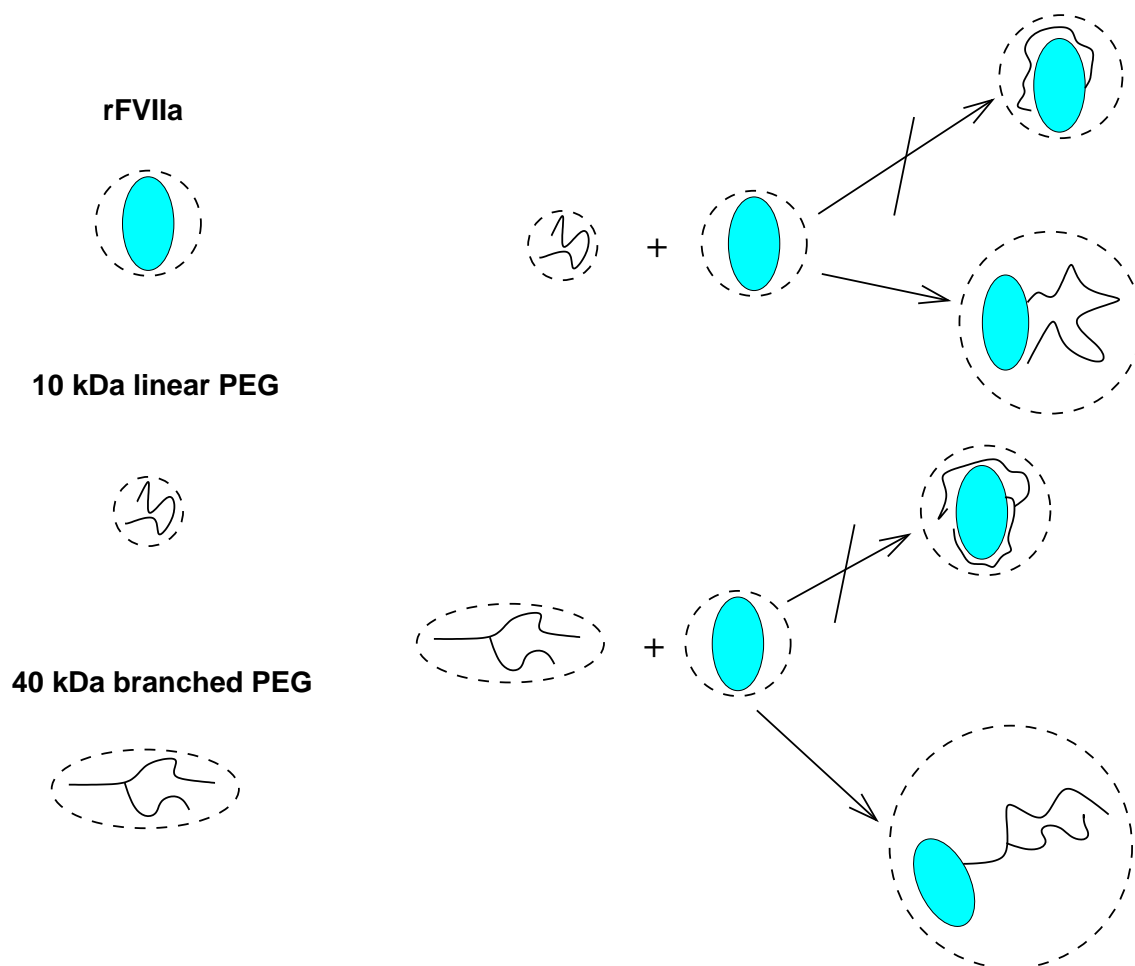
40 kDa branched PEG

Figure 7.5: The molar hydrodynamic volume of rFVIIa, pure PEG and GlycoPEGylated rFVIIa. The molar hydrodynamic volumes of the conjugated protein indicate that the PEG polymer is not wrapped around the protein, on the contrary it appears to be stretched out from the protein surface.
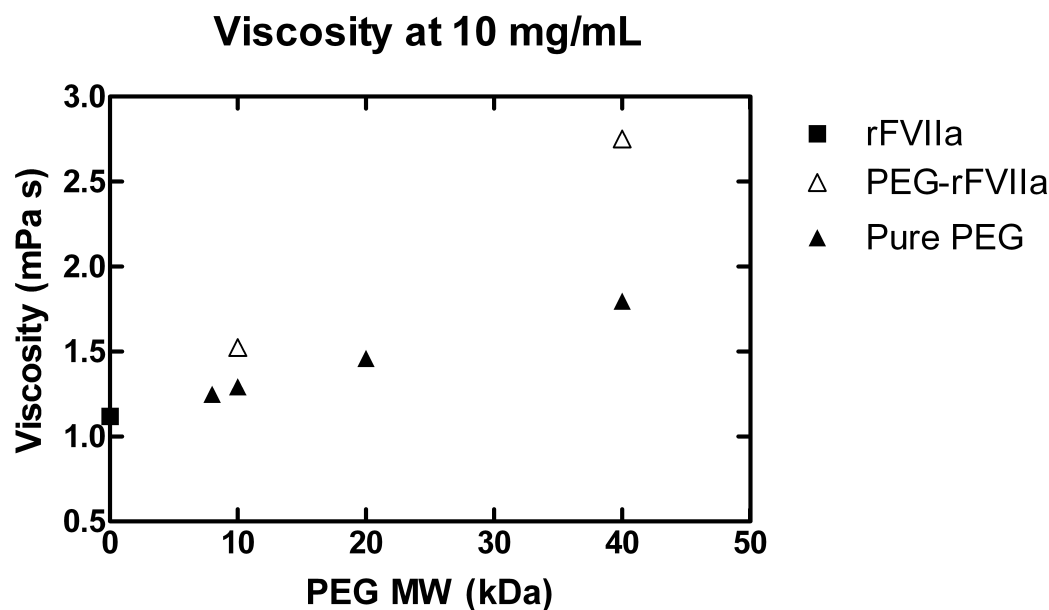
Viscosity at 10 mg/mL

Figure 7.6: The viscosities of pure PEG, unmodified rFVIIa and GlycoPEGylated rFVIIa at 10 mg/mL are plotted as a function of PEG molar mass. The concentrations for the two PEG-protein solutions are based on protein concentrations in the complex. The rFVIIa at zero molar mass is the unmodified rFVIIa. All viscosities at 10 mg/mL are calculated from the Ubbelohde viscometer measurements.

From the results represented in figure 7.6, it is clear that the viscosity of a 10 mg/mL protein solution increases significantly with GlycoPEGylation. The critical over-lap concentration, c^* $(1/[\eta])$, for 10 kDa GlycoPEGylated rFVIIa is approximately 33 mg/mL and 12 mg/mL for 40 kDa PEG-rFVIIa. Above this concentration the viscosity of the solution increases markedly with concentration as the solution reaches the semi-dilute regime.

If the overall purpose of PEGylating a pharmaceutical protein is increasing the circulation time while administration is through injection, a difficult balancing act arises. A large attached PEG will favourably increase the circulation time more than a smaller PEG, while the overall viscosity of the solution will increase unfavourably. The improved molar hydrodynamic properties of the protein conjugate will often result in an increased stability and thus favourable pharmacokinetic and immunological properties as compared to the unmodified protein [91]. However, the size and shape of the used PEG should be chosen as on the basis of which gives the best biological effect.

7.5   Conclusion

From the current study of the molar hydrodynamic volume of rFVIIa, pure PEG and GlycoPEGylated rFVIIa in solution it is evident, that the molar hydrodynamic volume of the conjugated protein is not just an addition of the molar hydrodynamic volume of the PEG and the protein. The molar hydrodynamic volume of the GlycoPEGylated protein is larger than the volume of its composites. These results suggest that both the linear and the branched PEG are not wrapped around the surface of rFVIIa but chains are significantly stretched out when attached to the protein.

Acknowledgements

8 Concluding remarks

As the title of this thesis implies the project has treated two different, but separately growing fields within protein pharmaceutics; highly concentrated protein solutions (Chapter 2) and PEGylated proteins in solution (Chapters 3, 4, 5, 6 and 7). The common feature is that all protein systems have been investigated using classical biophysical characterisation tools. To conclude the studies reported in this Thesis, future perspectives in relation to both highly concentrated protein solutions and PEGylated proteins solutions are given here.

The studies on highly concentrated lysozyme solutions were conducted to mimic the pharmaceutically relevant highly concentrated antibody solutions, and were initially intended as pilot experiments. However the surprising results that the unfolding temperature decreased with increasing protein concentration excited our curiosity and we continued working, hoping to find a reason for these unexpected findings. This was both exciting and challenging, and we did a number of experiments varying both the lysozyme and the salt concentration, trying to unravel the interplay between two opposite forces, the effect of excluded volume phenomena and the electrostatic interactions. During these experiments we discovered that the DSC scan of lysozyme under certain circumstances appeared to be biphasic, suggesting two domains of lysozyme unfolds. This unfolding behaviour was reversible, and the biphasic DSC scan reappeared even after heating, cooling and reheating the lysozyme sample.

It could be very interesting to do a more comprehensive study of the thermal stability of lysozyme in the pH range 2.5-4 as the surface charge difference between the native and unfolded state of the protein is pronounced here. By keeping the salt concentration at the lowest possible level, these experiments could be very complementary to those reported in chapter 2. By obtaining unfolding temperatures of lysozyme in the pH range mentioned above, we could attain a better picture of the thermal stability under these specifically interesting conditions. Meanwhile the use of zeta potentials measurements could be a great supplement to the surface charge values calculated by PropKa. Measuring the zeta potential of lysozyme at the different pH values and different salt concentrations could give a fine estimate of the real surface charges on lysozyme and assist in interpreting the results obtained by DSC. Studying the effect of salts in the Hofmeister series or di- and trivalent ions on the thermal stability would also be very relevant in order to see the effect on the surface charge of lysozyme.

Additionally experimental studies could include more heat scans with High Resolution Ultrasonic Spectroscopy (HRUS), as described in appendix A in order to get more infor-

mation on the formed soluble aggregates or heat scans with FTIR to determine possible changes in the secondary structure of the protein. As most of the other classical biophysical characterisation tools including CD and DLS need a substantially more dilute sample than the concentration of 40 mg/mL, which is the lowest used in these experiments, the number of useful experimental techniques is currently limited.

The effect of altering the salt concentration in the buffer was also investigated in the case with GlycoPEGylated rFVIIa (see chapter 6). As with lysozyme the thermal stability of rFVIIa and its GlycoPEGylated compounds was depending on the concentration of salt in the buffer. However, in this case the surface charge density was not the issue being in focus. Using $CaCl_2$ seemed like the most obvious salt to use when investigating different formulations of rFVIIa and GlycoPEGylated rFVIIa due to calcium's crucial role in the initiation of the blood coagulation cascade and because rFVIIa has specific binding sites for the Ca^{2+} ion. Still, it could be very interesting to investigate the effect of other salts like $MgCl_2$ and NaCl on the thermal stability of rFVIIa and its two GlycoPEGylated compounds. Comparing results obtained in a $MgCl_2$ or NaCl buffer with those obtained in $CaCl_2$ may clarify whether other di-valent ions can destabilise rFVIIa and GlycoPEGylated rFVIIa at high concentration, or if this is solely due to the interactions between $CaCl_2$ and rFVIIa.

The main focus in this thesis has been biophysical characterisation of PEGylated proteins using a range of disciplines ranging from calorimetry and spectroscopy to rheology and surface plasmon resonance. Throughout these investigations one main feature is consistent: There appears to no dependence on the molecular weight of the attached PEG polymer in the characteristics investigated. Intuitively one would expect that attaching a PEG polymer of similar size as the protein would have a different effect than attaching a PEG polymer, which size-vise is only a tenth of the molecular weight of the protein. But neither the structure, the apparent unfolding temperature nor the temperature of aggregation appear to be affected by the variations in PEG molecular weight. The only situation where a the molecular weight of the attached PEG seemed to have an effect was in the appearance of the DSC scan of PEGylated BSA. Here the biphasic appearance of the DSC scan changed slightly depending on the molecular weight of the PEG, the largest effect assigned the smallest PEG attached. This effect was interpreted along the lines of a smaller PEG stabilising the thermal unfolding of the two domains in BSA in a different way than a larger PEG. This effect is not found in the values of the apparent unfolding temperature, but purely by inspecting the DSC thermograms.

While some of these studies have focused on effects of protein PEGylation by changing the molecular weight of the attached linear PEG polymers, primarily, the exact same experiments could have been done on PEGylated proteins with branched or brush-shaped PEGs. If such experiments were conducted a number of issues could have been elucidated including investigations regarding the effect of PEG shape on the hydrodynamic volume and the binding properties. Would the binding profile of SDS to e.g. 10 kDa PEGylated BSA look the same if the 10 kDa PEG polymer was brush-shaped or branched? And would the hydrodynamic volume of a 10 kDa PEGylated protein be smaller if the PEG

was brush-shaped as opposed to linear, as one would guess by instinct? Further knowledge on the changes in the hydrodynamic volume upon PEGylation would be of great use in relation to optimising purification processes and developing liquid protein formulations of higher concentrations intended for injection.

Many studies throughout the past years have elucidated a lot of the issues related to PEGylation and PEGylated pharmaceutical proteins, the dynamics and conformation of the PEG chain and its preferred proximity to various regions on the protein surface is, as yet, unknown.

The biological function of a PEGylated protein depends on the dynamics and the conformation of the PEG chain (or chains for multiple PEGylation) but to our knowledge there have been no studies that have been specifically aimed at understanding the mechanisms by which a PEGylated protein may, on the one hand, resist proteolytic degradation yet, on the other, retain biological function. Both these phenomena involve interactions, and the protein is apparently able to recognize and interact with its binding partner or receptor while at the same time a heavily hydrated shell of PEG cause hindrance of interaction with the immune system through shielding of the protein surface. Being flexible, the PEG chain might be displaced as the protein binds to a receptor or a ligand but presumably the PEG is insensitive to the underlying protein construct i.e. whether it is a single protein or a protein complex. However only little is known of where the PEG chain is located once the PEG-protein complex is formed. The PEG chain might form a shell around the complex or it might be located as a 'polymer cloud' next to the protein as the hydrodynamic volume results indicate (chapter 7). The conformation of the PEG-protein complex is also yet unknown. While the modelling of the SPR data (appendix B) tried to estimate the conformation of the PEG chain as a random coil, an extended chain conformation or a "fried egg" conformation with the PEG flattened out round the surface construct ("yolk" = protein complex; "white" = PEG moiety), more experiments and subsequent calculations need to be conducted.

In addition it could be very interesting to measure the shape and conformation of PEGylated proteins Small Angle X-ray Scattering (SAXS) or Small Angle Neutron Scattering (SANS). Especially SANS could be interesting as one could choose to deuterate the protein and then PEGylated it, or deuterate the PEG group and then covalently attach this PEG group to the protein, and thus obtain signals from either group. The following data processing would then reveal which signal originated from with part of the PEG-protein complex.

Bibliography

[1] M. C. Manning, D. K. Chou, B. M. Murphy, R. W. Payne, and D. S. Katayama. Stability of Protein Pharmaceuticals: An Update. *Pharmaceutical Research*, 27(4): 544–575, 2010.

[2] E. Y. Chi, S. Krishnan, T. W. Randolph, and J. F. Carpenter. Physical stability of proteins in aqueous solution: Mechanism and driving forces in nonnative protein aggregation. *Pharmaceutical Research*, 20(9):1325–1336, 2003.

[3] B. Dani, R. Platz, and S. T. Tzannis. High concentration formulation feasibility of human immunoglubulin G for subcutaneous administration. *Journal of pharmaceutical sciences*, 96(6):1504–1517, 2007.

[4] R. J. Harris, S. J. Shire, and C. Winter. Commercial manufacturing scale formulation and analytical characterization of therapeutic recombinant antibodies. *Drug development research*, 61(3):137–154, 2004.

[5] S. J. Shire, Z. Shahrokh, and J. Liu. Challenges in the development of high protein concentration formulations. *Journal of Pharmaceutical Sciences*, 93(6):1390–1402, 2004.

[6] P.Qi, D.B. Volkin, H. Zhao, M.L. Nedved, R. Hughes, R. Bassand, S.C. Yi, M. E. Panek, D. Wang, P. Dalmonte, and M. D. Bond. Characterization of the Photodegradation of a Human IgG1 Monoclonal Antibody Formulated as a High-Concentration Liquid Dosage Form. *Journal of pharmaceutical sciences*, 98(9):3117–3130, 2009.

[7] R. J. Ellis and A. P. Minton. Cell biology - Join the crowd. *Nature*, 425(6953): 27–28, 2003.

[8] J. X. Guo, N. Harn, A. Robbins, R. Dougherty, and C. R. Middaugh. Stability of helix-rich proteins at high concentrations. *Biochemistry*, 45(28):8686–8696, 2006.

[9] N. Harn, C. Allan, C. Oliver, and C. R. Middaugh. Highly concentrated monoclonal antibody solutions: Direct analysis of physical structure and thermal stability. *Journal of pharmaceutical sciences*, 96(3):532–546, 2007.

[10] S. Matheus, W. Friess, and H. C. Mahler. FTIR and nDSC as analytical tools for high-concentration protein formulations. *Pharmaceutical Research*, 23(6):1350–1363, 2006.

[11] S. Matheus, H. C. Mahler, and W. Friess. A critical evaluation of t-m(ftir) measurements of high-concentration IgG(1) antibody formulations as a formulation development tool. *Pharmaceutical Research*, 23(7):1617–1627, 2006.

[12] J. Liu, M. D. H. Nguyen, J. D. Andya, and S. J. Shire. Reversible self-association increases the viscosity of a concentrated monoclonal antibody in aqueous solution. *Journal of pharmaceutical sciences*, 94(9):1928–1940, 2005.

[13] A. R. Patel, B. A. Kerwin, and S. R. Kanapuram. Viscoelastic Characterization of High Concentration Antibody Formulations Using Quartz Crystal Microbalance with Dissipation Monitoring. *Journal of pharmaceutical sciences*, 98(9):3108–3116, 2009.

[14] A. P. Minton. The Effect of Volume Occupancy Upon the Thermodynamic Activity of Proteins - Some Biochemical Consequences. *Molecular and Cellular Biochemistry*, 55(2):119–140, 1983.

[15] T. C. Laurent. Interaction between Polysaccharides and Other Macromolecules 5. Solubility of Proteins in Presence of Dextran. *Biochemical Journal*, 89(2):253–257, 1963.

[16] A. P. Minton. Excluded Volume As A Determinant of Macromolecular Structure and Reactivity. *Biopolymers*, 20(10):2093–2120, 1981.

[17] A. P. Minton and H. Edelhoch. Light-Scattering of Bovine Serum-Albumin Solutions - Extension of the Hard Particle Model to Allow for Electrostatic Repulsion. *Biopolymers*, 21(2):451–458, 1982.

[18] A. P. Minton. A Molecular-Model for the Dependence of the Osmotic-Pressure of Bovine Serum-Albumin Upon Concentration and pH. *Biophysical Chemistry*, 57(1): 65–70, 1995.

[19] A. P. Minton. Implications of macromolecular crowding for protein assembly. *Current Opinion in Structural Biology*, 10(1):34–39, 2000.

[20] A. P. Minton. Models for excluded volume interaction between an unfolded protein and rigid macromolecular cosolutes: Macromolecular crowding and protein stability revisited. *Biophysical journal*, 88(2):971–985, 2005.

[21] A. P. Minton. Influence of macromolecular crowding upon the stability and state of association of proteins: Predictions and observations. *Journal of pharmaceutical sciences*, 94(8):1668–1675, 2005.

[22] R. J. Ellis and A. P. Minton. Protein aggregation in crowded environments. *Biological Chemistry*, 387(5):485–497, 2006.

[23] A. P. Minton. The influence of macromolecular crowding and macromolecular confinement on biochemical reactions in physiological media. *Journal of Biological Chemistry*, 276(14):10577–10580, 2001.

[24] S. B. Zimmerman and A. P. Minton. Macromolecular Crowding - Biochemical, Biophysical, and Physiological Consequences. *Annual review of biophysics and biomolecular structure*, 22:27–65, 1993.

[25] G. Rivas, J. A. Fernandez, and A. P. MINTON. Direct observation of the self-association of dilute proteins in the presence of inert macromolecules at high concentration via tracer sedimentation equilibrium: Theory, experiment, and biological significance. *Biochemistry*, 38(29):9379–9388, 1999.

[26] C. Redfield and C. M. Dobson. Sequential H-1-NMR Assignments and Secondary Structure of Hen Egg-White Lysozyme in Solution. *Biochemistry*, 27(1):122–136, 1988.

[27] S. E. Radford, C. M. Dobson, and P. A. Evans. The Folding of Hen Lysozyme Involves Partially Structured Intermediates and Multiple Pathways. *Nature*, 358 (6384):302–307, 1992.

[28] L. S. Itzhaki, P. A. Evans, C. M. Dobson, and S. E. Radford. Tertiary Interactions in the Folding Pathway of Hen Lysozyme - Kinetic-Studies Using Fluorescent-Probes. *Biochemistry*, 33(17):5212–5220, 1994.

[29] C. M. Dobson, P. A. Evans, and S. E. Radford. Understanding How Proteins Fold - the Lysozyme Story So Far. *Trends in biochemical sciences*, 19(1):31–37, 1994.

[30] W. Pfeil and P. L. Privalov. Thermodynamic Investigations of Proteins .1. Standard Functions for Proteins with Lysozyme As An Example. *Biophysical Chemistry*, 4 (1):23–32, 1976.

[31] W. Pfeil and P. L. Privalov. Thermodynamic Investigations of Proteins .2. Calorimetric Study of Lysozyme Denaturation by Guanidine-Hydrochloride. *Biophysical Chemistry*, 4(1):33–40, 1976.

[32] W. Pfeil and P. L. Privalov. Thermodynamic Investigations of Proteins .3. Thermodynamic Description of Lysozyme. *Biophysical Chemistry*, 4(1):41–50, 1976.

[33] B. Batas and J. B. Chaudhuri. The influence of operational parameters on lysozyme refolding using size-exclusion chromatography. *Bioprocess and biosystems engineering*, 24(4):255–259, 2001.

[34] P. L. Privalov and N. N. Khechina. Thermodynamic Approach to Problem of Stabilization of Globular Protein Structure - Calorimetric Study. *Journal of molecular biology*, 86(3):665–684, 1974.

[35] W. J. Becktel and J. A. Schellman. Protein Stability Curves. *Biopolymers*, 26(11): 1859–1877, 1987.

[36] D. J. Segel, A. Bachmann, J. Hofrichter, K. O. Hodgson, S. Doniach, and T. Kiefhaber. Characterization of transient intermediates in lysozyme folding with time-resolved small-angle X-ray scattering. *Journal of molecular biology*, 288(3): 489–499, 1999.

[37] L. L. Chen, G. Wildegger, T. Kiefhaber, K. O. Hodgson, and S. Doniach. Kinetics of lysozyme refolding: Structural characterization of a non-specifically collapsed state using time-resolved X-ray scattering. *Journal of molecular biology*, 276(1):225–237, 1998.

[38] L. L. Chen, K. O. Hodgson, and S. Doniach. A lysozyme folding intermediate revealed by solution X-ray scattering. *Journal of molecular biology*, 261(5):658–671, 1996.

[39] N. Javid, K. Vogtt, C. Krywka, M. Tolan, and R. Winter. Protein-protein interactions in complex cosolvent solutions. *Chemphyschem*, 8(5):679–689, 2007.

[40] W. Eberstein, Y. Georgalis, and W. Saenger. Molecular-Interactions in Crystallizing Lysozyme Solutions Studied by Photon-Correlation Spectroscopy. *Journal of Crystal Growth*, 143(1-2):71–78, 1994.

[41] A. Tardieu, A. Le Verge, M. Malfois, F. Bonnete, S. Finet, M. Ries-Kautt, and L. Belloni. Proteins in solution: from X-ray scattering intensities to interaction potentials. *Journal of Crystal Growth*, 196(2-4):193–203, 1999.

[42] C. Tanford and R. Roxby. Interpretation of Protein Titration Curves - Application to Lysozyme. *Biochemistry*, 11(11):2192–2198, 1972.

[43] B. Ibarra-Molero and J. M. Sanchez-Ruiz. A model-independent, nonlinear extrapolation procedure for the characterization of protein folding energetics from solvent-denaturation data. *Biochemistry*, 35(47):14689–14702, 1996.

[44] A. S. Yang and B. Honig. On the pH Dependence of Protein Stability. *Journal of molecular biology*, 231(2):459–474, 1993.

[45] M. Cueto, M. J. Dorta, O. Munguia, and M. Llabres. New approach to stability assessment of protein solution formulations by differential scanning calorimetry. *International Journal of Pharmaceutics*, 252(1-2):159–166, 2003.

[46] P. L. Privalov. Stability of proteins: small globular proteins. In C. B. Anfinsen, J.T.Edsall, and F.M Richards, editors, *Advances in Protein Chemistry*, pages 167–241. Academic Press, 1 edition, 1979.

[47] A. Abuchowski, J. R. Mccoy, N. C. Palczuk, T. Vanes, and F. F. Davis. Effect of Covalent Attachment of Polyethylene-Glycol on Immunogenicity and Circulating Life of Bovine Liver Catalase. *Journal of Biological Chemistry*, 252(11):3582–3586, 1977.

[48] A. Abuchowski, T. Vanes, N. C. Palczuk, and F. F. Davis. Alteration of Immunological Properties of Bovine Serum-Albumin by Covalent Attachment of Polyethylene-Glycol. *Journal of Biological Chemistry*, 252(11):3578–3581, 1977.

[49] J. M. Harris and R. B. Chess. Effect of PEGylation on pharmaceuticals. *Nature Reviews Drug Discovery*, 2(3):214–221, 2003.

[50] S.A. Marshall, G. A. Lazar, A. J. Chirino, and J. R. Desjarlais. Rational design and engineering of therapeutic proteins. *Drug discovery today*, 8(5):212–221, 2003.

[51] P. Bailon, A. Palleroni, C. A. Schaffer, C. L. Spence, W. J. Fung, J. E. Porter, G. K. Ehrlich, W. Pan, Z. X. Xu, M. W. Modi, A. Farid, and W. Berthold. Rational design of a potent, long-lasting form of interferon: A 40 kDa branched polyethylene glycol-conjugated interferon alpha-2a for the treatment of hepatitis C. *Bioconjugate chemistry*, 12(2):195–202, 2001.

[52] C. S. Fishburn. The pharmacology of PEGylation: Balancing PD with PK to generate novel therapeutics. *Journal of pharmaceutical sciences*, 97(10):4167–4183, 2008.

[53] BioSpace, 2010. URL http://www.biospace.com/.

[54] Food and Drug Administration, 2010. URL http://www.fda.gov/.

[55] B. B. Heymann and H. Grubmuller. Elastic properties of poly(ethylene-glycol) studied by molecular dynamics stretching simulations. *Chemical Physics Letters*, 307 (5-6):425–432, 1999.

[56] K. Tasaki. Poly(oxyethylene)-water interactions: A molecular dynamics study. *Journal of the American Chemical Society*, 118(35):8459–8469, 1996.

[57] M. Rief F. Oesterhelt and H. E. Gaub. Single molecule force spectroscopy by AFM indicates helical structure of poly(ethylene-glycol) in water. *New Journal of Physics*, 1:6.1–6.11, 1999.

[58] P. Caliceti and F. M. Veronese. Pharmacokinetic and biodistribution properties of poly(ethylene glycol)-protein conjugates. *Advanced Drug Delivery Reviews*, 55(10): 1261–1277, 2003.

[59] A. S. Morar, J. R. L. Schrimsher, and M. D. Chavez. PEGylation of proteins: A structural approach. *Biopharm international*, 19(4):34–49, 2006.

[60] S. Zalipsky and J. M. Harris. Chemistry and biological applications of PEG. In J. M. Harris and S. Zalipsky, editors, *Poly(ethylene glycol) chemistry and biological application*, pages 1–13. American Chemical Society, Washington DC, 1997.

[61] S. Zalipsky. Chemistry of Polyethylene-Glycol Conjugates with Biologically-Active Molecules. *Advanced Drug Delivery Reviews*, 16(2-3):157–182, 1995.

[62] F. M. Veronese and G. Pasut. PEGylation, successful approach to drug delivery. *Drug discovery today*, 10(21):1451–1458, 2005.

[63] J. M. Harris, N. E. Martin, and M. Modi. PEGylation - A novel process for modifying pharmacokinetics. *Clinical pharmacokinetics*, 40(7):539–551, 2001.

[64] H. R. Stennicke, H. Ostergaard, R. J. Bayer, M. S. Kalo, K. Kinealy, P. K. Holm, B. B. Sorensen, D. Zopf, and S. E. Bjorn. Generation and biochemical characterization of glycoPEGylated factor VIIa derivatives. *Thrombosis and Haemostasis*, 100 (5):920–928, 2008.

[65] K. D. Hinds and S. W. Kim. Effects of PEG conjugation on insulin properties. *Advanced Drug Delivery Reviews*, 54(4):505–530, 2002.

[66] K. Yang, A. Basu, M. L. Wang, R. Chintala, M. C. Hsieh, S. Liu, J. Hua, Z. F. Zhang, J. Zhou, M. Li, H. Phyu, G. Petti, M. Mendez, H. Janjua, P. Peng, C. Longley, V. Borowski, M. Mehlig, and D. Filpula. Tailoring structure-function and pharmacokinetic properties of single-chain Fv proteins by site-specific PEGylation. *Protein Engineering*, 16(10):761–770, 2003.

[67] R. Clark, K. Olson, G. Fuh, M. Marian, D. Mortensen, F. Teshima, S. Chang, H. Chu, V. Mukku, E. CanovaDavis, T. Somer, M. Cronin, M. Winkler, and J. A. Wells. Long-acting growth hormones produced by conjugation with polyethylene glycol. *Journal of Biological Chemistry*, 271(36):21969–21977, 1996.

[68] F. M. Veronese, C. Monfardini, P. Caliceti, O. Schiavon, M. D. Scrawen, and D. Beer. Improvement of pharmacokinetic, immunological and stability properties of asparaginase by conjugation to linear and branched monomethoxy poly(ethylene glycol). *Journal of Controlled Release*, 40(3):199–209, 1996.

[69] P. Caliceti, O. Schiavon, and F. M. Veronese. Immunological properties of uricase conjugated to neutral soluble polymers. *Bioconjugate chemistry*, 12(4):515–522, 2001.

[70] C. Monfardini, O. Schiavon, P. Caliceti, M. Morpurgo, J. M. Harris, and F. M. Veronese. A Branched Monomethoxypoly(Ethylene Glycol) for Protein Modification. *Bioconjugate chemistry*, 6(1):62–69, 1995.

[71] F. M. Veronese. Peptide and protein PEGylation: a review of problems and solutions. *Biomaterials*, 22(5):405–417, 2001.

[72] F. M. Veronese, P. Caliceti, and O. Schiavon. Branched and linear poly(ethylene glycol): Influence of the polymer structure on enzymological, pharmacokinetic, and immunological properties of protein conjugates. *Journal of bioactive and compatible polymers*, 12(3):196–207, 1997.

[73] X. Zhao and J.M. Harris. *Novel degradable poly(ethylene glycol) esters for drug delivery.* Poly(ethylene glycol) - Chemistry and biological applications, Acs symposium series. American Chemical Society, Washington, 1997.

[74] S. Zalipsky and C Lee. Use of functionalized poly(ethylene glycol)s for modification of polypeptides. In J. M. Harris, editor, *Poly(ethylene glycol) chemistry: biotechnical and biomedical applications*, pages 347–370. Plenum Press, 1992.

[75] X. Y. Suo, C. Y. Zheng, P. Z. Yu, X. L. Lu, G. H. Ma, and Z. G. Su. Solid Phase Pegylation of Hemoglobin. *Artificial Cells Blood Substitutes and Biotechnology*, 37 (4):147–155, 2009.

[76] M. J. Roberts, M. D. Bentley, and J. M. Harris. Chemistry for peptide and protein PEGylation. *Advanced Drug Delivery Reviews*, 54(4):459–476, 2002.

[77] Mauro Sergi, Francesca Caboi, Carlo Maullu, Gaetano Orsini, and Giancarlo Tonon. Enzymatic techniques for pegylation of biopharmaceuticals. In F. Veronese, editor, *PEGylated Protein Drugs: Basic Science and Clinical Applications*, Milestones in Drug Therapy, pages 75–88. Birkhauser Verlag Press, Basel, 2009.

[78] H. Sato. Enzymatic procedure for site-specific pegylation of proteins. *Advanced Drug Delivery Reviews*, 54(4):487–504, 2002.

[79] S. DeFrees, Z. G. Wang, R. Xing, A. E. Scott, J. Wang, D. Zopf, D. L. Gouty, E. R. Sjoberg, K. Panneerselvam, ECM Brinkman-Van Der Linden, R. J. Bayer, M. A. Tarp, and H. Clausen. GlycoPEGylation of recombinant therapeutic proteins produced in Escherichia coli. *Glycobiology*, 16(9):833–843, 2006.

[80] G. E. Francis, D. Fisher, C. Delgado, F. Malik, A. Gardiner, and D. Neale. PEGylation of cytokines and other therapeutic proteins and peptides: the importance of biological optimisation of coupling techniques. *Int.J.Hematol.*, 68(1):1–18, 1998.

[81] S. Vanwetswinkel, S. Plaisance, Z. Zhi-Yong, I. Vanlinthout, K. Brepoels, I. Lasters, D. Collen, and L. Jespers. Pharmacokinetic and thrombolytic properties of cysteine-linked polyethylene glycol derivatives of staphylokinase. *Blood*, 95(3):936–942, 2000.

[82] Francesco M. Veronese, Anna Mero, and Gianfranco Pasut. Protein PEGylation, basic science and biological applications. In F. Veronese, editor, *PEGylated Protein Drugs: Basic Science and Clinical Applications*, Milestones in Drug Therapy, pages 11–31. Birkhauser Verlag Press, Basel, 2009.

[83] F. M. Veronese, P. Caliceti, A. Pastorino, O. Schiavon, L. Sartore, L. Banci, and L. M. Scolaro. Preparation, Physicochemical and Pharmacokinetic Characterization of Monomethoxypoly(Ethylene Glycol)-Derivatized Superoxide-Dismutase. *Journal of Controlled Release*, 10(1):145–154, 1989.

[84] J. Vincentelli, C. Paul, M. Azarkan, C. Guermant, A. El Moussaoui, and Y. Looze. Evaluation of the polyethylene glycol-KF-water system in the context of purifying PEG-protein adducts. *International Journal of Pharmaceutics*, 176(2):241–249, 1999.

[85] C. J. Fee. Protein conjugates purification and characterisation. In F. Veronese, editor, *PEGylated Protein Drugs: Basic Science and Clinical Applications*, Milestones in Drug Therapy, pages 113–125. Birkhauser Verlag Press, Basel, 2009.

[86] T. M. Pabst, J. J. Buckley, and A. K. Hunter. Comparison of strong anion-exchangers for the purification of a PEGylated protein. *Journal of Chromatography A*, 1147(2):172–182, 2007.

[87] C. J. Fee and J. M. Van Alstine. Prediction of the viscosity radius and the size exclusion chromatography behavior of PEGylated proteins. *Bioconjugate chemistry*, 15(6):1304–1313, 2004.

[88] F. Meng, B. N. Manjula, P. K. Smith, and S. A. Acharya. PEGylation of human serum albumin: Reaction of PEG-phenyl-isothiocyanate with protein. *Bioconjugate chemistry*, 19(7):1352–1360, 2008.

[89] D. D. Freitas and J. brahao Neto. Biochemical and biophysical characterization of lysozyme modified by PEGylation. *International Journal of Pharmaceutics*, 392 (1-2):111–117, 2010.

[90] G. Digilio, L. Barbero, C. Bracco, D. Corpillo, P. Esposito, G. Piquet, S. Traversa, and S. Aime. NMR structure of two novel polyethylene glycol conjugates of the human growth hormone-releasing factor, hGRF(1-29)-NH2. *Journal of the American Chemical Society*, 125(12):3458–3470, 2003.

[91] C. Dhalluin, A. Ross, L. A. Leuthold, S. Foser, B. Gsell, F. Muller, and H. Senn. Structural and biophysical characterization of the 40 kDa PEG-interferon-alpha(2a) and its individual positional isomers. *Bioconjugate chemistry*, 16(3):504–517, 2005.

[92] J. Ramon, V. Saez, R. Baez, R. Aldana, and E. Hardy. PEGylated interferon-alpha 2b: A branched 40K polyethylene glycol derivative. *Pharmaceutical Research*, 22(8): 1374–1386, 2005.

[93] P. Stigsnaes, S. Frokjaer, S. Bjerregaard, M. van de Weert, P. Kingshott, and E. H. Moeller. Characterisation and physical stability of PEGylated glucagon. *International Journal of Pharmaceutics*, 330(1-2):89–98, 2007.

[94] R. Lumry and H. Eyring. Conformation Changes of Proteins. *Journal of Physical Chemistry*, 58(2):110–120, 1954.

[95] R. S. Rajan, T. S. Li, M. Aras, C. Sloey, W. Sutherland, H. Arai, R. Briddell, O. Kinstler, A. M. K. Lueras, Y. Zhang, H. Yeghnazar, M. Treuheit, and D. N. Brems. Modulation of protein aggregation by polyethylene glycol conjugation: GCSF as a case study. *Protein science*, 15(5):1063–1075, 2006.

[96] S. Kubetzko, C. A. Sarkar, and A. Pluckthun. Protein PEGylation decreases observed target association rates via a dual blocking mechanism. *Molecular pharmacology*, 68(5):1439–1454, 2005.

[97] R. S. Larson, V. Menard, H. Jacobs, and S. W. Kim. Physicochemical characterization of poly(ethylene glycol)-modified anti-GAD antibodies. *Bioconjugate chemistry*, 12(6):861–869, 2001.

[98] H. Wang, L. He, M. Lensch, H. J. Gabius, C. J. Fee, and A. P. J. Middelberg. Single-Site Cys-Substituting Mutation of Human Lectin Galectin-2: Modulating Solubility in Recombinant Production, Reducing Long-Term Aggregation, and Enabling Site-Specific MonoPEGylation. *Biomacromolecules*, 9(11):3223–3230, 2008.

[99] A.D. Nielsen, K. Borch, and P. Westh. Thermochemistry of the specific binding of C12 surfactants to bovine serum albumin. *Biochimica et Biophysica Acta-Protein Structure and Molecular Enzymology*, 1479:321–331, 2000.

[100] A. O. Pedersen, B. Honore, and R. Brodersen. Thermodynamic parameters for Binding of Fatty-Acids to Human Serum-Albumin. *European Journal of Biochemistry*, 190(3):497–502, 1990.

[101] H. Aki and M. Yamamoto. Biothermodynamic Characterization of Monocarboxylic and Dicarboxylic Aliphatic-Acids Binding to Human Serum-Albumin - A Flow Microcalorimetric Study. *Biophysical Chemistry*, 46(1):91–99, 1993.

[102] S. Curry, P. Brick, and N. P. Franks. Fatty acid binding to human serum albumin: new insights from crystallographic studies. *Biochimica et Biophysica Acta-Molecular and Cell Biology of Lipids*, 1441(2-3):131–140, 1999.

[103] C. J. Halfman and T. Nishida. Method for Measuring Binding of Small Molecules to Proteins from Binding-Induced Alterations of Physical-Chemical Properties. *Biochemistry*, 11(18):3493–3498, 1972.

[104] H. Garcia-Arellano, B. Valderrama, G. Saab-Rincon, and R. Vazquez-Duhalt. High temperature biocatalysis by chemically modified cytochrome c. *Bioconjugate chemistry*, 13(6):1336–1344, 2002.

[105] D. Hall and A. P. Minton. Macromolecular crowding: qualitative and semiquantitative successes, quantitative challenges. *Biochimica et Biophysica Acta-Proteins and Proteomics*, 1649(2):127–139, 2003.

[106] S. N. Olsen. Applications of isothermal titration calorimetry to measure enzyme kinetics and activity in complex solutions. *Thermochimica Acta*, 448(1):12–18, 2006.

[107] A. Saluja and D. S. Kalonia. Application of ultrasonic shear rheometer to characterize rheological properties of high protein concentration solutions at microliter volume. *Journal of pharmaceutical sciences*, 94(6):1161–1168, 2005.

[108] N. A. Chebotareva, I. E. Andreeva, V. F. Makeeva, N. B. Livanova, and B. I. Kurganov. Effect of molecular crowding on self-association of phosphorylase kinase and its interaction with phosphorylase b and glycogen. *Journal of molecular recognition*, 17(5):426–432, 2004.

[109] T. B. Eronina, N. A. Chebotareva, and B. I. Kurganov. Influence of osmolytes on inactivation and aggregation of muscle glycogen phosphorylase b by guanidine hydrochloride. Stimulation of protein aggregation under crowding conditions. *Biochemistry-Moscow*, 70(9):1020–1026, 2005.

[110] B. G. Schlarb-Ridley, H. L. Mi, W. D. Teale, V. S. Meyer, C. J. Howe, and D. S. Bendall. Implications of the effects of viscosity, macromolecular crowding, and temperature for the transient interaction between cytochrome f and plastocyanin from the cyanobacterium Phormidium laminosum. *Biochemistry*, 44(16):6232–6238, 2005.

[111] D. S. Spencer, K. Xu, T. M. Logan, and H. X. Zhou. Effects of pH, salt, and macromolecular crowding on the stability of FK506-binding protein: An integrated experimental and theoretical study. *Journal of molecular biology*, 351(1):219–232, 2005.

[112] S. J. Shire, Z. Shahrokh, and J. Liu. Challenges in the development of high protein concentration formulations. *Journal of pharmaceutical sciences*, 93(6):1390–1402, 2004.

[113] C. N. Pace, F. Vajdos, L. Fee, G. Grimsley, and T. Gray. How to Measure and Predict the Molar Absorption-Coefficient of A Protein. *Protein science*, 4(11):2411–2423, 1995.

[114] Propka, the propka web interface 2.0, 2008. URL http://propka.ki.ku.dk/.

[115] H. Li, A. D. Robertson, and J. H. Jensen. Very fast empirical prediction and rationalization of protein pK(a) values. *Proteins-Structure Function and Bioinformatics*, 61(4):704–721, 2005.

[116] J. Wang, M. Dauter, R. Alkire, A. Joachimiak, and Z. Dauter. Triclinic lysozyme at 0.65 A resolution. *Acta crystallographica.Section D, Biological crystallography*, 63 (Pt 12):1254–1268, 2007.

[117] G. Pasut, A. Guiotto, and F. Veronese. Protein, peptide and non-peptide drug PEGylation for therapeutic application. *Expert Opinion on Therapeutic Patents*, 14 (6):859–894, 2004.

[118] L. N. Lin, A. B. Mason, R. C. Woodworth, and J. F. Brandts. Calorimetric Studies of the Binding of Ferric Ions to Ovotransferrin and Interactions Between Binding-Sites. *Biochemistry*, 30(50):11660–11669, 1991.

[119] H. Lund, B.P. Christensen, A.D. Nielsen, and P. Westh. Proton exchange coupled to the specific binding of alkylsulfonates to serum albumins. *Biochimica et Biophysica Acta-Proteins and Proteomics*, 1764:1243–1251, 2006.

[120] S. M. Vaiana, A. Emanuele, M. B. Palma-Vittorelli, and M. U. Palma. Irreversible formation of intermediate BSA oligomers requires and induces conformational changes. *Proteins-Structure Function and Bioinformatics*, 55(4):1053–1062, 2004.

[121] M. Yamasaki, H. Yano, and K. Aoki. Differential Scanning Calorimetric Studies on Bovine Serum-Albumin .1. Effects of pH and Ionic-Strength. *International Journal of Biological Macromolecules*, 12(4):263–268, 1990.

[122] M. Yamasaki, H. Yano, and K. Aoki. Differential Scanning Calorimetric Studies on Bovine Serum-Albumin .3. Effect of Sodium Dodecyl-Sulfate. *International Journal of Biological Macromolecules*, 14(6):305–312, 1992.

[123] M. Yamasaki, T. Y. Isoda, H. Yano, K. Tatsumi, and K. Aoki. Differential Scanning Calorimetric Studies on Bovine Serum-Albumin .4. Effect of anionic surfactants with various lengths of hydrocarbon chain. *International Journal of Biological Macromolecules*, 19(4):241–246, 1996.

[124] C. Giancola, C. DeSena, D. Fessas, G. Graziano, and G. Barone. DSC studies on bovine serum albumin denaturation - Effects of ionic strength and SDS concentration. *International Journal of Biological Macromolecules*, 20(3):193–204, 1997.

[125] M. Yamasaki, H. Yano, and K. Aoki. Differential Scanning Calorimetric Studies on Bovine Serum-Albumin .2. Effects of Neutral Salts and Urea. *International Journal of Biological Macromolecules*, 13(6):322–328, 1991.

[126] A. Michnik. Thermal stability of bovine serum albumin DSC study. *Journal of thermal analysis and calorimetry*, 71(2):509–519, 2003.

[127] S. M. Kelly, T. J. Jess, and N. C. Price. How to study proteins by circular dichroism. *Biochimica et Biophysica Acta-Proteins and Proteomics*, 1751(2):119–139, 2005.

[128] A. A. Bhattacharya, T. Grune, and S. Curry. Crystallographic analysis reveals common modes of binding of medium and long-chain fatty acids to human serum albumin. *Journal of molecular biology*, 303(5):721–732, 2000.

[129] L. G. Fagerstam, A. Frostell-Karlsson, R. Karlsson, B. Persson, and I. Ronnberg. Biospecific Interaction Analysis Using Surface-Plasmon Resonance Detection Applied to Kinetic, Binding-Site and Concentration Analysis. *Journal of chromatography*, 597(1-2):397–410, 1992.

[130] J. E. Gestwicki, H. V. Hsieh, and J. B. Pitner. Using receptor conformational change to detect low molecular weight analytes by surface plasmon resonance. *Analytical Chemistry*, 73(23):5732–5737, 2001.

[131] A. Helg, M. S. Mueller, A. Joss, F. Poltl-Frank, F. Stuart, J. A. Robinson, and G. Pluschke. Comparison of analytical methods for the evaluation of antibody responses against epitopes of polymorphic protein antigens. *Journal of Immunological Methods*, 276(1-2):19–31, 2003.

[132] B. Li, J. Chen, and M. Long. Measuring binding kinetics of surface-bound molecules using the surface plasmon resonance technique. *Analytical biochemistry*, 377(2):195–201, 2008.

[133] D. G. Myszka, X. He, M. Dembo, T. A. Morton, and B. Goldstein. Extending the range of rate constants available from BIACORE: Interpreting mass transport-influenced binding data. *Biophysical journal*, 75(2):583–594, 1998.

[134] D. G. Myszka, T. A. Morton, M. L. Doyle, and I. M. Chaiken. Kinetic analysis of a protein antigen-antibody interaction limited by mass transport on an optical biosensor. *Biophysical Chemistry*, 64(1-3):127–137, 1997.

[135] D. J. O'Shannessy and D. J. Winzor. Interpretation of deviations from pseudo-first-order kinetic behavior in the characterization of ligand binding by biosensor technology. *Analytical biochemistry*, 236(2):275–283, 1996.

[136] J. Homola. Surface Plasmon Resonance Based Sensors. volume 4 of *Springer Series on Chemical sensors and biosensor*. Springer, 2006. ISBN 978-3-540-33918-2 (Print) 978-3-540-33919-9 (Online).

[137] R. Mabry, M. Rani, R. Geiger, G. B. Hubbard, R. Carrion, K. Brasky, J. L. Patterson, G. Georgiou, and B. L. Iverson. Passive protection against anthrax by using a high-affinity antitoxin antibody fragment lacking an Fc region. *Infection and Immunity*, 73(12):8362–8368, 2005.

[138] ProteOn™ XPR36 Protein Interaction Array System - Version 2.1 User Manual, 2008. URL http://www.biorad.com.

[139] D. J. O'Shannessy, M. Brighamburke, K. K. Soneson, P. Hensley, and I. Brooks. Determination of Rate and Equilibrium Binding Constants for Macromolecular Interactions Using Surface-Plasmon Resonance - Use of Nonlinear Least-Squares Analysis-Methods. *Analytical biochemistry*, 212(2):457–468, 1993.

[140] A. Kausaite, M. van Dijk, J. Castrop, A. Ramanaviciene, J. P. Baltrus, J. Acaite, and A. Ramanavicius. Surface plasmon resonance label-free monitoring of antibody antigen interactions in real time. *Biochemistry and Molecular Biology Education*, 35 (1):57–63, 2007.

[141] M. M. Kurfurst. Detection and Molecular-Weight Determination of Polyethylene Glycol-Modified Hirudin by Staining After Sodium Dodecyl-Sulfate Polyacrylamide-Gel Electrophoresis. *Analytical biochemistry*, 200(2):244–248, 1992.

[142] O. W. Odom, W. Kudlicki, G. Kramer, and B. Hardesty. An effect of polyethylene glycol 8000 on protein mobility in sodium dodecyl sulfate-polyacrylamide gel electrophoresis and a method for eliminating this effect. *Analytical biochemistry*, 245 (2):249–252, 1997.

[143] Y. Tong, K. Zhong, H. Tian, X. D. Gao, X. Y. Xu, X. J. Yin, and W. B. Yao. Characterization of a monoPEG20000-Endostar. *International Journal of Biological Macromolecules*, 46(3):331–336, 2010.

[144] N. H. Chiem and D. J. Harrison. Monoclonal antibody binding affinity determined by microchip-based capillary electrophoresis. *Electrophoresis*, 19(16-17):3040–3044, 1998.

[145] R. L. Rich and D. G. Myszka. Survey of the year 2006 commercial optical biosensor literature. *Journal of molecular recognition*, 20(5):300–366, 2007.

[146] E. W. Davie, K. Fujikawa, and W. Kisiel. The Coagulation Cascade - Initiation, Maintenance, and Regulation. *Biochemistry*, 30(43):10363–10370, 1991.

[147] P. Wildgoose, D. Foster, J. Schiodt, F. C. Wiberg, J. J. Birktoft, and L. C. Petersen. Identification of a Calcium-Binding Site in the Protease Domain of Human Blood-Coagulation Factor-Cii - Evidence for Its Role in Factor-Vii Tissue Factor Interaction. *Biochemistry*, 32(1):114–119, 1993.

[148] M. J. Manco-Johnson, T. C. Abshire, A. D. Shapiro, B. Riske, M. R. Hacker, R. Kilcoyne, J. D. Ingram, M. L. Manco-Johnson, S. Funk, L. Jacobson, L. A. Valentino, W. K. Hoots, G. R. Buchanan, D. DiMichele, M. Recht, D. Brown, C. Leissinger, S. Bleak, A. Cohen, P. Mathew, A. Matsunaga, D. Medeiros, D. Nugent, G. A. Thomas, A. A. Thompson, K. McRedmond, J. M. Soucie, H. Austin, and B. L. Evatt. Prophylaxis versus episodic treatment to prevent joint disease in boys with severe hemophilia. *New England Journal of Medicine*, 357(6):535–544, 2007.

[149] B. A. Konkle, L. S. Ebbesen, E. Erhardtsen, R. P. Bianco, T. Lissitchkov, L. Rusen, and M. A. Serban. Randomized, prospective clinical trial of recombinant factor VIIa for secondary prophylaxis in hemophilia patients with inhibitors. *Journal of Thrombosis and Haemostasis*, 5(9):1904–1913, 2007.

[150] P. Sen, S. Ghosh, M. Ezban, U. R. Pendurthi, and L. V. M. Rao. Effect of glyco-PEGylation on factor VIIa binding and internalization. *Haemophilia*, 16(2):339–348, 2010.

[151] F. M. Veronese and M. Morpurgo. Bioconjugation in pharmaceutical chemistry. *Farmaco*, 54(8):497–516, 1999.

[152] A. D. Nielsen and C. Rischel. Biophysical Characterisation of GlycoPEGylated® recombinant human FVIIa. In *XXII International Society on Thrombosis and Haemostasis(ISTH)*, Boston, MA, USA, 11-16 July 2009.

[153] L. Palm, M. Renau, T. Jepsen, S. Fexby, A. D. Nielsen, and S. Valentin. Analysis and characterization of GlycoPEGylated® recombinant human FVIIa. In *XXII International Society on Thrombosis and Haemostasis(ISTH)*, Boston, MA, USA, 11-16 July 2009.

[154] M. Kunitani, G. Dollinger, D. Johnson, and L. Kresin. Online Characterization of Polyethylene Glycol-Modified Proteins. *Journal of chromatography*, 588(1-2):125–137, 1991.

[155] V. A. Bloomfield. Static and dynamic light scattering from aggregating particles. *Biopolymers*, 54(3):168–172, 2000.

[156] P. Westh. Preferential interactions of water and osmolytes at the membrane interface. *Recent Res.Devel.Biophys.*, 3:1–17, 2004.

[157] R. L. Baldwin. How Hofmeister ion interactions affect protein stability. *Biophysical journal*, 71(4):2056–2063, 1996.

[158] P. O. Freskgard, O. H. Olsen, and E. Persson. Structural changes in factor VIIa induced by Ca^{2+} and tissue factor studied using circular dichroism spectroscopy. *Protein science*, 5(8):1531–1540, 1996.

[159] P. O. Freskgard, L. C. Petersen, D. A. Gabriel, X. Li, and E. Persson. Conformational stability of factor VIIa: Biophysical studies of thermal and guanidine hydrochloride-induced denaturation. *Biochemistry*, 37(20):7203–7212, 1998.

[160] E. Persson, G. Bolt, T. D. Steenstrup, and M. Ezban. Recombinant coagulation factor VIIa - from molecular to clinical aspects of a versatile haemostatic agent. *Thrombosis Research*, 125(6):483–489, 2010.

[161] P. F. Neuenschwander and J. H. Morrissey. Roles of the Membrane-Interactive Regions of Factor VIIa and Tissue Factor - the Factor VIIa Gla Domain Is Dispensable for Binding to Tissue Factor But Important for activation of Factor X. *Journal of Biological Chemistry*, 269(11):8007–8013, 1994.

[162] A. K. Sabharwal, J. J. Birktoft, J. Gorka, P. Wildgoose, L. C. Petersen, and S. P. Bajaj. High-Affinity Ca^{2+}-Binding Site in the Serine-Protease Domain of Human Factor VIIa and Its Role in Tissue Factor-Binding and Development of Catalytic Activity. *Journal of Biological Chemistry*, 270(26):15523–15530, 1995.

[163] T. Arakawa and S. N. Timasheff. Mechanism of Protein Salting in and Salting Out by Divalent-Cation Salts - Balance Between Hydration and Salt Binding. *Biochemistry*, 23(25):5912–5923, 1984.

[164] B. Plesner, P. Westh, and A. D. Nielsen. Biophysical characterisation of GlycoPEGylated recombinant human Factor VIIa. *International Journal of Pharmaceutics*, 406:62–68, 2011.

[165] M. R. Cannon, R. E. Manning, and J. D. Bell. Viscosity Measurement - the Kinetic Energy Correction and A New Viscometer. *Analytical Chemistry*, 32(3):355–358, 1960.

[166] D. W. Banner, A. Darcy, C. Chene, F. K. Winkler, A. Guha, W. H. Konigsberg, Y. Nemerson, and D. Kirchhofer. The crystal structure of the complex of blood coagulation factor VIIa with soluble tissue factor. *Nature*, 380(6569):41–46, 1996.

[167] Huggins Maurice L. The Viscosity of Dilute Solutions of Long-Chain Molecules. IV. Dependence on Concentration. *Journal of American Chemical Society*, 64(11): 2716–2718, 1942.

[168] Elmer O. Kraemer. Molecular Weights of Celluloses and Cellulose Derivates. *Industrial and Engineering Chemistry*, 30(10):1200–1203, 1938.

[169] B. N. Manjula, S. Tsai, R. Upadhya, K. Perumalsamy, P. K. Smith, A. Malavalli, K. Vandegriff, R. M. Winslow, M. Intaglietta, M. Prabhakaran, J. M. Friedman, and A. S. Acharya. Site-specific PEGylation of hemoglobin at cys-93(beta): Correlation between the colligative properties of the PEGylated protein and the length of the conjugated PEG chain. *Bioconjugate chemistry*, 14(2):464–472, 2003.

[170] J. Maxfield and I. W. Shepherd. Conformation of Poly(Ethylene Oxide) in Solid-State, Melt and Solution Measured by Raman-Scattering. *Polymer*, 16(7):505–509, 1975.

[171] M. J. W. Povey. *Ultrasonic techniques fo fluids characterization.* Academic Press, San Diego, CA, 2007.

[172] L. S. Jung, C. T. Campbell, T. M. Chinowsky, M. N. Mar, and S. S. Yee. Quantitative interpretation of the response of surface plasmon resonance sensors to adsorbed films. *Langmuir*, 14(19):5636–5648, 1998.

[173] M. J. Cannon and D. G. Myszka. Methods for Structural Analysis of Protein Pharmaceuticals. American Association of Pharmaceutical Scientists, 1 edition, 2005.

[174] D. R. Lide. *CRC Handbook of Chemistry and Physics.* CRC Press, 2004.

[175] David B. Hand. The Refractivity of Protein Solutions. *Journal of Biological Chemistry*, 108(3):703–707, 1934.

[176] J. Brandrup and E. H. Immergut. *Polymer Handbook.* John Wiley and Sons, 1974.

[177] P. Kratochvil. *Classical Light Scattering from Polymer Solutions.* Elsevier, 1987.

[178] M. B. Huglin. Polymer handbook. In J. Brandrup and E. H. Immergut, editors, *Specific refractive index increments of polymers in dilute solutions*, pages VII/409–VII/471. John Wiley, New York, 1991.

[179] T. Tumolo, L. Angnes, and M. S. Baptista. Determination of the refractive index increment (dn/dc) of molecule and macromolecule solutions by surface plasmon resonance. *Analytical biochemistry*, 333(2):273–279, 2004.

[180] Philip Molyneux. *Water-Soluble synthetic polymers: properties and behaviour.* CRC Press, Boca Raton, Florida, 1983.

[181] S. H. Armstrong, M. J. E. Budka, K. C. Morrison, and M. Hasson. Preparation and Properties of Serum and Plasma Proteins .12. the Refractive Properties of the Proteins of Human Plasma and Certain Purified Fractions. *Journal of the American Chemical Society*, 69(7):1747–1753, 1947.

[182] B.S. Kendrick, B. A. Kerwin, B. S. Chang, and J. S. Philo. Online size-exclusion high-performance liquid chromatography light scattering and differential refractometry methods to determine degree of polymer conjugation to proteins and protein-protein or protein-ligand association states. *Analytical biochemistry*, 299(2):136–146, 2001.

A High Resolution Ultrasonic Spectroscopy

According to Povey [171] ultrasonic spectroscopy is one of the most useful techniques when it comes to measuring physical properties of highly concentrated protein solutions. Povey also state that measurements of the velocity of sound is the only direct way to determine the adiabatic compressibility, which, to a biophysicist, can be used in determining solute-solute and solute-solvent interactions [171]. We have used High Resolution Ultrasonic Spectroscopy (HRUS) as a supplement to DSC in characterising highly concentrated lysozyme solutions. HRUS measures how sound waves propagate through a sample by detecting the velocity and attenuation of the sound wave through the media and its reference. The changes in velocity and attenuation can also be measured as a function of temperature. The variations in the speed of sound relates to the compressibility, density and hydration of the sample whereas the attenuation relates to the possible formation of aggregates [171].

Here HRUS has been used to measure the effect of concentration and changing pH on highly concentrated lysozyme solutions. Basically freeze-dried lysozyme was dissolved in Milli Q water and filtered through a 22 μ filter. Subsequently pH was adjusted and the samples were diluted (if needed). Unlike the experimental procedure described in section 2.2 these samples were not diluted and then concentrated through an Amicon tube, repeating the procedure 6 times to remove excess ions. In addition the solutions were diluted with Milli Q water, and not with a NaCl-buffer with the same salt concentration as the concentrated protein solution. In other words, these samples are not as well characterised as the lysozyme samples used in chapter 2, but these experiments serve purely as supporting data, reflecting the same tendency as seen in chapter 2.

The results of the velocity measurements are differentiated with respect to temperature in order to obtain the point where the change in velocity with temperature is largest. This point is denoted T_m. The attenuation results are plotted as a function of temperature without further data processing.

The results are summarised in table A.1 and further illustrated in figure A.1, A.2 and A.3.

As seen on figure A.1 there are noticeable differences between the measurements of the highly concentrated lysozyme solutions. The experiments can roughly be categorised in three groups (i) pH 1.5, (ii) pH 2.0, pH 3.0, pH 3.5 and (iii) pH 4.0, pH 4.5 and pH 5.0. It appears as though the protein solutions in group (i) and (iii) are the most stable solutions,

pH	T_m (℃)		pH	Conc. (mg/mL)	T_m (℃)
1.5	48.0 ± 0.5		1.5	200	48.0 ± 0.5
2.0	67.4 ± 0.5		1.5	160	59.7 ± 0.5
3.0	68.7 ± 0.5		1.5	120	67.4 ± 0.5
3.5	68.5 ± 0.5		1.5	80	68.3 ± 0.5
4.0	65.7 ± 0.5				
4.5	66.2 ± 0.5		4.0	200	65.7 ± 0.5
			4.0	160	66.7 ± 0.5
			4.0	120	67.9 ± 0.5
			4.0	80	68.8 ± 0.5
			4.0	40	66.6 ± 0.5

Table A.1:
Left panel: The apparent unfolding temperature, T_m, measured by HRUS at 200 mg/mL and 7 pH values (fig. A.1a).
Right panel: The apparent unfolding temperature, T_m, measured at two pH values and 4-5 different concentrations (fig. A.2a and fig. A.3a).
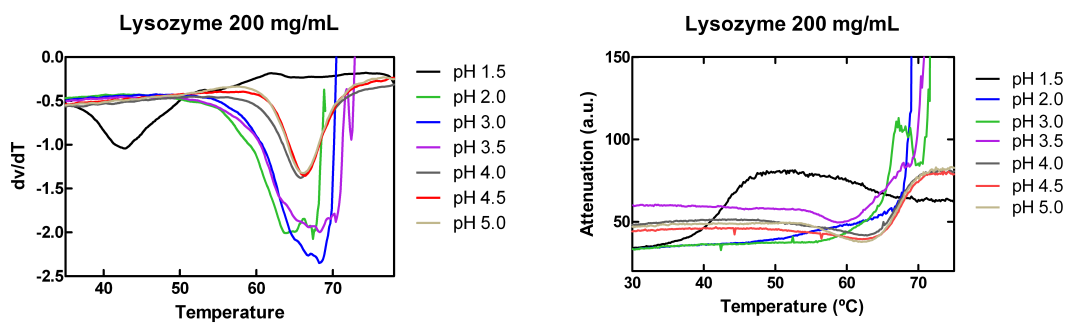
(a) The change in velocity with temperature as a function of temperature for highly concentrated lysozyme solutions.

(b) The attenuation change as a function of temperature for high concentration lysozyme solutions.

Figure A.1: dv/dT (A.1a) and attenuation (A.1b) for high concentration lysozyme solutions.

whereas group (ii) seems more unstable illustrated by the uneven change in attenuation and velocity with temperature.
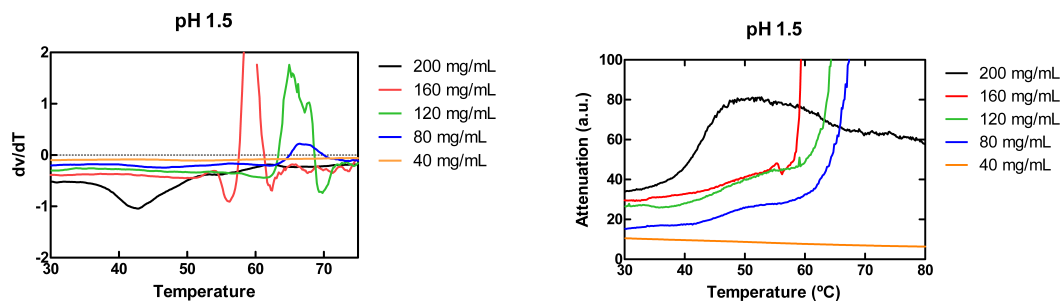
(a) The change in velocity with temperature as a function of temperature for lysozyme at pH 1.5.

(b) The attenuation change as a function of temperature for lysozyme at pH 1.5.

Figure A.2: HRUS results for the measurements of highly concentrated lysozyme solutions at pH 1.5

From the results presented in figure A.2 it is evident that the lysozyme solutions at pH 1.5 depend strongly on the concentration of lysozyme.
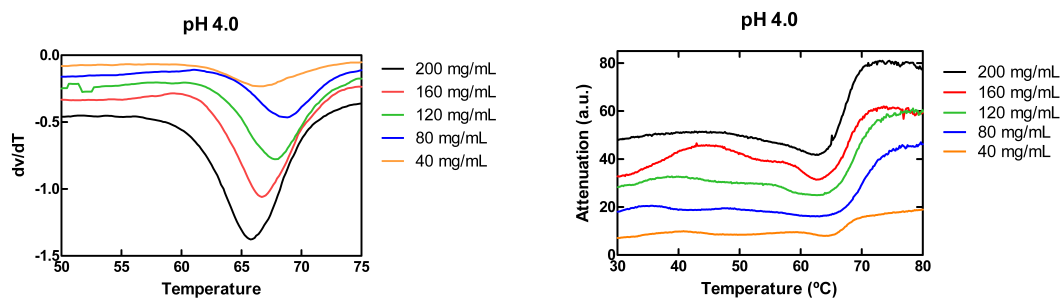
(a) The change in velocity with temperature as a function of temperature for lysozyme at pH 4.0

(b) The attenuation change as a function of temperature for lysozyme at pH 4.0.

Figure A.3: HRUS results for the measurements of highly concentrated lysozyme solutions at pH 4.0

The HRUS results obtained with the lysozyme solutions at pH 4.0 are a very nice example of how the attenuation and the velocity changes with lysozyme concentration. Both experimental parameters strongly indicate that the protein unfolding temperature decrease with increasing protein concentration.

B   Using SPR to estimate the conformation of PEGylated BSA

A novel approach to using SPR

A spinoff of the SPR experiments represented in chapter 4 was modelling the raw SPR data without focusing on the binding properties of the ligand and the analyte. This work is a very tentative exploratory investigation into the possibility that PEG conformation could explain the SPR responses seen in chapter 4. It is our perception that this work is not yet fully developed, but serves as a basis for further exploration and development in the future. Normally SPR is used to determine the binding kinetics between an antibody and an antigen, see section 4.1. But here we have interpreted the SPR data in a new way and used the SPR response in estimating the conformation of an immobilised PEGylated BSA molecule. The data do not reflect binding kinetics but solely the SPR response to the immobilisation of a protein onto the SPR chip. The SPR response data are generated by activating the SPR chip with a 10 times diluted activation solution. The activation is deliberately low to diminish the number of intermolecular interactions between the immobilised proteins on the chip surface. After activation the native BSA and various PEGylated BSA species were immobilised onto a SPR chip, see figure B.1.
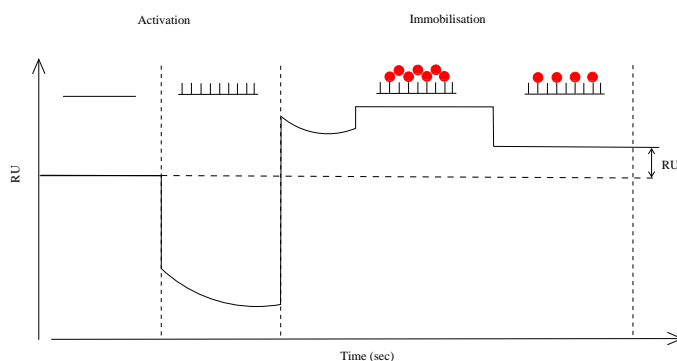
Figure B.1: The SPR response to activation and immobilisation as a function of time. The response equalling the adsorption of BSA or PEGylated BSA is used for the modelling process. The response is illustrated as RU on the figure, and the measured RU is plotted as a function of PEG molecular weight on figure B.2. The red dots illustrate the immobilised protein molecules.

The corresponding SPR response, RU, was used as one of the modelling parameters. The RU is plotted as a function of the molecular weight of the attached PEG polymer (PEGylated BSA) in figure B.2.
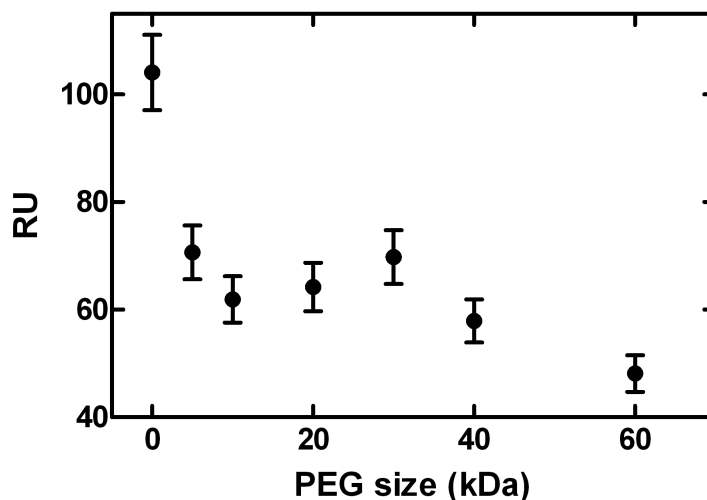
Figure B.2: The SPR response to the immobilisation of BSA and various PEGylated BSA species. The RU values are decreasing with increasing molecular weight of the PEGylated BSA.

The SPR response data show a decrease in response with increasing PEG size, see figure B.2. This observation is surprising as the SPR response normally increases with increasing molecular weight of the immobilised protein [136]. Jung et al. [172] have shown how the SPR response also depends on the thickness of the adsorbed surface adlayer and the difference in refractive index between the adsorbed layer and the bulk solution. We put forward a model which is based on those calculations, the viscosity radius calculations in Fee and Van Alstine [87], and our own measurements of the refractive index of PEGylated BSA, see appendix C.

Basically 3 different models are put forward, all of which describe different possible locations of the polymer around the immobilised BSA. The fundamental basis for the modelling is the PEG molecular weight dependent viscosity radius, which is described in Fee and Van Alstine [87], and in section C, and the thickness of the adsorbed layer.

Our basis model is found in figure B.3a, which represents PEGylated BSA in free solution. The thickness of the adlayer will serve as the main parameter determining whether the polymer is wrapped around the protein, figure B.3b, sits as a sphere, figure B.3c, or as an elongated sphere on top of the immobilised protein, figure B.3d. All models are summarized in figure B.3.
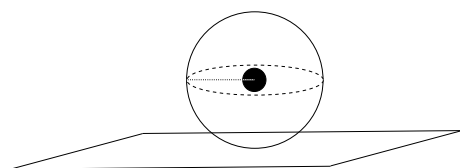
(a) Model 1, the sphere. PEGylated BSA in free solution. The BSA is represented by the black sphere, the PEG polymer is represented by the transparent sphere surrounding the BSA.
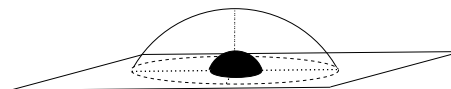
(b) Model 2, the hemisphere. PEGylated BSA on the SPR chip, the overall structure is a hemisphere, where the transparent sphere is the PEG polymer wrapped around the BSA, represented by a black sphere.
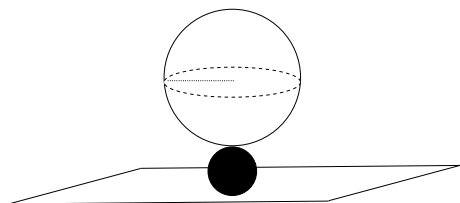
(c) Model 3, sphere on top of sphere. PEGylated BSA on the SPR chip. BSA, the black sphere, is attached to the SPR chip, the PEG polymer, represented by the transparent sphere, is floating on top of the protein.
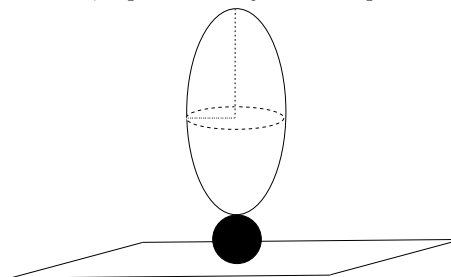
(d) Model 4, elongated sphere. PEGylated BSA on the SPR chip. BSA, the black sphere, is attached to the SPR chip. The PEG polymer, represented by the transparent, elongated sphere is floating on top of protein.

Figure B.3: The thickness of the adlayer (from the chip to the top of the molecule) is modelled as a function of the viscosity radius of BSA and the attached PEG polymer. Model 1 illustrates the PEGylated BSA molecule in free solution. Models 2, 3 and 4 are realistic illustrations of how the PEGylated BSA can be located on the SPR chip.

The SPR response, RU, is directly proportional to the change in refractive index between the bulk solution and the protein adsorbed onto the chip at a certain distance from the chip surface [172].

$$RU \propto (n_{protein} - n_{buffer}) \tag{B.1}$$

The refractive index of the protein is calculated from equation C.1, using the Refractive Index Increments reported in appendix C. The model also depends on the concentration of protein on the SPR chip, and this concentration depends on the surface coverage. In our modelling the surface coverage has either been independent or dependent on the molecular weight of the immobilised PEGylated protein. In the case where the surface coverage is dependent on the molecular weight of the protein, it is estimated that the surface coverage

decreases with 1 % per 1 kDa PEG attached to the BSA. Thus the surface coverage decreases with 60 % when immobilising a 60 kDa PEGylated BSA compared to a native BSA. If the surface coverage is independent of the molecular weight of the immobilised PEGylated protein, the same value for the surface coverage is used for all species. This value is calculated based on the SPR response to immobilising native BSA onto the SPR chip, which is described further on page 142.

Viscosity Radius

Fee and Van Alstine used Size Exclusion Chromatography (SEC) to determine the viscosity radii of equivalent spheres for proteins covalently grafted with PEG. The viscosity radius of a PEGylated protein depends on the molecular weight of the protein and the PEG as well as the viscosity radii of both species [87]. The radius of PEGylated BSA serves as the basis for modelling the SPR response. The radius is used to calculate the occupied volume of a spherical PEGylated BSA molecule. The occupied volume is independent of the model used, and depends only on the size of the PEG.

Modelling

Model 1

It is assumed that the PEGylated BSA in aqueous solution occupies a sphere with a radius corresponding to the viscosity radius. The first model, model 1, describes the PEGylated BSA free in solution, and as seen on figure B.4, BSA, black sphere, is not attached to the chip surface. PEG is illustrated as the transparent sphere surrounding the protein. This model serves mainly as the basis for the other three models.
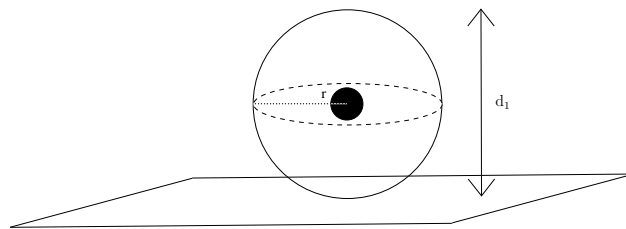
Figure B.4: Model 1. PEGylated BSA in free solution. The distance d_1 equals two viscosity radii of PEGylated BSA. The volume of the free PEGylated BSA in solution is calculated from $V_{\text{PEGylated BSA}} = \frac{4}{3}\pi r^3$, where r is the viscosity radius.

The distance d_1 refers to the distance from the surface of the chip to the top of the adlayer, in this case 2 times the viscosity radius of a PEGylated BSA molecule. d_1 is an estimate of the bilayer thickness, see table B.1.

PEG MW (kDa)	d_1 (nm)
5	8.2
10	9.7
20	11.8
30	13.7
40	15.5
60	18.8

Table B.1: The bilayer thickness, d_1, calculated from the viscosity radius of PEGylated BSA [87].

Model 2

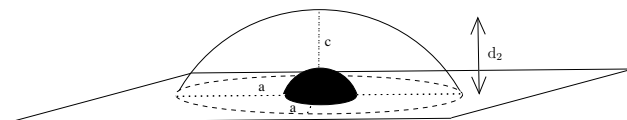Model 2 illustrates the case, where the PEG polymer is wrapped around the BSA molecule, see figure B.5.

Figure B.5: Model 2. PEGylated BSA on the SPR chip, hemisphere. The distance d_2 equals c, which is found from the volume of this hemisphere: $V_{\mathrm{PEGylated\ BSA}} = \frac{2}{3}\pi a^2 c$.

The distance d_2 refers to the distance from the surface of the chip to the top of the adlayer. d_2 equals the distance c on figure B.5. The volume of a PEGylated BSA molecule and the distance c is found as:

$$c = d_2 = \frac{3 \cdot V_{\mathrm{PEGylated\ BSA}}}{2 \cdot \pi \cdot a^2} \tag{B.2}$$

Here a is defined as:

$$a = R_{\mathrm{h\ BSA}} + x \cdot R_{\mathrm{h\ PEG}} \tag{B.3}$$

Here $R_{\mathrm{h\ BSA}}$ refers to the viscosity radius of BSA, and $R_{\mathrm{h\ PEG}}$ refers to the viscosity radius of pure PEG [87].

And the unknown factor x is found by fitting this hemispherical model to the measured SPR response data, the values for x is found when the difference between the measured and calculated SPR response was a minimum. From the data fitting two different values for a has been found; One describing the case where the surface coverage is independent of the molecular weight of the PEGylated BSA. The other one describing the case where the surface coverage is depending on the molecular weight of the PEGylated BSA, see table B.2.

PEG MW (kDa)	a (nm) (independent of surface coverage)	d_2 (nm)	a (nm) (dependent on surface coverage)	d_2 (nm)
5	3.5	12.7	3.4	13.3
10	4.0	14.3	4.0	14.1
20	5.0	16.7	5.3	14.7
30	5.2	24.5	5.9	18.6
40	5.7	29.0	6.9	19.1
60	6.2	42.9	9.3	18.9

Table B.2: From the data fitting two different values for a, and then d_2 has been found. One describing the case where the surface coverage is independent of which PEGylated BSA species is immobilised. The other one describing the case where the surface coverage is decreasing with increasing PEGylated BSA MW.

Model 3

Model 3 illustrates the situation where the PEG polymer floats like a sphere on top of the grafted BSA, see figure B.3. The thickness of the bilayer corresponds to two viscosity radii of native BSA and two viscosity radii of PEG, as determined when it is attached to the BSA ($R_{h\ PEGylated\ BSA}$-$R_{h\ BSA}$).
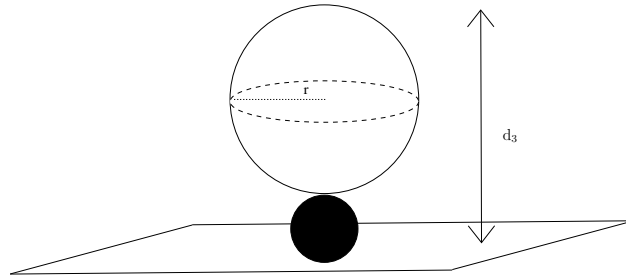
Figure B.6: PEGylated BSA on the SPR chip, two spheres. The distance d_3 equals 2 $R_{h\ BSA}$+ 2 r. The volume of the PEG molecule attached to the BSA is calculated from $(V_{PEGylated\ BSA} - V_{BSA}) = \frac{4}{3}\pi r^3$.

PEG MW (kDa)	d_3(nm) (independent of surface coverage)	d_3(nm) (dependent on surface coverage)
5	10.1	13.5
10	10.9	15.2
20	12.2	17.7
30	13.3	19.8
40	14.2	21.7
60	15.9	25.1

Table B.3: From the data fitting two different values for a, and then d_3 has been found. One describing the case where the surface coverage is independent of which PEGylated BSA species is immobilised. The other one describing the case where the surface coverage is decreasing with increasing PEGylated BSA MW.

Model 4

Model 4 describes the situation where the PEG polymer floats as an elongated sphere on top of the BSA molecule, which is immobilised onto the SPR chip, see figure B.7.
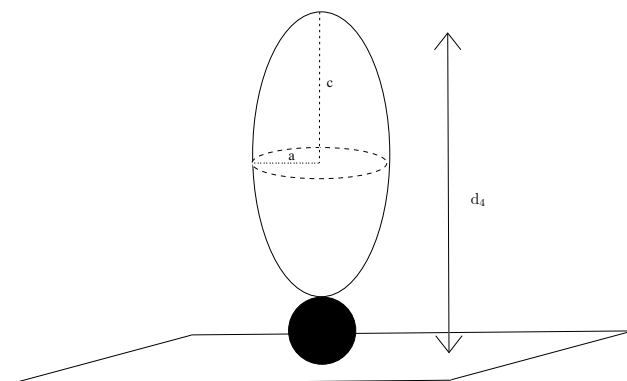
Figure B.7: PEGylated BSA on the SPR chip, elongated sphere on top of sphere. The distance d_4 equals $2 R_{h \, BSA} + 2 c$. The volume of the PEG attached to the BSA is calculated from $(V_{\text{PEGylated BSA}} - V_{\text{BSA}}) = \frac{4}{3}\pi a^2 c$.

The bilayer thickness, d_4, is calculated from the viscosity radii of BSA and the volume of the attached PEG polymer.

$$d_4 = 2 \cdot R_{H \ BSA} + 2 \cdot \frac{3 \cdot (V_{\text{PEGylated BSA}} - V_{\text{BSA}})}{4 \cdot \pi \cdot a^2} \tag{B.4}$$

In figure B.7 the distance a describes the 'semi-minor axis' and it is defined as

$$a = x \cdot R_{h\ PEG} \tag{B.5}$$

$R_{h\ PEG}$ is the viscosity radius of pure PEG [87].

Modelling the data gives two different values for a, depending on the value of the surface coverage, and whether the surface coverage is depending on the molecular weight of the grafted PEGylated BSA or not, see table B.4.

PEG MW (kDa)	**a** (nm) (independent of surface coverage)	d_4 (nm)	**a** (nm) (dependent on surface coverage)	d_4 (nm)
5	3.7	12.7	3.5	13.3
10	4.5	14.3	4.6	14.1
20	5.8	16.7	6.5	14.7
30	5.7	24.1	6.9	18.6
40	6.2	28.9	8.3	19.1
60	6.6	42.9	11.3	18.9

Table B.4: From the data fitting two different values for a, and then d_4 has been found. One describing the case where the surface coverage is independent of whatever PEGylated BSA species is immobilised. The other one describing the case where the surface coverage is decreasing with increasing PEGylated BSA molecular weight.

Results

The results in figure B.8 show that the hemispherical model, model 2, and the elongated spherical model, model 4, with the distances d_2, table B.2 and d_4, table B.4 are the best fit to the model. However looking at the values for the bilayer thickness they seem to be fairly large compared to the values for the free PEGylated BSA molecule, see table B.1. The value of bilayer thickness when describing an immobilised 60 kDa PEGylated BSA molecule is almost 2.5 times larger in model 2 and model 4 compared to model 1. Model 1 has mainly been used when developing the other models as it can be useful to take the behaviours at the extremes of the system boundaries under consideration, even if they appear to be absurd, as these help to bound the solution space under consideration. The results in figure B.9 show the modelling results, where the surface coverage depends on the molecular weight of the grafted molecule.

The decrease in surface coverage with larger molecular weight of the grafted PEGylated BSA can be taken into account in the modelling process profitably. All the 3 realistic models describe the measured data quite well. The values for the parameter a in model 2 found in table B.2 indicate that the height of the hemisphere is 2-4 times larger than the width, which will make the grafted PEGylated BSA somewhat cylinder shaped. The values of a in model 4 found in table B.4 show that the PEG is best described as an
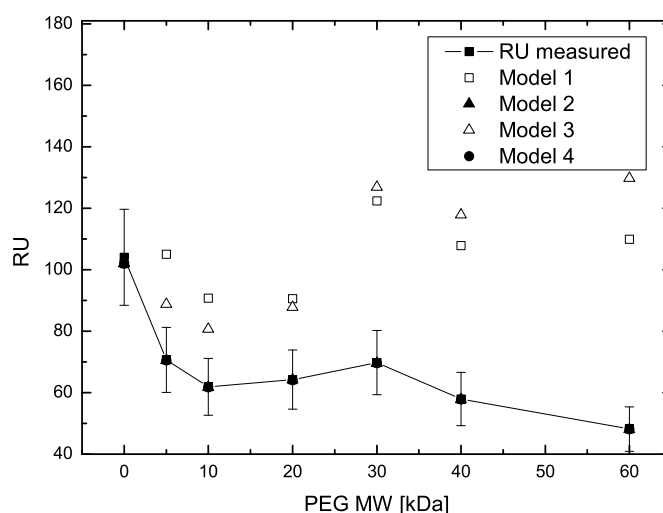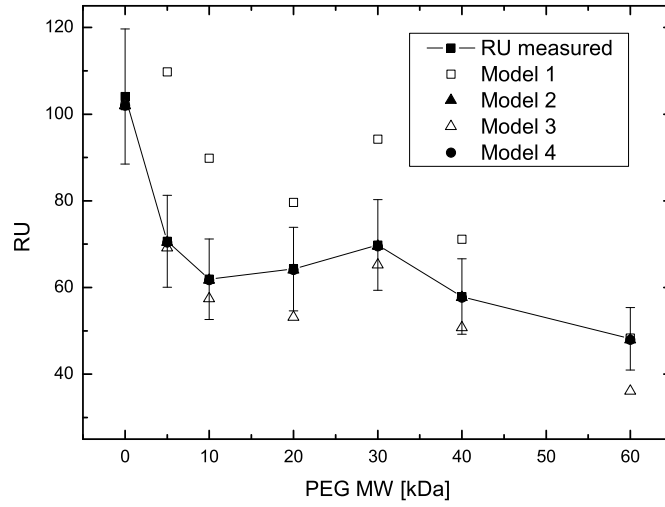
Figure B.8: The RU response versus the PEG molecular weight. This graph shows the modelling results based on values of the surface coverage being independent of the molecular weight of the PEGylated BSA.

ellipsoid on top of the spherical BSA molecule, sitting like an oblate spheroid on top of the BSA molecule.

In conclusion, the models which describe the case where the surface coverage is depending on the molecular weight of the PEGylated BSA are overall the best models. Based on these results the immobilised PEGylated BSA is best described as a hemisphere, where BSA is encased by PEG, or a sphere, BSA, with an oblate spheroid, PEG, sitting on top.

Concluding remarks

Traditionally SPR has been used as a screening tool for the investigation of the binding kinetics between antibodies and their corresponding antigens, and it is as such an excellent instrument. Especially with the growing marked within PEGylated pharmaceutical proteins the use of SPR will inevitably increase, and hopefully the content of this appendix will shed the light on the various potentials of the Surface Plasmon Resonance technique.

Figure B.9: The RU response versus the PEG molecular weight. This graph shows the modelling results based on values of the surface coverage is depending on the molecular weight of the PEGylated BSA.

Background calculations

The SPR response, RU, is directly proportional to the change in refractive index between the bulk solution and the protein adsorbed onto the chip at a certain distance from the chip surface.

$$\text{RU} \propto \left(\text{n}_{\text{protein}} - \text{n}_{\text{buffer}} \right)$$

The refractive index is defined as

$$\text{n}_{\text{protein}} = \text{n}_{\text{buffer}} + \text{C}_{\text{protein}} \cdot \frac{dn}{dc}$$

The refractive index increment of all the PEGylated BSA solutions was measured, and used in the modelling process.

The concentration of protein at the surface of the chip was

$$C_{\text{protein}} = \text{C} \cdot MW_{BSA} + MW_{PEG} \frac{\text{surface coverage}}{d}$$

The constant, C, contains unit conversion factors and Avagagro's Number, d is the thickness of the adsorbed adlayer and the surface coverage is amount of protein molecules per

nm^2. The surface coverage is calculated from the SPR response of the immobilised native BSA;

$$RU = m(n_{\text{protein}} - n_{\text{buffer}})$$

Here m in an instrument specific constant, n_{buffer} is the refractive index of the buffer and n_{protein} is the refractive index of the protein dissolved in the buffer. By knowing the molecular weight of the protein in question, Avagadro's Number, the thickness of the adlayer and the protein concentration an estimate of the surface coverage can be made. The thickness of the adlayer is, at first, based on d being 6.2 nm, which correspond to twice the viscosity radii of BSA[87].

The radius of PEGylated BSA serves as the basis for modelling the SPR response, as:

$$R_{h\ \text{PEG-BSA}} = \frac{A}{6} + \frac{2}{3A}R_{\text{PEG}}^2 + \frac{1}{3}R_{h\ \text{PEG}}$$

where

$$A = \left[108\ R_{h}{}^3{}_{\text{BSA}} + 8R_{h\ \text{PEG}}^3 + 12(81R_h{}^6{}_{\text{BSA}} + 12R_h{}^3{}_{\text{BSA}}R_h{}^3{}_{\text{PEG}})^{1/2}\right]^{1/3}$$

Viscosity radius of BSA is

$$R_{h\ \text{BSA}} = (0.82 \pm 0.02)66.7^{1/3} \tag{B.6}$$

where 66.7 is the molecular weight of BSA in kDa. And the viscosity radius of PEG is depending on the molecular weight of the polymer.

$$R_{h\ \text{PEG}} = 0.1912 \cdot MW_{\text{PEG}}^{0.559} \tag{B.7}$$

All the radii have the unit Å.

C Refractive index of PEGylated BSA

Refractive Index

In connection with the SPR measurements we modelled the SPR response as described in appendix B. Besides being sensitive towards the accumulated mass on the chip surface [173], the induced surface plasmons are sensitive to changes in the refractive index of the medium to an extent which makes the SPR response directly proportional to the difference in refractive index between the bulk solution and the liquid solution to be analysed [172]. Thus the refractive index of the protein solution must also be taken into account when interpreting SPR data.

Experiments with binding of PEGylated BSA with various linear PEG molecular weights to anti-BSA have resulted in lower SPR response compared to the similar experiments with non PEGylated BSA C.1.
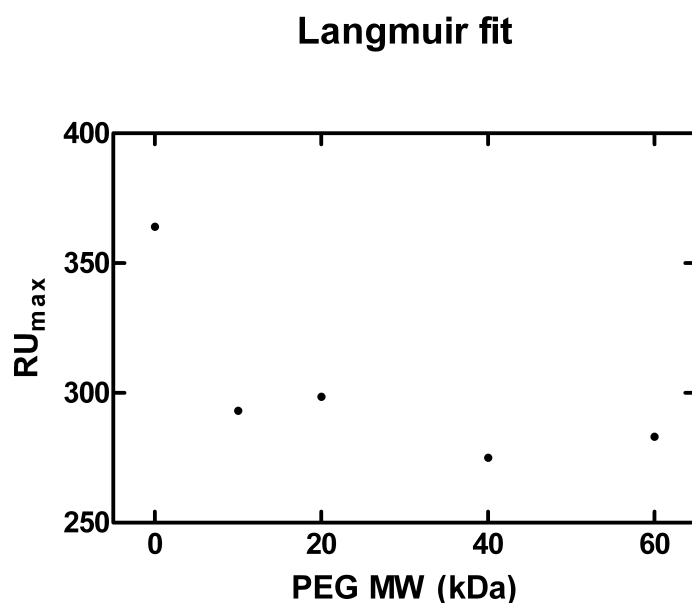
Figure C.1: The maximum response versus the PEG molecular weight, based on the Langmuir modelling. Error bars are too small to be seen.

The response might be low because the PEG is sterically hindering the binding of BSA to the immobilised anti-BSA. But the response is not affected by the molecular weight of the grafted PEG, which is surprising as the SPR response is proportional to the mass of the adsorbed protein [136, 172, 173]. It would be a curious coincident if an equilibrium exists between the lower response resulting from the steric hindrance and the higher response from the higher mass bound to the surface chip, which just cancels out for all the molecular weight PEGs in question.

A comparable study conducted by Kubetzko et al. [96] shows that the RU_{max} is much lower for the 20 kDa PEGylated species compared to the RU_{max} from the measurements of the native protein. The response is 1/3 even with a 3 times higher concentration of native protein. This supports our results, as we also see a reduction in the SPR response depending on PEGylation.

Another study, conducted by Yang et al. [66], shows the same tendency, almost a 10 fold decrease in the SPR response with PEGylation. The response from non-PEGylated antibody is 54 RU with a concentration of 135 nM, whereas the response of the 40 kDa PEG is 62 RU with a concentration of 3141 nM.

The reason for the unexpected low response might be found by looking at the index of refraction (RI) of the proteins in solution. Basic knowledge about the changes in the RI of the PEGylated protein compared to the non-PEGylated protein and free PEG in solution is needed in order to interpret our SPR data properly.

The RI relates to the media's dielectric constant and is depending on the state of the media, the temperature as well as the wavelength at which the RI is measured. Pure water has a RI of 1.333 at 20 °C and 589 nm [174]. Most dry, crystalline proteins have a RI near 1.6 [175], whereas PEG has a RI is 1.4563 [176]. It is a widely held view that the RI response of a mixture of different molecules or a hybrid molecule is the sum of the RI responses of the two components. Kunitani et al. [154] state that the RI of a specific component is a characteristic of the electron density of that component. Since PEG is attached to the protein by a single covalent bond it is the assumption, that the electron density of each component should essentially remain unchanged and approximation of their individual RI additivity should be accurate [177].

Measurements

The index of refraction (RI) of BSA, 5, 8 and 20 kDa PEG[1] and 5, 10, 20, 30, 40 and 60 kDa PEGylated BSA[2], all dissolved in PBS buffer, are measured. A Differential Refractometer Detector RID-10 A from Shimadzu is used to measure the difference in RI between the buffer solution and the different solutions of BSA, PEG and PEGylated BSA, respectively. All sample solutions are measured at different protein and PEG concentrations to get an experimental value for the refractive index increment.

---

[1] Fluka Chemie GmbH (Switzerland)
[2] PEGylated proteins from the PEGylation reaction described on page 60

The refractive index of each individual BSA or PEGylated BSA sample was measured at 5 different concentrations from a dilution series starting at the highest possible protein concentration from the pooled samples. The concentrations range from 1.35 mg/mL to 100 μg/mL. The pure PEG samples were made of either dissolved mPEG-SPA or pure PEG to cover the entire range of molecular weight PEGs used for PEGylation. Each sample was 100 μL and the measurements were done 3 times in immediate continuation of each other. The obtained values were averaged and the experiments were repeated the following day. Thus the refractive index of a certain concentration of protein or PEG was measured at least 6 times.

Theoretical model for the refractive index of PEGylated BSA

Fee and Van Alstine [87] have shown that the viscosity radius of PEGylated proteins depends on the molecular weight of the native protein and the total weight of the grafted PEG but not on the PEG molecular weight. The viscosity radius can be used to determine the volume of a PEGylated protein. The volume of a PEGylated protein can be divided into two parts, the contribution from the protein and the contribution from the attached PEG. The volume contribution from the PEG is smaller when attached to the protein, than when it is free in solution. This observation might be reflected in the measured refractive index of PEGylated BSA. Kunitani et al. [154] and Jung et al. [172] both suggest using the Lorenz-Lorenz Equation to estimate the refractive index of an unknown fluid solution, when all the constituting components are known. The refractive index of a PEG-protein solution would then be defined as:

$$n = n_{\text{buffer}} + \left(\frac{dn}{dc}\right)_{\text{PEG}} \cdot C_{\text{PEG}} + \left(\frac{dn}{dc}\right)_{\text{protein}} \cdot C_{\text{protein}} \quad \text{(C.1)}$$

Where n_{buffer} is the refractive index of the buffer, $(\frac{dn}{dc})_{\text{PEG}}$ and $(\frac{dn}{dc})_{\text{protein}}$ are the specific refractive index increments for PEG and protein, respectively, and C_{PEG} and C_{protein} are the weight concentrations of the PEG and protein per unit volume. The refractive index of mono-PEGylated BSA corresponds to a 1:1 molar ratio mixture of the two compounds. It can be calculated theoretically from equation C.1 and the viscosity radius from Fee and Van Alstine [87] and the refractive index of the dry protein and dry PEG. The theoretical model is a mixture of the properties of PEG, BSA and PEGylated BSA dissolved in buffer and as dry powder. The plot of the correlation between the index of refraction and the size of the PEG shows a difference in the index of refraction from the PEG-BSA mixture to the PEGylated BSA, especially at relatively low PEG size, see figure C.4. The PEGylated BSA has got a higher refractive index than PEG-BSA mixtures.

Refractive Index Results

The refractive index is a linear function of the concentration over a wide range of concentrations. The slope of the plot of the refractive index versus concentration is known as the refractive index increment (RII). The differential refractometer was used to determine the RII of BSA, PEG and PEGylated BSA in PBS buffer, see figure C.2.
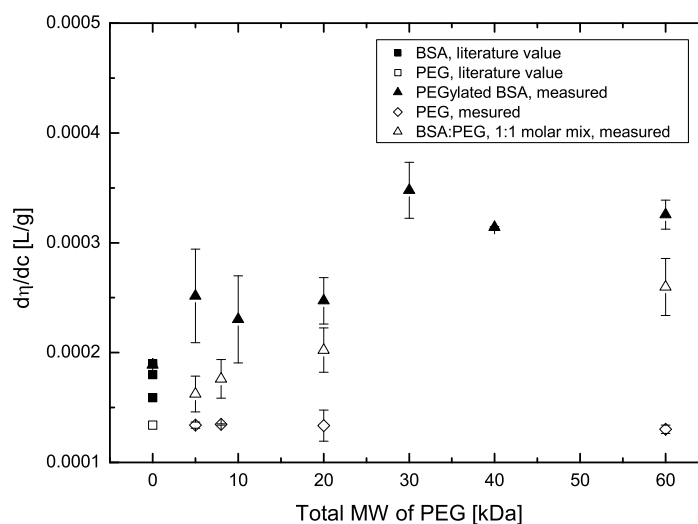
Figure C.2: The refractive index increment of BSA, PEG and PEGylated BSA in PBS. The RII is increasing with increasing molecular weight of the PEGylated BSA. The RII of pure PEG is independent of the molecular weight of PEG. There is a significant difference between the RII of the 1:1 molar mix of PEG and BSA and the PEGylated BSA. The RII of native BSA and pure PEG are comparable to the literature values. There is no difference in the RII between using dissolved activated PEG or pure PEG of the same molecular weight. The RII at 0 PEG molecular weight corresponds to native BSA.

From figure C.2 it is evident, that the refractive index increment is increasing with increasing molecular weight of the PEGylated BSA. The RII of pure PEG is independent of the molecular weight of the polymer, which is also found in the literature [176]. The RII of the 1:1 molar mix of PEG and BSA is clearly lower than the corresponding for the PEGylated BSA. There is no difference in the RII between using dissolved activated PEG or pure PEG of the same molecular weight. The maleimido-propionamide group attached to the activated PEG has thus no influence on the refractive index.

Discussion

It is essential to know the refractive index of a protein solution to be able to interpret data from various biophysical experiments including Static Light Scattering (SLS), Dynamic Light Scattering (DLS), Surface Plasmon Resonance (SPR) and other chromatographic and spectroscopic methods. Experimental results of measurements of the RI as well as the RII of PEGylated proteins found in the literature have been very sparse. Kubetzko et al. [96] have set the refractive index increment to 0.166 mg/L for PEGylated mini-antibodies or to 0.185 mg/L for nonPEGylated mini-antibodies. We have found that PEGylating

a protein result in a larger refractive index increment compared to the nonPEGylated species.

Our measurements of the RII of BSA are comparable to the literature values [175], [178], [179], see table C.1. There is no apparent correlation between the refractive index and the size of the protein. The slight difference between the refractive indices is most likely depending on the content of the protein bulk solution (whether the bulk solution contained phenols, alcohol, chaotropic or kosmotropic agents), small temperature differences or difference in the reagent purity.

BSA	PEG
$1,89 \cdot 10^{-4} \pm 0.01 \cdot 10^{-4}$ L/g (in PBS)	$1.33 \cdot 10^{-4} \pm 0.053 \cdot {}^{-4}$ L/g (in PBS)
$1.571\text{-}1.590 \cdot 10^{-4}$ L/g (in $(NH_4)_2SO_4$)[175]	$1.34 \cdot 10^{-4}$ L/g (in water)[180]
$1.90 \cdot 10^{-4} \pm 0.02 \cdot 10^{-4}$ L/g (in Milli-Q water)[179]	
$1.83 \cdot 10^{-4}$ L/g (in Milli-Q water) [179]	

Table C.1: The experimental values, on top, and the literature values for the refractive index increment of native BSA and different MW PEGs.

Studies have shown that the index of refraction of *dry* proteins range from 1.35-1.6 [172, 175, 181].

The absolute index of refraction of a solutions is calculated from the refractive index increment of the solute added the refractive index of the solvent, equation C.1. For a protein solution of a given concentration, the experimental measurements of the refractive index can be compared to theoretical calculations of the same solution when the RI of the buffer and the RII of the solute is known, see figure C.3.

From figure C.3 it is clear, that the measured refractive indices of the PEGylated BSA solutions are larger than the refractive index of the 1:1 molar ratio of BSA and PEG by themselves.

Kendrick et al. [182] argue that the refractive index increment is a function of its chemical groups and independent of higher order structures. We see a slightly different tendency in our measurements. As seen in figure C.2 the RII of a solution of BSA and PEG is depending on whether they are covalently linked or not. So the RII is not only a function of the chemical groups, but also dependent of higher order structures.

Background calculations

The difference between these two models is mainly the amount of occupied volume. The occupied volume of the PEGylated BSA molecule is more than the mixture of BSA and PEG.
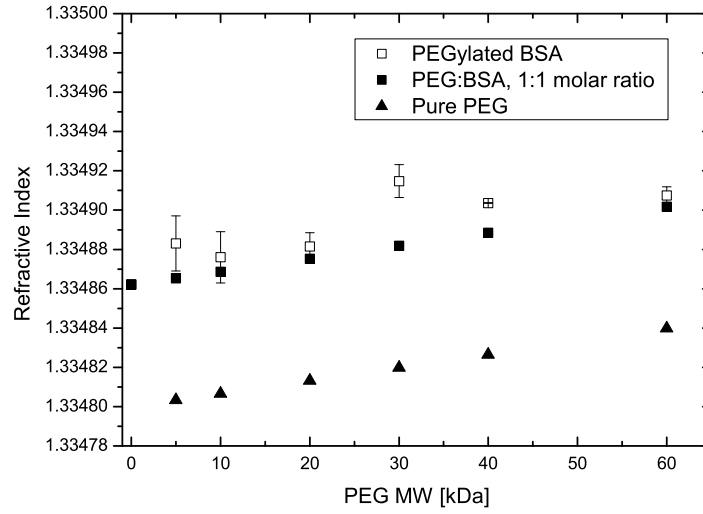
Figure C.3:   The refractive index of various 0.33 mg/mL solutions is plotted versus the molecular weight. The filled squares and triangles are calculated values, whereas the open squares are experimentally measured values.

The refractive index of a mixture of PEG and BSA can be calculated from a variation of equation C.1.

$$n_{\mathrm{BSA\ PEG\ mixture}} = n_{\mathrm{BSA}} \cdot \frac{V_{\mathrm{BSA}}}{V_{\mathrm{BSA}} + V_{\mathrm{PEG}}} + n_{\mathrm{PEG}} \cdot \frac{V_{\mathrm{PEG}}}{V_{\mathrm{BSA}} + V_{\mathrm{PEG}}} \qquad (\mathrm{C.2})$$

The volume of BSA is

$$V_{\mathrm{BSA}} = \frac{4 \cdot \pi (R_{\mathrm{H\ BSA}})^3}{3} = \frac{4 \cdot \pi (0.82 \cdot MW_{\mathrm{BSA}}^{1/3})^3}{3} \qquad (\mathrm{C.3})$$

The volume of PEG is

$$V_{\mathrm{PEG}} = \frac{4 \cdot \pi (R_{\mathrm{HPEG}})^3}{3} = \frac{4 \cdot \pi (0.1912 \cdot MW_{\mathrm{PEG}}^{0.559})^3}{3} \qquad (\mathrm{C.4})$$

For the PEGylated BSA the refractive index can also be calculated from equation C.1:

$$n_{\mathrm{PEGylated\ BSA}} = n_{\mathrm{BSA}} \cdot \frac{V_{\mathrm{BSA}}}{V_{\mathrm{BSA}} + V_{\mathrm{PEG\ attached}}} + n_{\mathrm{PEG}} \cdot \frac{V_{\mathrm{PEG\ attached}}}{V_{\mathrm{BSA}} + V_{\mathrm{PEG\ attached}}} \qquad (\mathrm{C.5})$$

The volume of the attached PEG is found by calculating the viscosity radius of PEGylated BSA, using the equations given in Fee and Van Alstine [87]:

$$
\begin{aligned}
R_{H\ PEG-BSA} = &\frac{1}{6}\left[108\ (R_{H\ PEG})^3 + 12(81(R_{H\ BSA})^6 + 12(R_{H\ BSA})^3(R_{H\ PEG})^3)^{1/2}\right]^{1/3} + \\
&\frac{2}{3}\left[\frac{(R_{H\ PEG})^2}{(108\ (R_{H\ PEG})^3 + 12(81(R_{H\ BSA})^6 + 12(R_{H\ BSA})^3(R_{H\ PEG})^3)^{1/2})}\right]^{1/3}\right]
\end{aligned}
\tag{C.6}
$$

$$
R_{H\ PEG\ attached} = R_{H\ PEG-BSA} - R_{H\ BSA}
\tag{C.7}
$$

$$
V_{PEG\ attached} = \frac{4 \cdot \pi \cdot (R_{H\ PEG\ attached})^3}{3}
\tag{C.8}
$$

The index of refraction of the BSA and PEG mixture (n_mix) and the PEGylated BSA (n_PEGylated BSA) as a function of PEG molecular weight in Da is plotted in figure C.4.
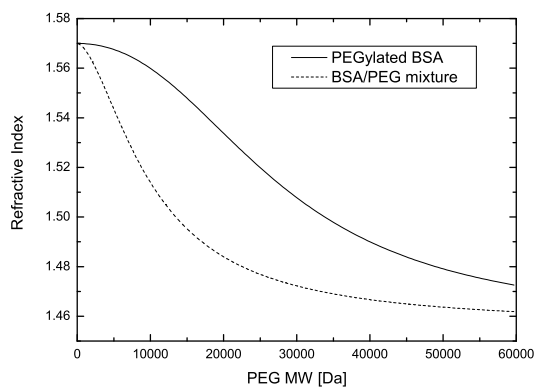
Figure C.4: The theoretical change in refractive index (RI) versus PEG MW for a 1 mg/mL PEGylated BSA and a 1:1 molar, 1 mg/mL mixture of PEG and BSA. Red line shows the RI of a 1:1 molar mixture of PEG and BSA, whereas the blue dotted line shows the RI of PEGylated BSA. The refractive index of a solution 1:1 molar solution of PEG and BSA depends clearly on whether they are covalently attached to each other

Index